Application of laser Doppler vibrocardiography for human heart auscultation

by

Suretha Koegelenberg

Thesis presented in partial fulfilment of the requirements for the degree of Master of Science in Mechatronic Engineering in the Faculty of Engineering at Stellenbosch University

Department of Mechanical and Mechatronic Engineering,
University of Stellenbosch,
Private Bag X1, Matieland 7602, South Africa.

Supervisor: Prof. C. Scheffer and Dr. M. Blanckenberg

April 2014

Declaration

By submitting this thesis electronically, I declare that the entirety of the work contained therein is my own, original work, that I am the sole author thereof (save to the extent explicitly otherwise stated), that reproduction and publication thereof by Stellenbosch University will not infringe any third party rights and that I have not previously in its entirety or in part submitted it for obtaining any qualification.

Date: . . . .

Abstract

Application of laser Doppler vibrocardiography for human heart auscultation

S. Koegelenberg

Department of Mechanical and Mechatronic Engineering,
University of Stellenbosch,
Private Bag X1, Matieland 7602, South Africa.

Thesis: MScEng (Mech)

April 2014

This thesis investigates the feasibility of the laser Doppler vibrometer (LDV) for use in the autonomous auscultation of the human heart. As a non-contact measurement device, the LDV could become a very versatile biomedical sensor. LDV, stethoscope, piezoelectric accelerometer (PA) and electrocardiogram (ECG) signals were simultaneously recorded from 20 volunteers at Tygerberg Hospital. Of the 20 volunteers, 17 were confirmed to have cardiovascular disease. 3 patients with normal heart sounds were recorded for control data.

The recorded data was successfully denoised using soft threshold wavelet denoising and ensemble empirical mode decomposition. The LDV was compared to the PA in common biomedical applications and found to be equally accurate. The heart sound cycles for each participant were segmented using a combination of ECG data and a simplicity curve. Frequency domain features were extracted from each heart cycle and input into a k-nearest neighbours classifier. It was concluded that the LDV can form part of an autonomous, non-contact auscultation system.

Uittreksel

Toepassing van laser Doppler vibrasiemeter vir menslike hart beluistering

("Toepassing van laser Doppler vibrasiemeter vir menslike hart beluistering')

S. Koegelenberg

Departement Meganiese en Megatroniese Ingenieurswese,
Universiteit van Stellenbosch,
Privaatsak X1, Matieland 7602, Suid Afrika.

Tesis: MScIng (Meg)

April 2014

Hierdie tesis ondersoek die haalbaarheid daarvan om die laser Doppler vibrasie-meter (LDV) vir die outonome beluistering van die menslike hart te gebruik. As 'n kontaklose meettoestel kan die LDV werklik 'n veelsydige biomediese sensor word. Twintig vrywilligers by die Tygerberg Hospitaal se LDV-, stetoskoop-, piëso-elektriese versnellingsmeter (PV)- en elektrokardiogram (EKG) seine is gelyktydig opgeneem. Uit die 20 vrywilligers was daar 17 bevestigde gevalle van kardiovasku-lêre siektes. Die data van drie pasiënte met normale hartklanke is as kontroledata opgeneem.

Geraas is suksesvol uit die opgeneemde data verwyder deur 'n kombinasie van sagtedrempelgolf en saamgestelde empiriese modus ontladingstegnieke. Die LDV was vergelyk met die PV vir algemene biomediese gebruike en daar was gevind dat dit vergelykbare akkuraatheid het. Die hartklanksiklusse van elke deelnemer is gesegmenteer deur EKG data en 'n eenvoudskromme te kombineer. Frekwensie-gebiedskenmerke is uit elke hartsiklus onttrek en in 'n k-naastebuurpunt klassifi-seerder ingevoer. Daar is tot die gevolgtrekking gekom dat die LDV deel van 'n outonome, kontaklose beluisteringstelsel kan uitmaak.

Acknowledgements

I would like to express my sincere gratitude to my supervisors for their patience and my parents for their continuous support.

Dedications

This thesis is dedicated to my First Love.

Contents

CONTENTS viii

List of Figures

List of Tables

Nomenclature

Abbreviations

AR	Aortic regurgitation
AS	Aortic stenosis
CV	Cross validation
ECG	Electrocardiogram
$EEMD$	Ensemble empiracle mode decomposition
EMD	Empiracle mode decomposition
FFT	Fast Fourier transform
HR	Heart rate
ICP	Integrated circuit piezoelectric
IMF	Intrinsic mode function
LDV	Laser Doppler vibrometer
$LOOCV$	Leave-one-out cross validation
MA	Moving average
MR	Mitral regurgitation
MS	Mitral stenosis
PA	Piezoelectric accelerometer
PAT	Participant number
PC	Personal computer
PR	Pulmonary regurgitation
PS	Pulmonary stenosis
RMS	Root mean square
SNR	Signal to noise ratio
$STFT$	Short time fourier transform
SVC	Support vector classifier
TR	Tricuspid regurgitation
VSD	Ventricular sepal defect

Chapter 1

Introduction

1.1 Introduction

Cardiovascular disease (CVD) is a worldwide health issue and has become a growing concern for developing countries such as South Africa. These poor and underdeveloped countries are being forced to allocate sparse health care resources into the treatment and prevention of CVD. The Heart and Stroke Foundation predicts a 41% increase in the premature deaths of people aged 35–64 in the years 2000–2030. Since this age group makes up the largest fraction of the country's workforce, CVD could cause significant economic hardship in South Africa (Steyn, 2007). Maredza *et al.* (2011) has remarked that South Africa is increasingly influenced by international trends and lifestyles. These influences prompt South Africans to adopting lifestyles with increased CVD risk factors, such as tobacco smoking and unhealthy diets.

The Heart and Stroke Foundation's 2007 report stated that, on average, 195 people died every day due to CVD in South Africa (Steyn, 2007). The World Health Organization reported in 2010 that South Africa showed an estimated mortality rate due to CVD of 11% in 2008 (WHO, 2010). By contrast, the mortality rate due to CVD of the United States of America was 35%. Maredza *et al.* (2011) indicates that South Africa's health care focuses on "acute care" which necessitates that the management of HIV/AIDS currently uses most of the country's health care resources. Due to its rapid growth and the lack of availability of health care resources, the care and treatment of CVD must be efficiently managed.

The management of CVD includes the development of methods which make its early detection possible. Those living in rural areas often do not have access to sufficient medical care or qualified doctors who can provide such a service. Telemedicine and automated diagnosis tools are therefore an important step towards providing basic medical care to South Africans, especially those living outside of urban areas.

1.2   Background

Various researchers have tested a wide range of sensors such as accelerometers (Salerno *et al.*, 1991), rigid reference frame surface velocity analyzers (Smith *et al.*, 1983) and laser-based vibration sensors (Umberto *et al.*, 2007) for their applicability to auscultation, and reported varying degrees of success. Recently, interest has been shown in the laser Doppler vibrometer (LDV) as a non-contact auscultation tool (Scalise, 2012). In this work its applicability as part of an automated diagnostic system for heart sounds and murmurs will be explored. In this section some brief background on two popular auscultation tools, the stethoscope and a piezoelectric accelerometer, as well as the LDV is provided.

1.2.1   Stethoscope

Immediate auscultation is the act of placing an ear against a patient's chest to listen to their heart sounds. This technique has been used to diagnose illness since the time of the Hippocratics (460 to 370 BC). The need for a method which required less physical contact with the patient led to the development of the stethoscope which later became the primary tool for auscultation (Bedford, 1972). Advances in electronics and sensors have led to the further development of the stethoscope as well as more sophisticated auscultation devices.

The traditional stethoscope is a robust and readily available tool. Despite its simplicity, in the hands of an experienced physician it is a useful component of a diagnostic system (Noimanee *et al.*, 2007). The first stethoscope was invented by French physician Renè Théophile Hyacinthe Laënnec, in 1816 (Reiser, 1979). Laënnec experimented with various wooden sticks and cylinders and found that a rod of solid wood placed between his ear and the patient's chest, best improved the transmission of the sound. When the rod was pierced by a narrow bore, this transmission became even more efficient.

Initially, physicians were slow to adopt the stethoscope. They often did not have the necessary knowledge and training to use the stethoscope as a diagnostic tool, but word of this "new technology" had spread to their patients and meant that their competence would be questioned if they did not possess one. Their lack of skills hindered the stethoscope's progress and therefore the development of auscultation in general (Reiser, 1979). As physicians' diagnostic skills improved, the design of the stethoscope grew more sophisticated, spawning various designs (Dalmay *et al.*, 1995).

A traditional stethoscope has a two-sided head – one with a flat membrane, or diaphragm, to pick up high frequency sounds and the other with a "bell" to pick up low frequency sounds. The bell's frequency range is approximately 20 to 200 Hz, making it useful for listening to heart sounds (3M, 2012). Stethoscope design has made advances since the early days of Laënnec. Today, highly complex dig-

ital stethoscopes are available which incorporate advanced ambient noise rejection within the stethoscope itself (ThinkLabs, 1995). Wireless stethoscopes have also been developed for many years, allowing remote access to patients and use in telemedicine (Hök *et al.*, 1988). The basic operation of the stethoscope is shown in Figure 1.1.
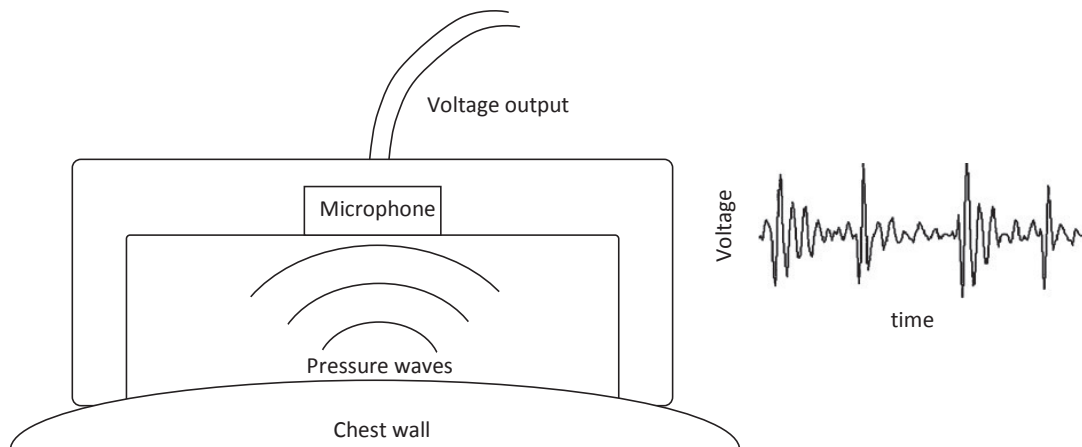
Figure 1.1: The stethoscope housing directs the pressure waves which are caused by the vibration of the skin towards a microphone. The microphone produces a voltage output directly proportional to the input waves which can be recorded for playback or analysis.

1.2.2 Piezoelectric accelerometer

Piezoelectric accelerometers (PA) are constructed from two major components – a seismic mass and piezoelectric material, such as a quartz crystal lattice structure (see Figure 1.2). When the seismic mass undergoes acceleration it applies a load on the crystal. As the crystal deforms it produces a voltage output proportional to the applied force, which is in turn proportional to the acceleration of the seismic mass (PCB Piezotronics, 2012). This is phenomenon was discovered by the Curie brothers in 1880 and is known as the piezoelectric effect (Katzir, 2003).

The piezoelectric effect has been used in sensors for nearly a century. It was first used to measure pressure in 1919 and vibration in 1921 (Gautschi, 2002). Due to the insensitivity and size of early accelerometers, they were considered to be of limited use in the medical field at the time (Umberto *et al.*, 2007).

Recently accelerometers have become both sensitive and small enough to be of practical use in medical applications (Umberto *et al.*, 2007). One such use includes

the detection of the heart's underlying motion by monitoring the vibrations of the chest wall. In the 1990's seismocardiography, a technique to monitor and diagnose heart sounds with a seismic instrument, often an accelerometer (Wilson *et al.*, 1993), was introduced. Today, seismocardiography is reported to be of comparable accuracy to the ECG's when measuring heart rate (HR) assessment (Wilson *et al.*, 1993).
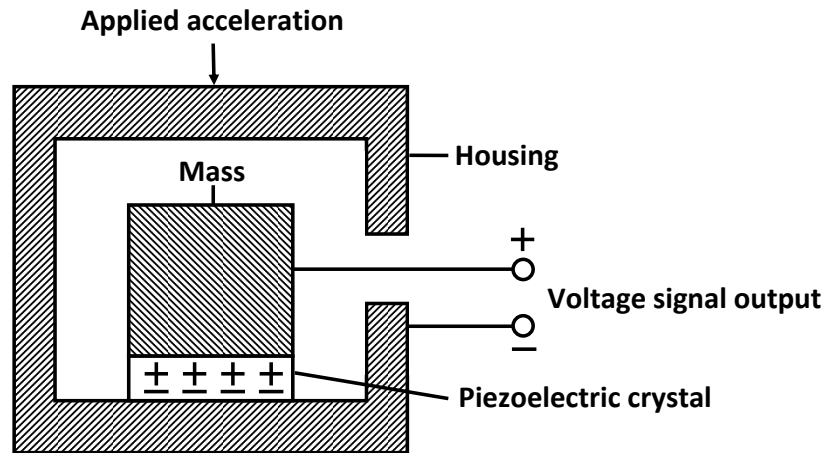
Figure 1.2: The piezoelectric accelerometer contains a mass inside a housing. When undergoing a given acceleration, this mass applies a proportional force to the acceleration to the piezoelectric material on which it is mounted. The piezoelectric material then outputs a measurable voltage proportional to the force it is experiencing.

1.2.3 Laser Doppler vibrometer

The LDV has been the object of numerous biomedical studies, discussed in Section 2.5.3. As it does not require contact with the patient, it is suitable for monitoring vital signs in situations where a contact sensor can not be used. The LDV has also been proven to be largely insensitive to environmental noise (Avargel and Cohen, 2011).

The operation of the LDV is explained in Figure 1.3. A laser beam is sent from the diode through a Bragg cell acousto-optic modulator (AOM). The beam is split in two: one part is diffracted, frequency shifted and directed towards the object of interest while the other part of the beam is stopped by the beam stop. The beam which was directed at the object is reflected back and part of the scattered light is sent back towards the AOM. Here the light is diffracted and frequency shifted again and sent to the laser diode where it is mixed with the reference beam – a part of the laser diode beam which is used to monitor the laser power. The returned beam

has three added frequency components – two from when passing though the Bragg cell twice and as well as the Doppler frequency shift returned from the object being measured. This frequency shifted beam is detected by a built-in photo-diode which produces the corresponding voltage output. Electronics in the electric controller box process this output in real time to calculate the frequency and amplitude of the object's vibration.
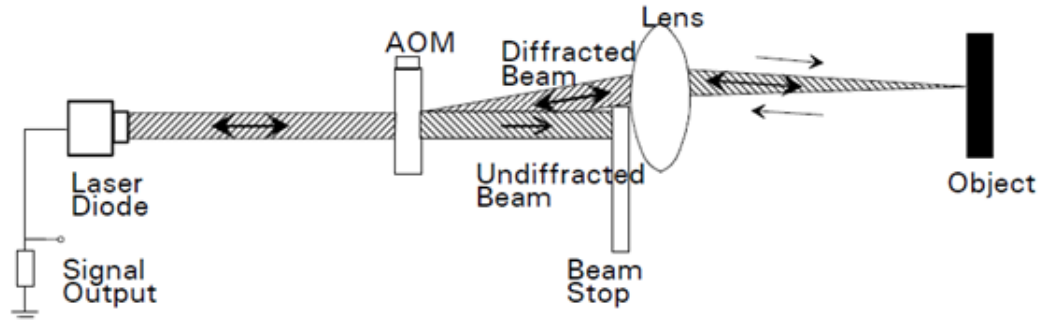
Figure 1.3: The laser Doppler vibrometer directs a laser beam at an object. The reflected light is compared to a reference beam where the frequency shift in the returned beam is used to calculate the velocity of the measured object. (MetroLaser Inc., 2010)

1.3 Motivation

The LDV is a promising alternative to traditional methods of auscultation such as a stethoscope or accelerometer. The LDV has several advantages over the common contact sensors. It is ideal for monitoring the vital signs of patients for whom contact is painful or could cause infections, such as burn victims. It is also well suited for monitoring the vital signs of infants where limited space is available for traditional sensors. Furthermore, the LDV can be used in bio-hazardous environments: contact sensors in such an environment would need to be discarded or sterilized while the LDV could be kept outside of the environment itself, avoiding this necessity (Umberto *et al.*, 2007).

As the phonocardiogram is widely studied as an auscultation instrument, the performance of the LDV should be tested against it. Although not the main focus of this work, it is also informative to benchmark the LDV against alternative auscultation techniques. The accelerometer and its use in seismocardiography are therefore also investigated.

1.4   Objectives

The project goal is to use and characterize the LDV as an auscultation device by comparing it to the well documented phonocardiogram as well as a piezoelectric accelerometer. To that end certain objectives were identified:

1. Record simultaneous data from the LDV, accelerometer and stethoscope and synchronize it with ECG data

2. Find features which can be used to classify various heart murmurs

3. Implement a proof of concept classifier for automated diagnosis of heart murmurs using the LDV and PA data

4. Characterize the LDV output for various heart murmurs and compare its output to the well-known phonocardiogram and PA recordings

1.5   Thesis outline

Chapter 1 provided an overview of the history of the LDV, stethoscope and accelerometer as biomedical sensors. Chapter 2 discusses relevant literature regarding the heart and auscultation, the electrocardiogram and previous research on the topics of signal processing techniques, methods of classification, and the LDV as a biomedical sensor. The current project is also compared with previous research.

Chapter 3 describes the hardware used in the study and provides an overview of how the data was recorded in the clinical environment. Chapter 4 describes how the data was denoised as well as how the heart cycles were segmented for further analysis. The different heart murmurs as recorded on the LDV are shown and the accelerometer and LDV's data are directly compared. Features sets and classification are discussed. Chapters 5 shows the results of the classification and Chapter 6 discusses the conclusions and recommendations of the study.

1.6   Chapter summary

An overview of the background and operating principles of the stethoscope, accelerometer and laser Doppler vibrometer have been given in this chapter. The motivation behind the current work is to characterize the LDV as a non-contact auscultation tool for use of an autonomous classifier of heart sounds. The objectives and a general outline of the work presented was discussed.

Chapter 2

Literature review

2.1 Introduction

In this chapter, an overview of the cardiovascular system is presented and the common heart sounds and heart murmurs are discussed. The electrocardiogram is briefly described and literature discussing denoising, segmentation, signal processing and classification methods are examined. The current work is compared with previous projects, and the LDV and its role as a biomedical sensor is also discussed.

2.2 The cardiovascular system

The heart is the pump which drives the circulatory system of the body. The circulation of the blood through the heart is summarized from Rangayyan (2001). The cells within the body all require oxygen to function and survive. They draw oxygen from the blood distributed to them by the body's veins and arteries. This leaves the blood de-oxygenated, which requires that the blood be pumped towards the lungs to become oxygenated again. The heart forces the blood through the veins and arteries, driving continuous movement of oxygenated and de-oxygenated blood. Figure 2.1 shows a basic diagram of the circulatory system, indicating how de-oxygenated blood flows through the heart to the lungs where it is oxygenated, and then back through the heart to be distributed to the rest of the body. The blue sections of the diagram represents the flow of de-oxygenated blood and the red sections represent the flow of oxygenated blood.

The heart has two halves, separated by the septum. Each of these halves can further be divided into two chambers: the top chamber, or atrium and the lower chamber, or ventricle. The atria collect the blood coming into the heart. The right atrium receives de-oxygenated blood from the circulatory system and the left atrium receives oxygenated blood from the lungs. The heart chambers can be filled with blood when they are relaxed (polarized) and eject the blood when they contract

7
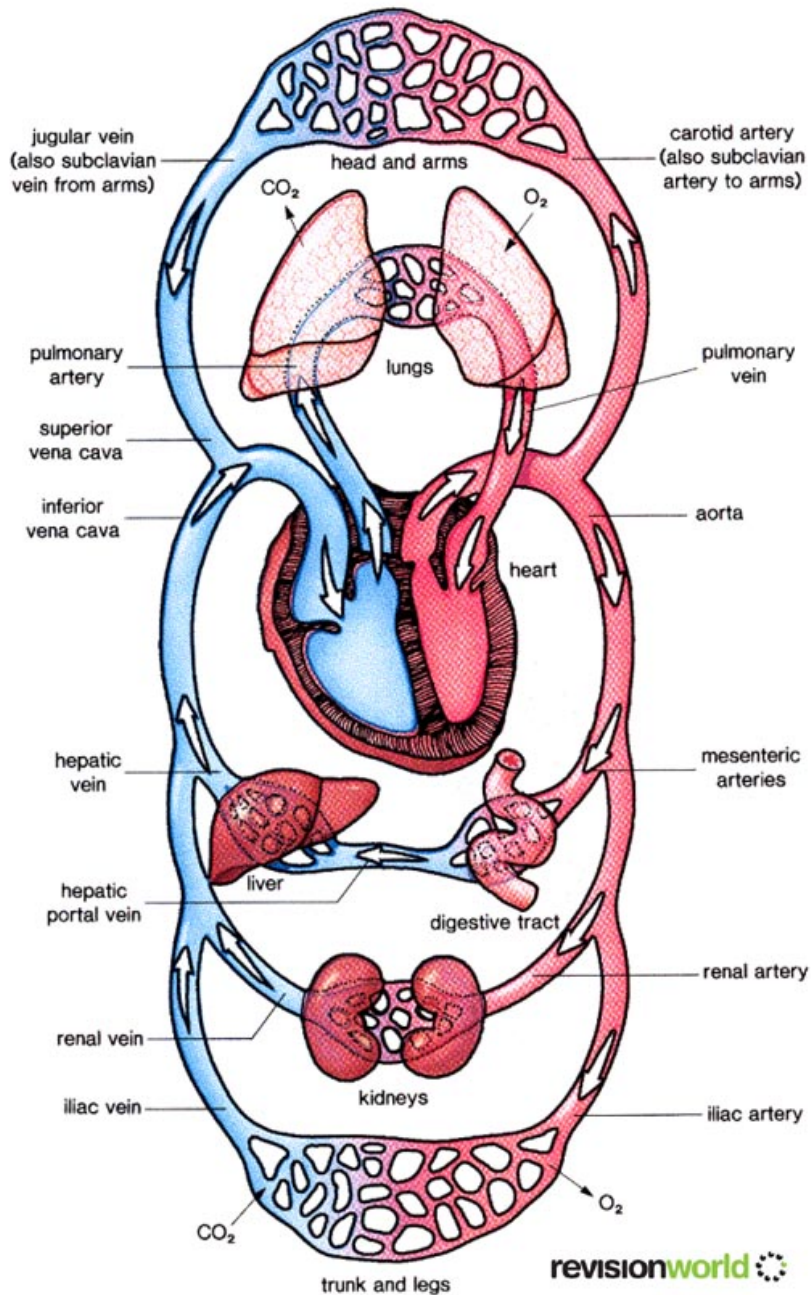
Figure 2.1: The circulation of blood through the cardiovascular system where red indicates oxygen-rich (oxygenated) blood circulating towards the body cells and blue represents oxygen-poor (de-oxygenated) blood returning from the body cells (Revision World, 2012).

(depolarize). Blood is forced to the lungs and rest of the body by contractions of the right and left ventricles respectively. When a chamber is in rest it is in the diastolic phase, while a contracting chamber is in the systolic phase. Blood flow within the heart is kept one-directional by four one-way mechanical valves. They are the tricuspid, pulmonary, mitral and aortic valves (Figure 2.2).

The contractions of the various heart chambers are governed by electrical pulses. Figure 2.2 shows the main components of the nerve system - the sinoatrial (SA) node, found at the top of the right atrium, the atrioventricular node (AV) node, found at the center of the heart between the atria and ventricles, and attached to the AV node are the His bundle and Purkinje fibers. An action potential originates in the SA node and is conducted through the atria towards the AV node, causing the atria to contract. The AV node is specialized to be the only conductive point between the atria and ventricles, and conducts electrical impulses slowly. The AV node therefore creates a time delay between the contractions of the atria and ventricles. When the action potential has passed through the AV node it is relayed towards the bundle of His, where it is further conducted along the bundles' branches and the Purkinje fibers. The Purkinje fibers stimulate the various cells surrounding them to contract (Johnson, 2003).
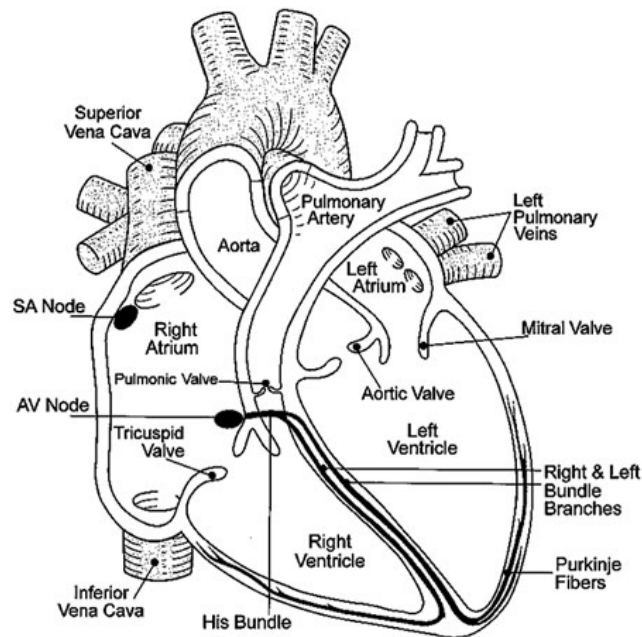
Figure 2.2: The physical anatomy of the heart showing the positions of the heart chambers, -valves and the structures responsible for the propagation of electricity within the heart muscle (NursingMedic, 2010).
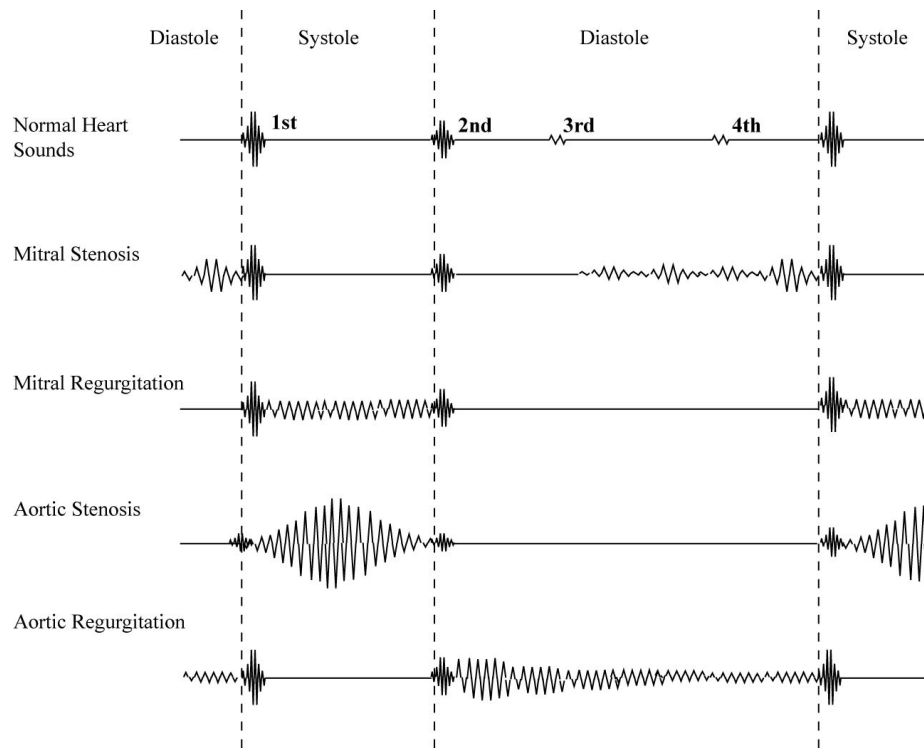
Figure 2.3: Characteristic shapes of heart murmurs as seen on a phonocardiogram (Lammers, 2013).

2.3 Heart sounds and auscultation

Initially the heart sounds were ascribed to the movement of the four heart valves. Further study revealed that the sounds are actually caused by pressure gradients triggering vibrations of the entire cardiovascular system (Rangayyan, 2001). A normal heart typically has two heart sounds, denoted as S1-S2 (Figure 2.3). In rare cases a third and fourth heart sound can also be heard. S1 and S2 are often described as a "lub-dub" sound combination, due to their characteristic sounds when auscultating a normal heart using a stethoscope. When audible, S3 is just after S2 and S4 is at the start of S1. S3 and S4 are very often obscured by the much louder S1 and S2. S3 is normal in people under 40 years of age but could be a sign of severe mitral regurgitation when it is detected in older people (Shah *et al.*, 2008). S4 is heard during late diastole and is the result of the atria contracting and pushing blood forward into the relaxed ventricles.

Murmurs are high-frequency noises occurring between S1 and S2, and between S2 of a given cycle and S1 of the following cycle. They occur when the blood's velocity increases from passing through a narrowed section in its path and the blood flow transitions to turbulence. Heart murmurs can be classified into two

groups: innocent and abnormal. Innocent murmurs are usually heard in infants and newborns and are not indicative of an abnormal heart. Abnormal murmurs are usually heard in older children and adults, and indicate the presence of faulty heart valves.

One common cause of heart murmurs is valvular stenosis (VS) – the stiffening of the heart valves. VS is often caused by a build-up of calcium deposits. These stiffened heart valves cannot fully open so that they create an obstruction in the path for the passing blood. In contrast, valvular insufficiency is observed when the valves cannot close properly and regurgitation or reverse leakage is facilitated (Rangayyan, 2001). Figure 2.3 shows several heart murmurs as seen on a phonocardiogram. These murmurs are well documented and have characteristic shapes and durations which are often used for classification.

2.4   The electrocardiogram

The electrocardiogram (ECG) is an electronic visualization of the electrical activity in the heart. The ECG is considered the golden standard for calculating heart rate and heart rate variability and as such is widely used in many medical applications (Burke and Nasor, 2002). The wave shapes seen on an ECG are a representation of the net electrical pulses as seen by the each of the ECG leads. The ECG waveform usually has clearly visible peaks which make calculating the heart beats per minute straightforward (Rangayyan, 2001). Figure 2.4 shows a characteristic ECG shape with the labels of the important peaks and waves. Additionally this figure shows the state of the heart valves during the cycle as well as the corresponding timing of S1 and S2. S1 can be observed just after the R peak and S2 can be seen just before the end of the T-wave.

Figure 2.5 shows how the physical and electrical activity of the heart relate to one another (Visagie, 2007).

1. De-oxygenated blood from the body enters the right atrium from the superior and inferior vena cavae as atrial depolarization is started (Figure 2.5.1).

2. Once the atrium is completely depolarized, the atrium is full and contracts (Figure 2.5.2).

3. Ventricular depolarization then starts and the blood is pushed into the right ventricle. The atria start repolarizing at this point (Figure 2.5.3).

4. The tricuspid valve then briefly opens to allow the blood through. Once closed the valve prohibits the blood from flowing back into the atrium. During ventricular depolarization the ventricles contract (Figure 2.5.4), pushing the blood out to the pulmonary arteries
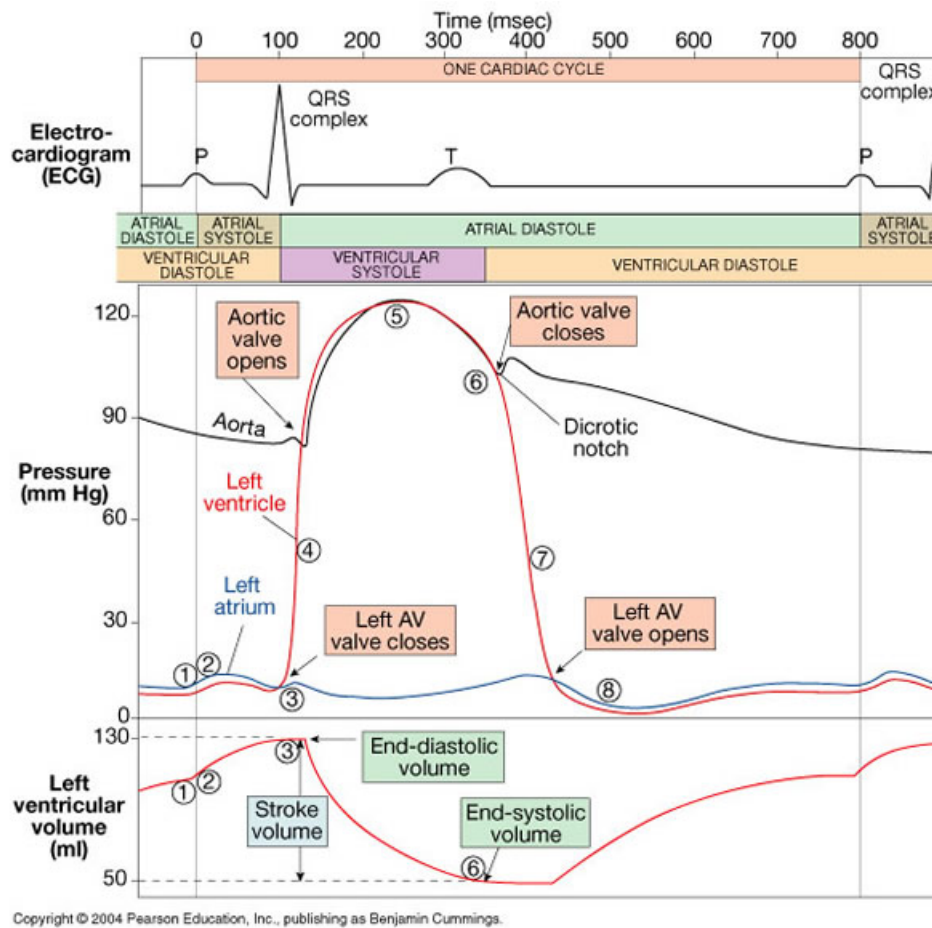
Figure 2.4: The polarization and depolarization electrical activity propagating in the heart tissue as recorded on an electrocardiogram trace (Cummings, 2004).

5. The pulmonary valve allows the blood to flow out to the arteries but stops any flow in the opposite direction. The ventricles now repolarize (Figure 2.5.5–6).

   The de-oxygenated blood then flows through the pulmonary arteries to the lungs to be re-oxygenated. Oxygenated blood leaves the lungs and is pumped towards the left atrium via the pulmonary veins. When the atrium has filled with blood, it contracts and pumps the blood into the left ventricle. The mitral valve briefly opens and closes to facilitate this transfer. Once closed, the mitral valve prevents blood from flowing back into the left atrium. When the left ventricle is filled with blood it contracts, pumping the blood out into the aorta to be circulated to the rest of the body. The aortic valve allows blood to flow from the left ventricle to the aorta but stops any flow in the opposite direction (Rangayyan, 2001).
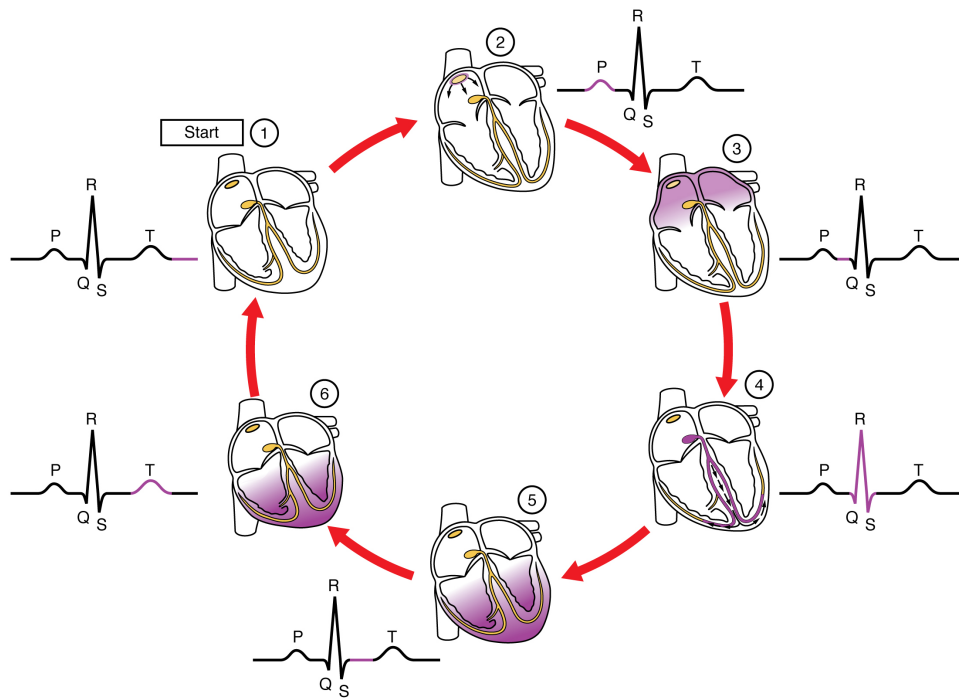
Figure 2.5: An electrocardiogram trace with the synchronized timing of the heart sounds as well as the periods for which the heart valves are open and closed (Telleen, 2013).

2.5 Previous research

The Biomedical Research Group of Stellenbosch University has conducted much research into analyzing heart sounds and murmurs for automatic diagnostic systems. Visagie (2007) and Botha (2010) created prototypes which could automatically gather the sounds generated by the heart and lungs. Visagie (2007) designed a jacket with built-in microphones and an ECG which recorded the participant's heart sounds and subsequently classified the signals using neural networks. Botha (2010) continued with this project, using his own version of the wearable device with built-in stethoscopes to record heart sounds. Both of these projects produced systems which could discriminate between normal and abnormal heart sounds with relative accuracy. The current work will differ from Botha (2010) and Visagie (2007)'s work as it focuses on the LDV and its ability to be used as part of an autonomous diagnostic system. Commonly used signal processing and classification techniques will be discussed in the following sections. A brief overview of the LDV as a biomedical sensor will also be presented.

2.5.1 Signal processing techniques

Both the time and frequency domain of a biological signal can provide useful information for analysis. Time domain analysis of the phonocardiogram has included the use of synchronized envelope averaging (Karpman *et al.*, 1975; Beyar *et al.*, 1984) to improve the signal to noise ratio of the recorded heart sounds. The four heart sounds have been detected by using both an envelope generated from the Hilbert-Huang transformation of the signal (Xu *et al.*, 2010) and the normalized average Shannon energy (Liang *et al.*, 1997).

Frequency domain information extracted from time domain signals such as phonocardiograms are often used for a variety of applications. Older techniques are often re-visited and improved on (such as zero crossing analysis (Grillo *et al.*, 2012) and bandpass filter banks (Ricke *et al.*, 2005)). The fast Fourier transform (FFT) has been extensively used to investigate the frequency spectrum of the heart sounds (Yoganathan *et al.*, 1976*b*,*a*), and the short time Fourier transform (STFT) has been used to classify normal and abnormal heart sounds when combined with artificial neural networks (Mokhlessi *et al.*, 2011).

Signal analysis can be used to gather parameters from the recorded data and create a model of the underlying system, or the signal can be decomposed, revealing the components from which the signal is composed of. The empirical mode decomposition (EMD), breaks down the observed signal to its frequency modes, called intrinsic mode functions (IMFs) (Wu and Huang, 2009). The ensemble empirical mode decomposition (EEMD) proposed by Wu and Huang (2009) improves on the EMD method by making it more robust to noisy signals, a process explained in Section 4.2.3. EEMD analysis has been proven to be useful across a wide range of applications, such as noise reduction in seismic signals (Chen *et al.*, 2012) and the removal of artifacts introduced in signals recorded in unstable environments such as ambulances (Sweeney *et al.*, 2012).

Nigam and Priemer (2005) proposed a segmentation method which calculates coefficients corresponding to the signal's complexity. They found that S1 and S2 are less complex compared to murmurs and found it possible to segment the signal accordingly. They report that the simplicity based method gives better results than those achieved by frequency and amplitude methods.

Heart sounds are considered to be non-stationary signals from a statistical perspective and are therefore best analyzed by a combination of time and frequency domain techniques (Daliman and Sha'ameri, 2003). They investigated the S-transform as a method to distinguish between the opening snap of the mitral valve, which is observed very close to S2, and S3 which also occurs shortly after S2. (Livanos *et al.*, 2000) reported that the S-transform gave better results than the continuous wavelet transform and the STFT. Wavelet analysis has rapidly replaced the traditional Fourier analysis techniques for heart sounds.

2.5.2 Classification

To classify objects into different groups, called classes, various distinguishing features of each class must be identified. Automated classification is the process in which content is divided into classes using numerical techniques. This process requires that the raw data be represented by a set of compact and relevant features. Amit (2009) listed potential domain-specific features such as the dominant frequency of a signal's spectrum, the bandwidth of the dominant frequencies, mean and total spectral energy, and the intensity ratio of S1 and S2. Amit also notes the use of model-based analysis, where the parameters of the model are a natural feature set, such as the coefficients of a 12-order all pole model. Bentley *et al.* (1998) created a search scheme which found the optimal feature set for the recorded data.

Popular classification schemes include artificial neural networks (ANN), support vector machines (SVM) (Kumar *et al.*, 2010) and k-nearest neighbor classifiers (KNN) (Kofman *et al.*, 2012). ANNs have been explored extensively for the automatic diagnosis of heart sounds. ANN classifiers are capable of classifying complex non-linear data sets (Wisconsin-Madison, 2007). Visagie (2007) trained a feed-forward network and reported a sensitivity of 85.7% and specificity of 94.1% to differentiate between normal and abnormal patients. Botha (2010) used an ensemble of neural networks to classify heart sounds. This approach combines the individual outputs of each of the individual networks to ultimately assign a classification to a data point.Botha (2010) reported a sensitivity rating of 82% and a specificity rating of 88%. While ANN is well suited for classifying large sets of data, there are some limitations for its use. Backpropagation networks, for example, are considered to be 'black boxes' with very little input from the user as the network learns on its own. ANN can be computationally expensive with larger sets of data. With a small set of data, ANN can overfit the data, which would mean the classification results would be biased and therefore meaningless (Wisconsin-Madison, 2007).

SVM classifiers mathematically transform data to a multi-dimentional space and use a hyperplane to separate the data. By definition SVMs are limited to only separating two classes of data at a time. The computation time for a SVM is quadratic, meaning that a data set twice as large will take four times as long to train, which could become a restriction with large data sets. The optimal choice of a kernel for the SVM is still an open research question, and can be suceptible to overfitting data (Noble, 2006).

In contrast to ANN, KNN classifiers are uncomplicated systems which are computationally inexpensive in low dimensions. In higher dimension systems, a number of methods have been proposed which could be implemented to speed up the nearest neighbour retrieval (Cunningham and Delany, 2007). KNN classifiers require no complicated parameter choices apart from choosing the value of K, the number of neighbours to consider. KNN classifiers are very robust as they are completely

data driven. They are also well suited for multi-class classification. Singh *et al.* (2002) used a K = 2 KNN classifier to identify different prostate examples, and reported a 90% accuracy using leave-one-out cross validation.

2.5.3 The laser Doppler vibrometer as a biomedical sensor

Several authors have used the LDV to measure vibration within the human body. Wang *et al.* (2007) performed an experimental study using a pulsed laser vibrometer to monitor vital signs using any surface on the body. They found that they could monitor vital signs successfully even while the subject was wearing clothing, thereby eliminating the need for exposed skin. Scire (2010) proposed a compact and lightweight LDV stethoscope which would be used in noisy spacecraft environments. The stethoscope would use the LDV principle to detect the movement of a membrane stretched across the bell-end of the housing and a microphone would record the ambient noise. The prototype was tested on volunteers and showed good performance at noise levels where both the conventional and electronic stethoscopes were no longer effective. Scalise *et al.* (2004) is currently researching the LDV as a tool for evaluating the design and quality control of mechanical heart valves. Because it does not require contact, the LDV could test the heart valves in vitro by using an ad-hock experimental setup which mimics the circulatory system. Researchers affiliated with the Polytechnic University of Marche (PUM) have been studying the LDV as a biomedical sensor. One branch of their research is the use of the LDV as an auscultation device. PUM have tested the LDV as a suitable alternative to an ECG (Umberto *et al.*, 2007) and also compared the LDV to the phonocardiogram (De Melis *et al.*, 2007). They found that they could calculate heart rate variability (HRV) indicators with the LDV data. The indicators proved to be very accurate when compared to those calculated with the data from the ECG, the golden standard for HRV calculations. They could also identify deflections in the recorded LDV signal which corresponded to the heart sounds as well as the closure of the heart valves.

The LDV also sees use in other biomedical areas. Avargel and Cohen (2011) used a LDV to measure low frequency speech. By combining a LDV with a microphone, an improvement in the signal to noise ratio was reported. Rosowski *et al.* (2008) used a laser vibrometer to investigate the relationship between hearing loss and the measured velocity of the tympanic membrane in the middle ear. Results indicated that it is possible to identify the presence of abnormalities. A laser vibrometer has also been used to measure skin tissue's viscoelastic material properties. Force was applied to the skin with a mechanical shaker and then the skin's surface vibrations were measured with the laser vibrometer and analyzed using a surface wave method (Zhang *et al.*, 2008).

2.5.4 Comparing the present study with previous research

Botha (2010) and Visagie (2007) classified heart sounds as either normal or abnormal. They used data from a stethoscope array built into auscultation devices which could be worn by participants. The current project will characterize the performance of the LDV as an auscultation device, and attempt to classify the recorded signals into their various underlying pathology classes.

Researchers at PUM tested the LDV as a replacement for the ECG (Umberto *et al.*, 2007) and have compared it to the phonocardiogram (De Melis *et al.*, 2007). The current study will be testing the LDV as an aid to the ECG and as a replacement of the stethoscope and resulting phonocardiogram. Scalise *et al.* (2008) showed that the LDV can successfully be used to monitor vital signs (such as HR, HRV, pulse transit time and respiration rate). No examples of LDV classification could be found in the literature.

2.6 Chapter summary

The cardiology system and the resulting heart sounds and their auscultation was briefly described. The characteristic ECG waveform was described in terms of the underlying heart function. Previous research which related to the current work was discussed and a comparison was made to the current work and the work completed by the previous students within the author's own research group. No example of heart sound classification with a LDV could be found in the literature.

Chapter 3

Hardware and data acquisition

3.1 Introduction

In this chapter the process of acquiring data is described. In Section 3.2 the main components of the measurement system are outlined where necessary. Specification sheets for the components are provided in Appendix A. Section 3.3 provides an overview of the clinical study undertaken to gather participant data for analysis, feature extraction and classification.

3.2 Hardware and data acquisition

The LDV, stethoscope, PA and ECG simultaneously record data from the participant. These sensors, along with the data acquisition system (DAQ) were mounted on a specifically designed mobile frame, shown in Figure 3.1. The connections between the sensors and their respective signal conditioners and DAQ are shown in Figure 3.2. In subsequent subsections, each sensor is briefly discussed. Consult Appendix A for data sheets where applicable.

3.2.1 Laser Doppler vibrometer

The LDV used in this study is the VibroMet Model 500V, single-point measurement system, shown in Figure 3.3. It is classified as a class 3B laser, which requires protective eye wear to prevent ocular harm. In the interest of safety, protective eye wear was provided to all participants during the recording process and no persons were allowed in the recording room without protective eye wear.

Figure 3.1 shows the LDV mounted at the top of the test frame, pointing downwards, with the laser beam orientated perpendicularly to the patient's chest wall. In this orientation, the LDV outputs a velocity profile representing the vibrations of the chest wall in the vertical axis. To improve signal quality and reduce the
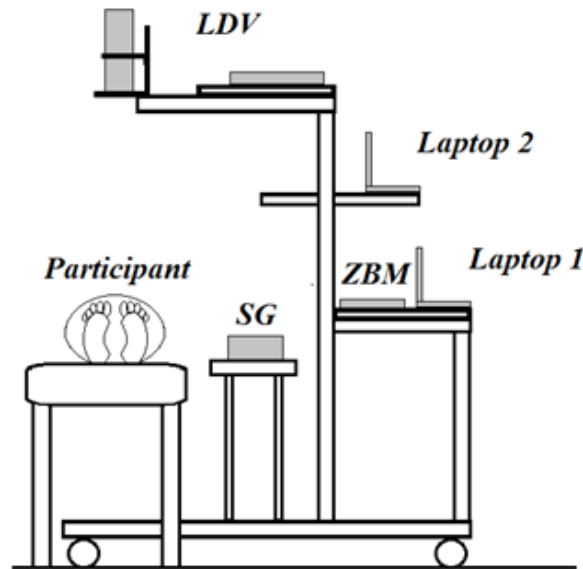
Figure 3.1: The test frame setup showing the positions of the data acquisition units and sensors relative to the participant. The laser Doppler vibrometer (LDV) is mounted with the laser beam perpendicular to the participant's chest. Laptop 1 controls the ECG data acquisition and Laptop 2 controls the stethoscope and accelerometer (not shown) data acquisition from the ZonicBook Medallion (ZBM). The signal generator (SG) is used to synchronize the data from the two laptops during post-processing.

occurrence of signal drop-outs, described in Section 4.2.1, a small white sticker was attached to the participant's chest. Umberto *et al.* (2007) stated that it was possible to record vibrations from the skin directly, but in this study a white surface gave consistent results which were not affected by the participant's skin colour or condition.

3.2.2 Stethoscope

The stethoscope used in this work is a back electret microphone (Panasonic W-61A) with a sensitivity of 35±4 dB and a frequency range of 20 to 20000 Hz (see Appendix A). The microphone is mounted in a plastic housing which was designed by Minai (unpublished) and manufactured by the Stellenbosch University mechanical workshop.

The output of the microphone is amplified by custom-built amplification circuitry for the current project before being sent to the DAQ. The schematic of the circuit board used for the stethoscope is shown in Figure 3.4. The stethoscope was attached to the participant with adhesive tape during testing.
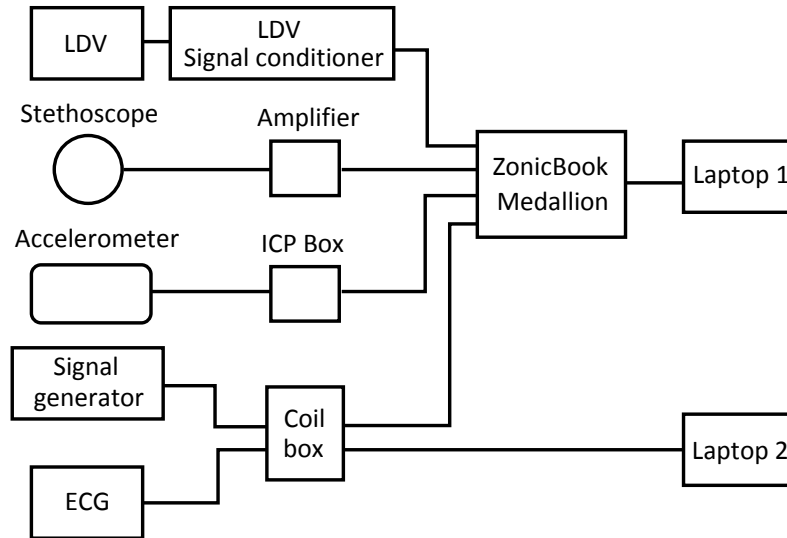
Figure 3.2: The connections between the sensors, synchronization equipment and data acquisition units.

The original stethoscope was destroyed by another student shortly before the clinical trials began. During the trials, it was discovered that the new stethoscope batteries were depleted at a far more rapid rate than anticipated. Once the battery voltage dropped below a certain threshold, recordings became unreliable, resulting in the periodic unavailability of stethoscope data during the clinical trials. As a consequence, usable stethoscope data was only obtained for a small number of participants.

3.2.3 Piezoelectric accelerometer

The model 352A24 piezoelectric accelerometer from PCB Piezotronics was used in the current work. It is a miniature, lightweight ICP ceramic shear accelerometer with a sensitivity of 100 mV/g and a 5% frequency range of 1 to 8000 Hz (see Appendix A). It is powered by an ICP power supply from PCB Piezotronics (PCB Piezotronics, 2012), as shown in Figure 3.5. The accelerometer was attached to the patient with an ECG sticker.

Figure 3.3: The MetroLaser Inc. Laser Doppler Vibrometer 500V used in the study. By directing the laser beam at the participant's chest wall, a velocity profile related to the underlying mechanics of the heart can be detected (MetroLaser Inc., 2010).
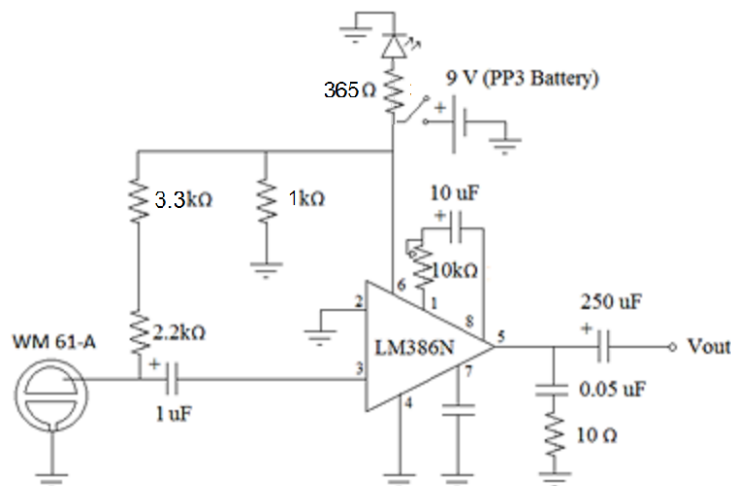
Figure 3.4: The wiring schematic of the electronic stethoscope used in the study. The output from the microphone is amplified by an LM386 audio amplifier before being passed into the data acquisition unit.

3.2.4   ECG

A full 12 lead ECG, the 1200 HR PCECG from Norav Medical, was used to record the ECG data. It was connected to Laptop 2 via a USB interface (Figure 3.6). Unfortunately, the proprietary Norav Medical RestECG software used to record the ECG data only allowed 10 seconds of ECG data to be recorded at a time.

ECG data is commonly used for very accurate segmentation of signals into heart
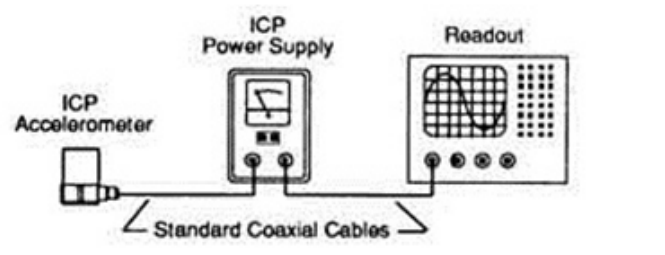
Figure 3.5: The model 352A24 piezoelectric accelerometer connected to an ICP power supply as used in the study (PCB Piezotronics, 2012).

sound cycles. Since the ECG was recorded on Laptop 2 and the rest of the sensors were recorded through a DAQ, the ECG and DAQ signals had to be synchronized. This process is described in Section 3.2.5.

Figure 3.6: The Norav Medical 1200HR Electrocardiogram used in the study (Norav Medical Inc., 2011).

3.2.5 The coil box

The ECG data and the data recorded by the DAQ had to be synchronized so that the data could be segmented into individual heart sounds (described in Section 4.3). Synchronization was accomplished by adding an electronic artifact to both the ECG and ZonicBook's data. The chosen artifact was a sinusoidal signal as it would be easy to identify during post-processing and could be generated with readily-available equipment. Figure 3.7 shows the connections of the coil box relating to the ECG.
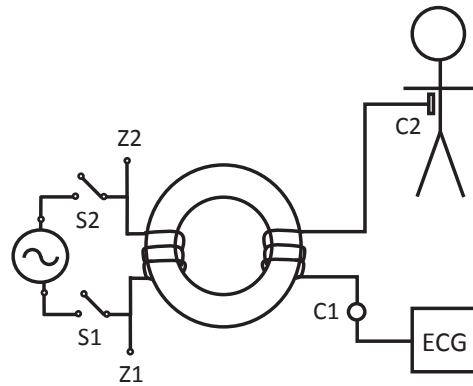
Figure 3.7: The coil box which was used to synchronize the ECG and ZonicBook data. It added a sinusoidal artifact to one of the input leads of the ECG and was one of the inputs for the ZonicBook. The sinusoidal waves were then aligned during post-processing.

A signal generator outputting a 20 Hz sinusoidal signal was used to produce the artifact signal. The output from the signal generator was sent directly to the ZonicBook (Z1 and Z2 on Figure 3.7), but exceeded the maximum voltage which could be input on the ECG and so had to be de-amplified. An iron core torus was used as a transformer to ramp down the voltage from the signal generator. A connecting lead was attached between the ECG sticker and its original lead (Figure 3.7). The connecting lead was looped through the torus and then attached to the relevant ECG lead. A switch (S1 and S2 on Figure 3.7) was used to start and stop the artifact signal.

3.2.6   DAQ systems

The ZonicBook Medallion from IOtech was used as the DAQ (see Figure 3.8). The stethoscope, piezoelectric accelerometer, LDV and one output from the coil box (see Section 3.2.5) were connected to the ZonicBook unit. The ZonicBook was connected to Laptop 1 shown in Figure 3.1. The ECG and second output of the coil box are connected to Laptop 2 as labeled in Figure 3.2. The ZonicBook is equipped with a built-in 80 dB anti-aliasing filters for each of its channels. Most heart sounds fall well below 2kHz frequency range. The Nyquist theorem states that the minimum sampling frequency for a signal should be twice that of the maximum frequency component of the signal, therefore 5120 Hz is adequate to capture heart sound data. The ZonicBook was thus set to a sampling frequency of 5120 Hz.
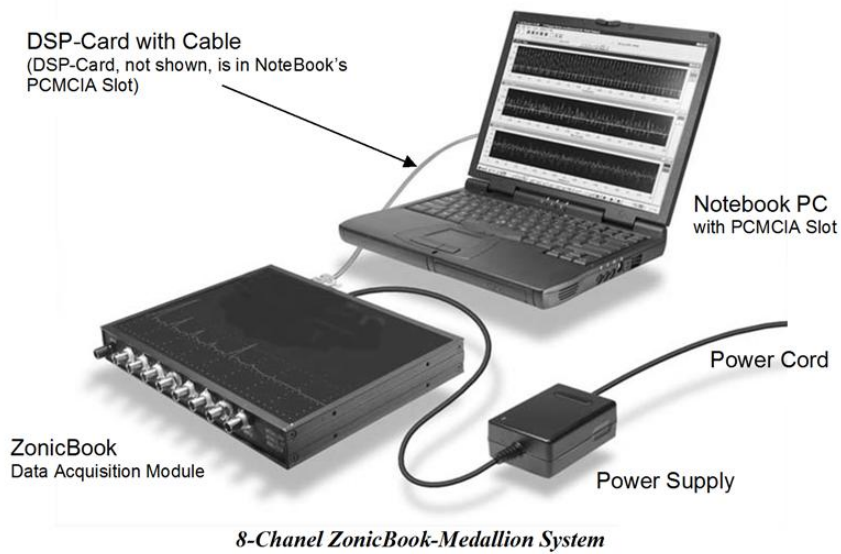
Figure 3.8: The IOtech ZonicBook Medallion data acquisition unit used in the study (IOtech, 2001).

3.3 Clinical study

The participants were recorded at Tygerberg hospital and consisted of patients from the cardiology clinic, students from Stellenbosch University and the general public. The inclusion criteria were as follows: the participants had to have been for an echocardiogram within the last year and they were to have a heart murmur and no prosthetic valve, or a normal heart. All participants were auscultated by a cardiologist from Tygerberg Hospital to confirm that they were suitable for the study. For each participant, the cardiologists completed a diagnostic sheet, shown in Appendix B, indicating their diagnosis. They then checked their diagnosis against the echocardiogram.

Each participant read and completed the consent forms provided and the participant's age and gender was recorded for statistical analysis. The English version of the form is included in Appendix B. Medical staff and other patients translated the document for those participants who did not speak Afrikaans or English and fingerprints were used in the cases where participants could not sign their own name.

Stethoscope recordings were taken at the four main auscultation sites as indicated in Figure 3.9. The accelerometer was alternated between the two main positions for seismocardiography, the sternum (Xu *et al.*, 1996) as well as the apex of the heart (Phan *et al.*, 2008), as shown in Figure 3.9. The LDV's position was
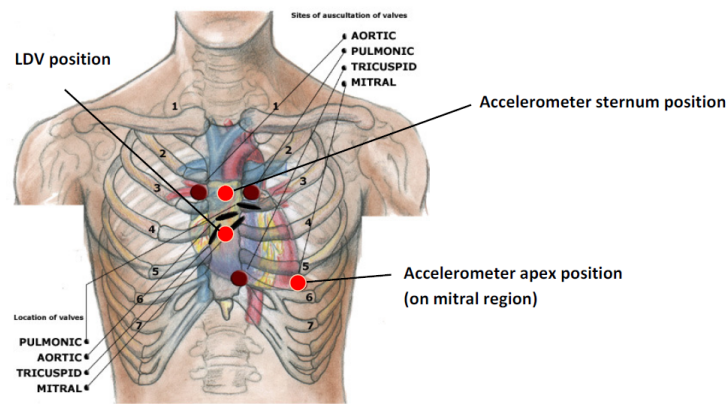
Figure 3.9: In this figure, the four auscultation sites used for the stethoscope recordings are shown. Additionally, the recording position of the laser Doppler vibrometer and the two sites used for recording the accelerometer data are indicated (Stethographics, 2012).

taken from the work of Umberto *et al.* (2007) and De Melis *et al.* (2007). Multiple recordings were made at each position to ensure sufficient data would be available for processing. Some participants were obese and uncomfortable or had bad circulation and so could not remain motionless for the duration of the test. Data with excessive noise and major artifacts caused by patient movement, as determined by visual inspection, were discarded.

A total of 20 patients were recorded, 17 abnormal and 3 normal. Table 3.1 shows the gender, age, diagnosis and cardiologist's notes for each participant. Table 3.2 shows the occurrences of the abnormal pathologies recorded. The number of participants recorded was sufficient to test the feasibility of the current work. Additional participants would enable more statistically significant conclusions to be made.

3.4 Chapter summary

The hardware used in the current work as well as the configuration of the recording setup was discussed. The participants and recording procedure used in the clinical study were described. In Chapter 4, the denoising of the data recorded with the experimental setup is discussed

Table 3.1: Patient data and diagnosis summary

PAT	Gender	Age	Diagnosis	Notes
1	F	36	AS and MR	Split S2
2	F	43	AS and MR	
3	F	71	AS	Split S2
4	F	38	AS	
5	F	37	MR	Tachycardic
6	F	32	MS and MR	Split S2, audible opening snap
7	F	83	AS	Severe AS, peaks late
8	F	34	MS	
9	M	57	Normal	
10	M	25	Normal	
11	F	35	VSD	Doctor diagnosis: PS
12	F	30	AS	Mild AS
13	M	60	HOCM	
14	M	26	MS	With pulmonary hypotention
15	F	47	MS and MR	Moderate MS and mild MR
16	M	40	MR, AR, PS, PR and PHT	Moderate MR, AR, PS, severe PR, PHT
17	F	80	MR	
18	M	61	AS	
19	F	49	AS and AR	Severe AS, moderate AR
20	M	65	Normal	

Table 3.2: The occurrences of abnormal pathologies

Pathology	Number of participants
MR	2
MS	2
AS	5
AS and MR	2
MS and MR	2
AS and AR	1
HOCM	1
VSD	1

Chapter 4

Signal processing

4.1 Introduction

In this chapter the denoising and processing of data gathered by the experimental setup described in Chapter 3 is discussed. The denoising and segmentation process is summarized in Figure 4.1. Three series of participant data were collected from both laptops and processed in MATLAB: sensor outputs, synchronization data and ECG data. The LDV, PA and stethoscope were recorded with the ZonicBook Medallion DAQ, at a sampling rate of 5120 Hz. The ZonicBook was in turn connected to Laptop 1 shown in Figure 3.1 and controlled by the eZ Analyst software. eZ Analyst produced a text file which contained the time history data for each recording. The Norav Medical ECG had to be connected to Laptop 2 as Laptop 1 could not run both programs simultaneously. Norav Medical's RestECG software was used to record the ECG, at a sampling rate of 500 Hz. RestECG stored the data in a MATLAB format for later processing. The data from the two laptops had to be synchronized to perform segmentation as described in the Section 4.3. This was achieved electronically with a third system (the "coil box" discussed in Section 3.2.5) which was connected to each DAQ

4.2 Denoising the recorded signals

The denoising process for the stethoscope and accelerometer data started with the removal of signal dropouts and the splitting of data into two streams. Stream 1 was passed through a 4th order BP Butterworth filter with high and low cut-off frequencies of 15 Hz and 700 Hz respectively (Safara *et al.*, 2012) as this is the range in which heart sounds commonly occur. This produces a wave form similar to a phonocardiogram (De Melis *et al.*, 2007). Stream 2 was passed through a low-pass Butterworth filter which provides a detailed velocity profile of the chest wall (Umberto *et al.*, 2007). Examples of Stream 1 and Stream 2 data are plotted
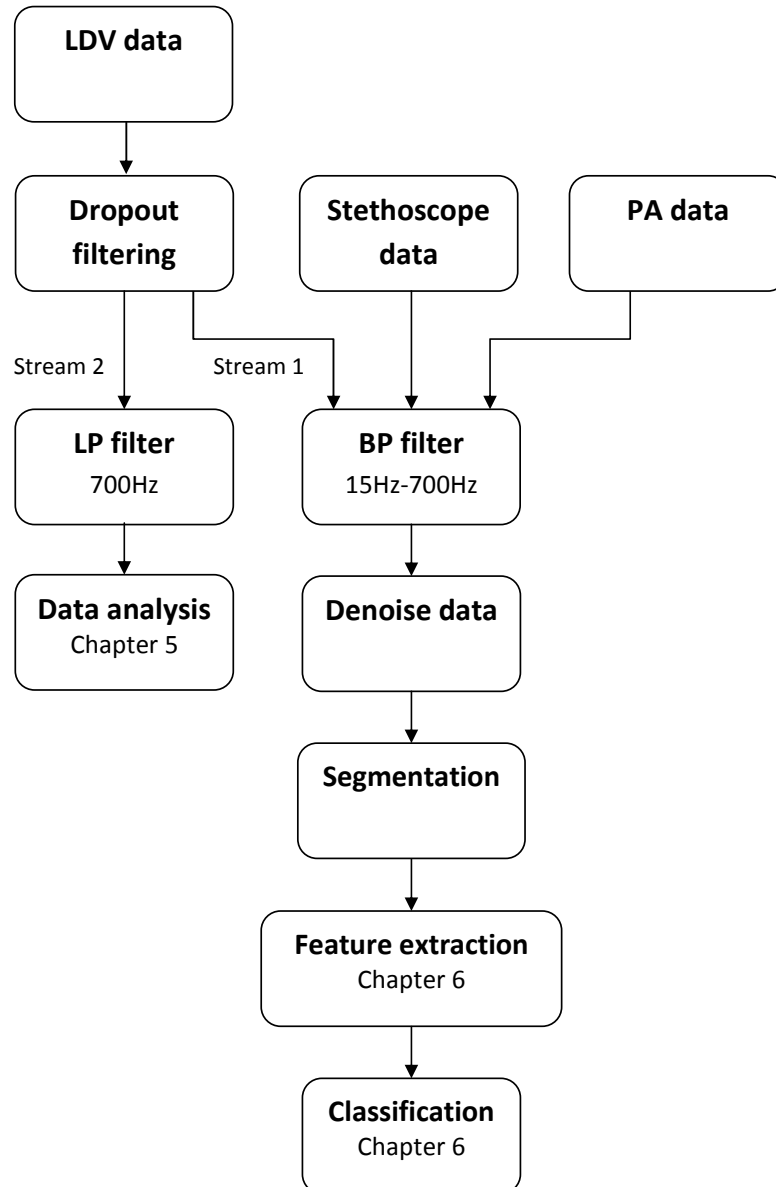
Figure 4.1: The flow of data as the signals are processed and segmented. Signal dropouts are removed from the recorded LDV data, where after the signals are filtered and denoised. The denoised data are then segmented and analyzed in Chapter 5 and Chapter 6.
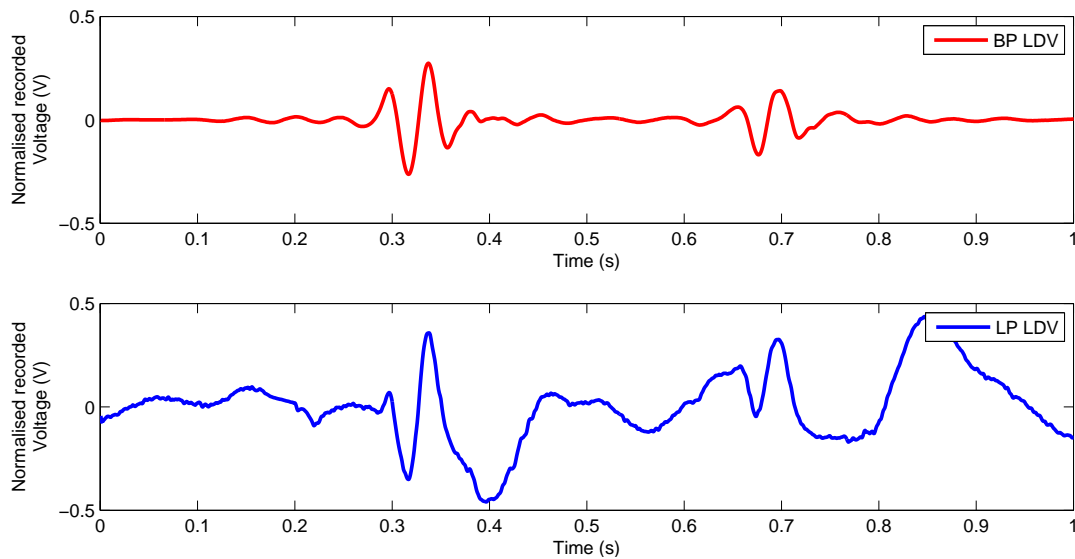
Figure 4.2: The velocity profile from the laser Doppler vibrometer data is filtered with a low-pass (LP) filter and compared to the same signal which has been filtered with a band-pass (BP) filter. The LP filtered data provides a velocity profile of the chest wall where the BP filtered data is visually very similar to a phonocardiogram.

in Figure 4.2. The LDV BP signal, stethoscope and accelerometer data were also further denoised using multi-resolution wavelet analysis, described in Section 4.2.2.

4.2.1   Laser dropouts

A typical example of LDV output is shown in Figure 4.3. The laser beam's recorded amplitude varies with the physical properties of the measured surface. When many wavelengths are observed (an "optically rough" surface) the measurement is described as granular and creates an effect referred to as speckle noise (Gatzwiller *et al.*, 2002). The LDV's demodulation unit requires the amplitude of the returned Doppler signal to exceed a minimum threshold value for the unit to derive an analogue velocity waveform. Speckle noise creates an amplitude variation in the Doppler signal. In the event that the amplitude of the Doppler signal falls below the minimum required value, the velocity waveform cannot be derived and a dropout occurs (Gatzwiller *et al.*, 2002). The effect of speckle noise and dropping below the threshold value is shown in Figure 4.4.

Vanlanduit *et al.* (2002) developed a method for dealing with outliers in the study of a vibrating plate using a LDV. Their method involves detecting and rejecting outliers and then applying a global least-squares fit to the data to replace the missing values. The outliers detection and rejection technique described by Vanlanduit *et al.* (2002) was used in the current study.
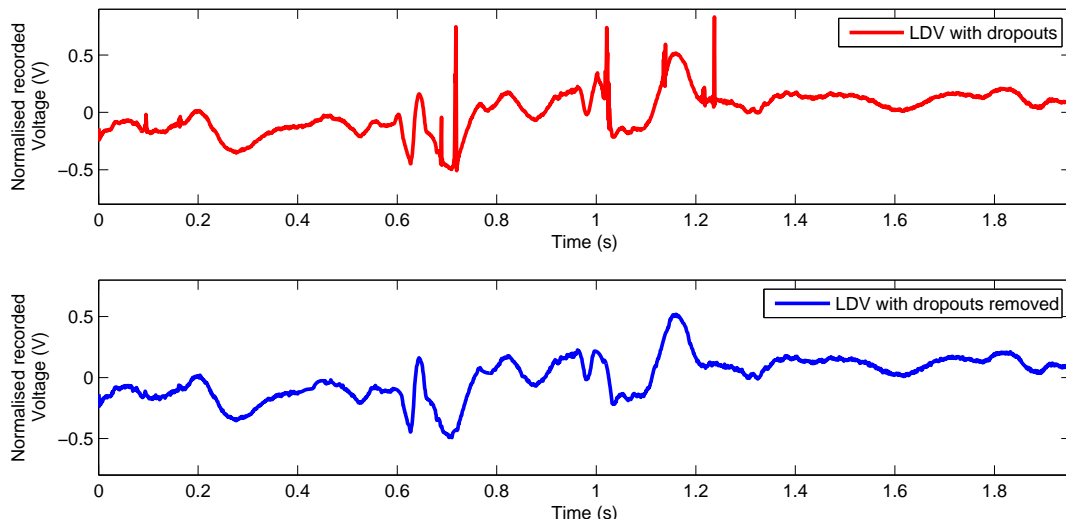
Figure 4.3: A segment of laser Doppler vibrometer signal before and after the dropouts have been removed. Dropouts were removed by detecting outliers, deleting them and interpolating. This is discussed in Section 4.2.1.
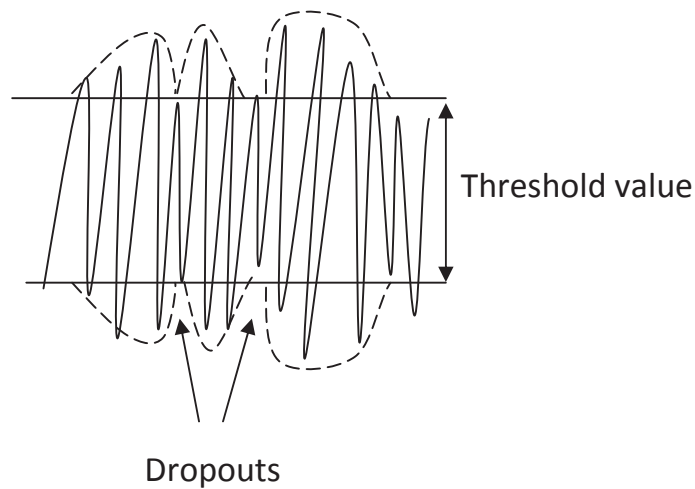
Figure 4.4: The strength of the signal observed by the laser Doppler vibrometer must be above a certain threshold value for the internal photo detector circuitry to function. An observed signal below this threshold produces a sharp fall in the recorded signal where it is labeled as a signal drop-out.

Data points corresponding to 0.1×MAD, where MAD is the median absolute deviation as calculated by Equation 4.1, were removed from the dataset and replaced by interpolated data points calculated with a piecewise cubic Hermite interpolation method. The algorithm to remove the laser dropouts was as follows:

1. Compute $\hat{x}$ by applying a 4th order one-dimensional median filter to the input data, x

2. Compute the median absolute deviation for the residual data $e = x - \hat{x}$ with the equation

$$\text{MAD(e)} = median(|e - median(e)|) \tag{4.1}$$

3. Compute the set of time samples (I) which are outliers and remove from x

$$I = \left\{ i \big| |e(i\delta t)| > 0.1 \times MAD \right\} \tag{4.2}$$

4. Fit a piecewise cubic Hermite interpolation curve to the remaining data points

5. Use the interpolator to resample the removed data points and add to $\hat{x}$

Figure 4.3 shows a section of data before and after the dropouts were removed. It is clear that the algorithm effectively removes the dropouts found in the data. Factors which could reduce the occurrence of dropouts are discussed in Section 7.4.2.

4.2.2 Wavelet analysis

Wavelet analysis is the process of expanding a function in terms of basis functions known as wavelets. These wavelets are translated and scaled versions of the mother wavelet, which is a fixed function (Antoniak, 2011). An example of a mother wavelet and corresponding wavelets is shown in Figure 4.5. As part of wavelet analysis, the signals are decomposed into wavelet coefficients and a threshold parameter determines which coefficients are used to reconstruct the signal. The band pass filtered LDV, stethoscope and accelerometer signals were all analyzed with wavelets.

The wavelet decomposition process is similar to the well known Fourier transform, which uses trigonometric polynomials to analyze and reconstruct the observed signal. The short-time Fourier transform has been shown to be less well suited to analyzing short pulse data as it assumes the small window of data it is analyzing is stationary. This is not the case for heart sounds which are brief, impulsive events, and are localized with respect to both time and frequency (Messer *et al.*, 2001). Murmurs can occur in various parts of the heart cycle and can vary slightly in their length and position within each patient's heart cycles. Wavelet analysis is therefore a good choice for reconstructing heart sounds as a close correlation can be achieved
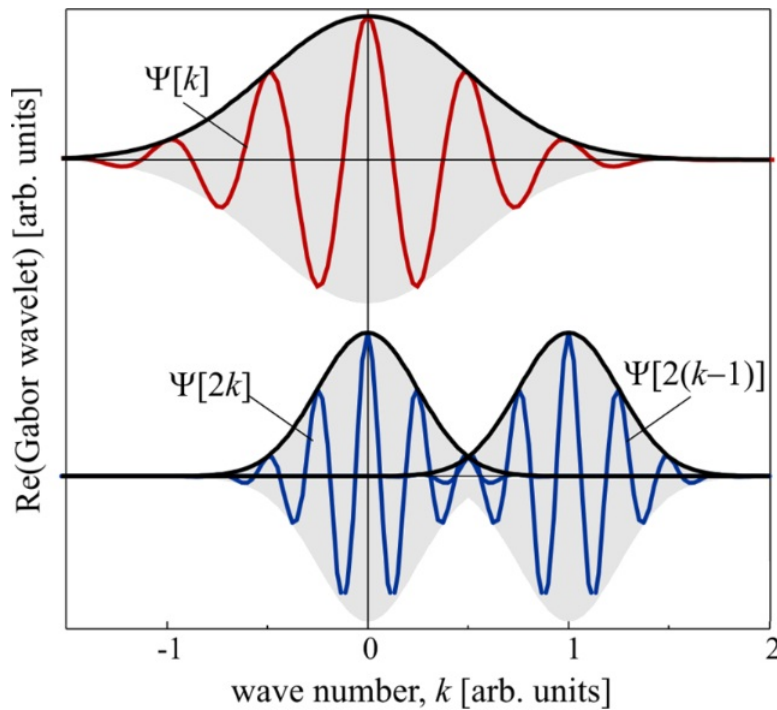
Figure 4.5: Wavelet denoising is the process where mother wavelets (red curve) are translated and dilated (blue curve) to form wavelets which are then added together to recreate the a denoised version of observed signal (Antoniak, 2011).

between the wavelet coefficients and the signal to be approximated. This ensures good numerical stability when the signal is reconstructed and subsequently manipulated, and makes wavelets very useful for non-stationary processing (Lee and Yamamoto, 1994; Unser and Aldroubi, 1996).

Daubechies 7 (db7) wavelets, at decomposition level 7, from the wavelet toolbox in Matlab were used to denoise the data. Figures 4.6a and 4.6b shows examples of wavelet denoised LDV and stethoscope data, respectively. The data has been visibly smoothed for both waveforms.

4.2.3   Ensemble empirical mode decomposition

The Hilbert Huang transform (HHT) is commonly used to analyze the instantaneous frequency components of non-stationary and nonlinear data. The empirical mode decomposition (EMD) breaks down a signal into time-energy distribution functions which are called intrinsic mode functions (IMF). By applying the HHT to each IMF, the instantaneous frequencies present in the signal can be computed. Cho and Yejin (2013) calculate the IMFs as follows:
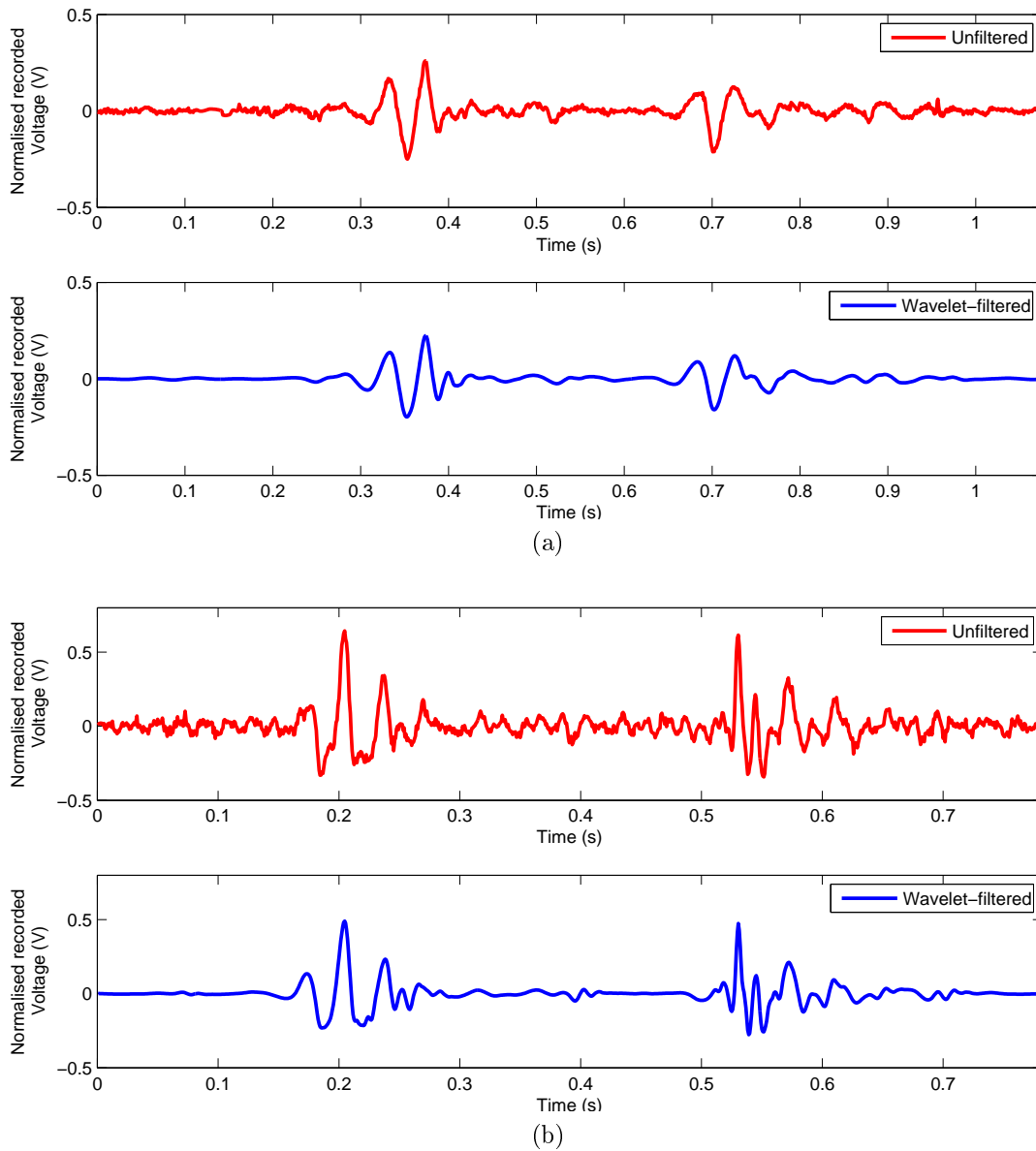
Figure 4.6: a) laser Doppler vibrometer and b) stethoscope signal before and after wavelet filtering. The resulting signal has been visibly smoothed.

1. Set $x(t)$ as the initial signal

2. Set the number of IMFs to be extracted as $\log_2(N)$ where N is the number of data points in $x(t)$. Fix the number of iterations at $i = 10$ per sifting cycle

3. Calculate a single IMF

   a) Find the extrema for $x(t)$

   b) Fit separate cubic splines to the maximum and minimum extrema, creating an upper and lower envelope for $x(t)$

   c) Calculate the mean of the two envelopes, $m(t)$

   d) Set $x(t) = x(t)$ - $m(t)$

   e) Repeat 3.1-3.4 i times. On the ith repeat set $x(t)$ as the IMF

4. Repeat Step 3 with $x(t) = x(t)$ - IMF until $\log_2(N)$-1 IMFs have been calculated

5. Set the last $x(t)$ calculated as the residual, r

EMD is susceptible to the appearances of a feature called mode mixing, where more than one scale of the signal will appear on the same IMF or that the same scale will appear on various IMFs. The effects of mode mixing can be greatly reduced by using a modified version of the EMD called ensemble empirical mode decomposition (EEMD). EEMD adds Gaussian white noise to the original signal. In a sufficiently large ensemble, the added white noise will average to zero and only the underlying IMF will remain (Wu and Huang, 2009). The procedure to calculate the EEMD is as follows (Wu and Huang, 2009):

1. Add random white noise to the original signal

2. Extract IMFs from the noise-added data as per the EMD method

3. Pepeat Steps 1 and 2 with a different white noise series NE times, where NE is a sufficiently large number

4. Obtain the actual IMF by taking the mean of the ensemble of IMFs

The white noise series were chosen to have an amplitude calculated as N_{std} x the standard deviation of the original heart sound signal, with $N_{std} = 0.1$ and NE = 1000 as based on work done by Botha (2010).

Figure 4.7 shows the full EEMD decomposition of the band pass filtered LDV signal of a single heart cycle for a normal patient. Figure 4.8 shows the full EEMD of the same cycle in the stethoscope signal. Every IMF is a single oscillatory mode
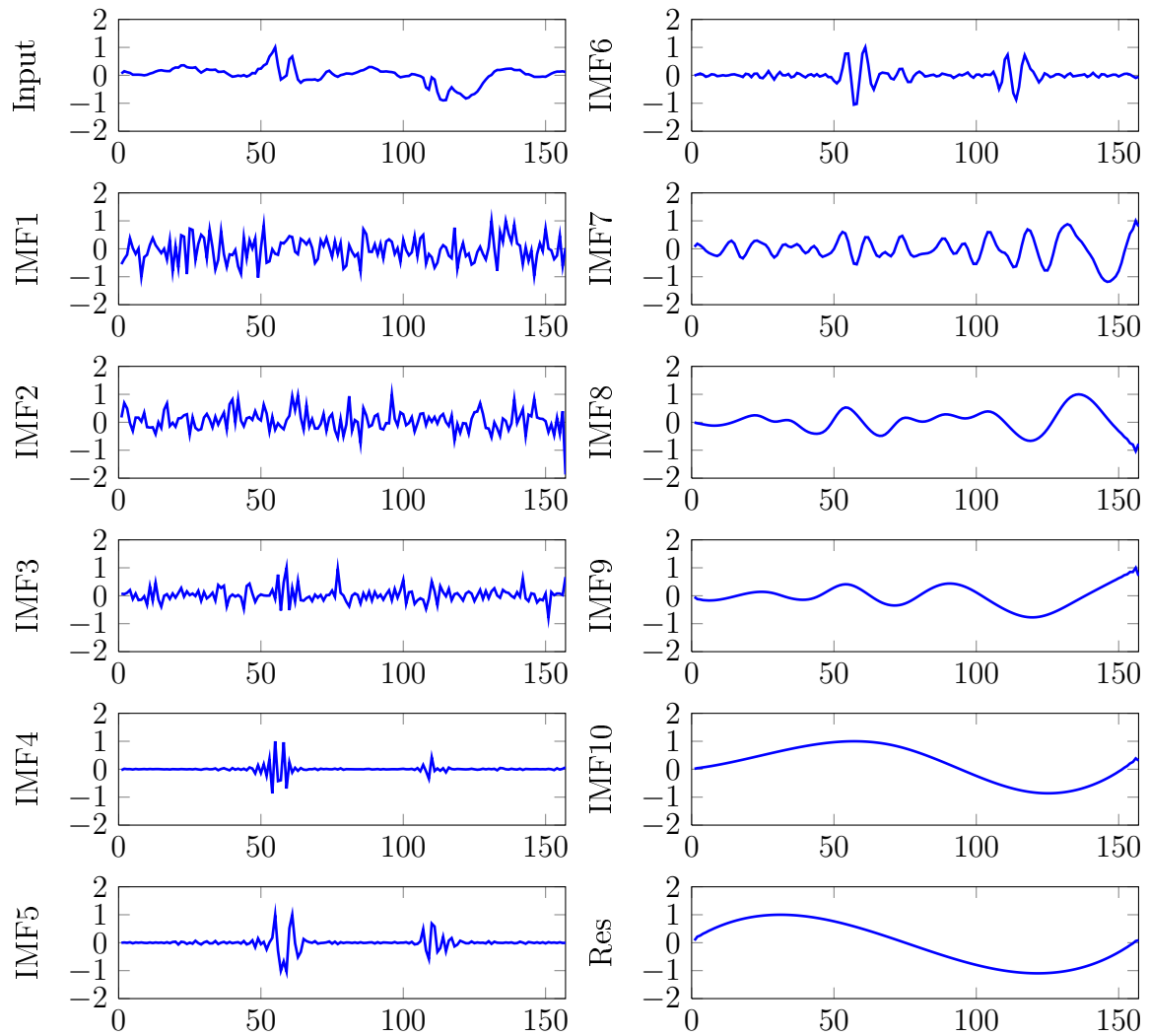
Figure 4.7: The full EEMD decomposition of a heart cycle recorded by the LDV. The IMFs become progressively less complex until $\log_2(N)$ IMFs are reached. The residual function is shown as Res.

within the original signal. The IMF shapes become less complex as the mean of the signal's envelopes becomes more intricate with each fitted envelope mean.

In this work, EEMD was originally explored as a method for feature extraction, however it was observed that signals which were decomposed using EEMD and then reconstituted were further denoised. This is to be expected as the EEMD decomposition involves the reconstruction of the denoised signal from a finite number of modes, the most significant of which will represent the signal, not noise. The denoising capability of the EEMD is confirmed by Agarwal and Tsoukalas (2007).
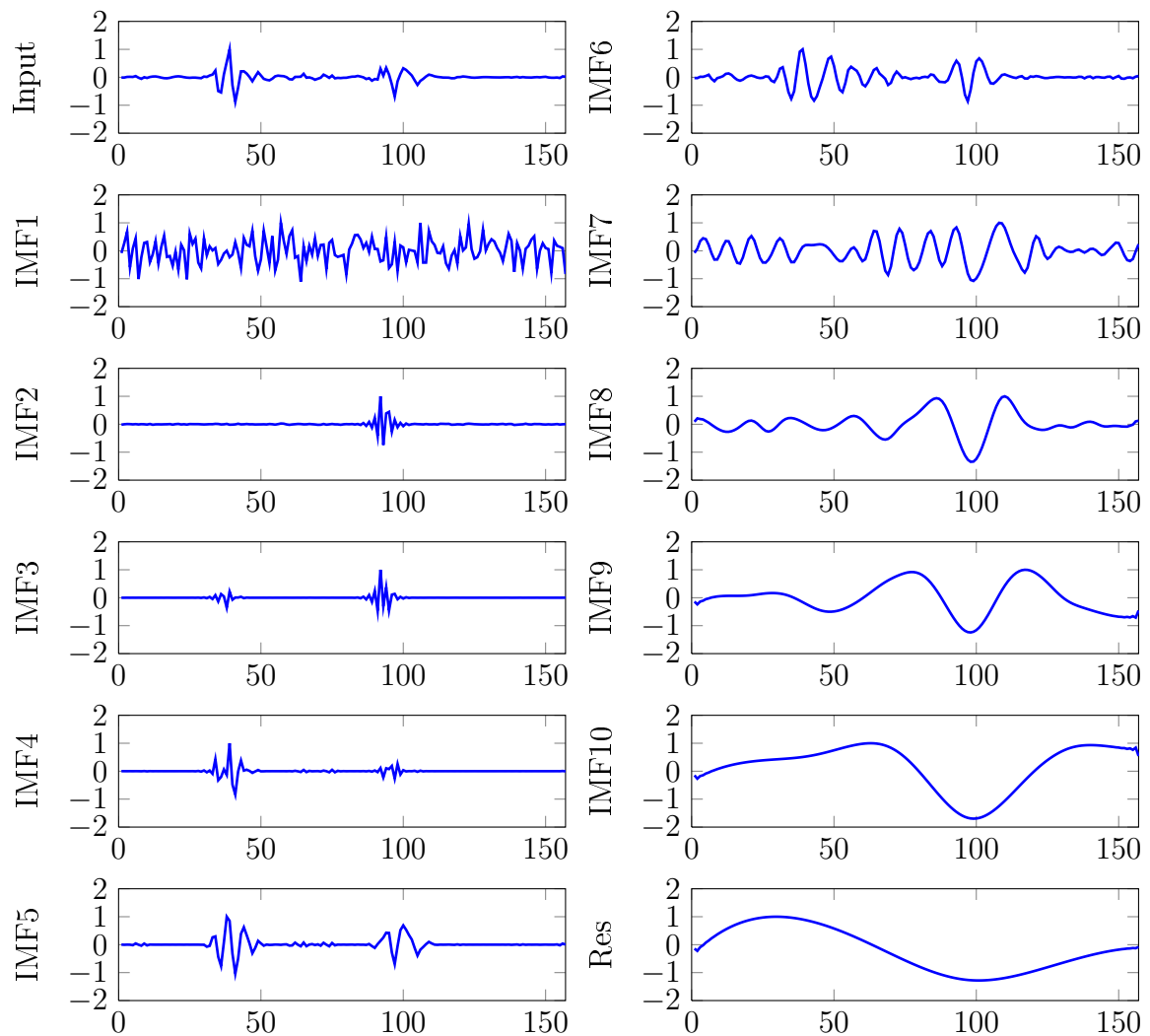
Figure 4.8: The full EEMD decomposition of a heart cycle recorded by the stethoscope. The IMFs become progressively less complex until $\log_2(N)$ IMFs are reached. The residual function is shown as Res.

There are interesting similarities in the LDV and stethoscope decomposed signals. For both signals, the heart sounds only become notable from the 4th IMF onward. For the LP Butterworth filtered LDV signal, a filtering process had to be chosen which would remove the noise without altering the subtle peaks within the signal. Studying the output of the EEMD analysis reveals that most of the noise in the data was captured in the first three IMF's. Reconstructing the data from the 4th IMF onwards produced a noise-free signal. The results of this procedure are shown in Figure 4.9.
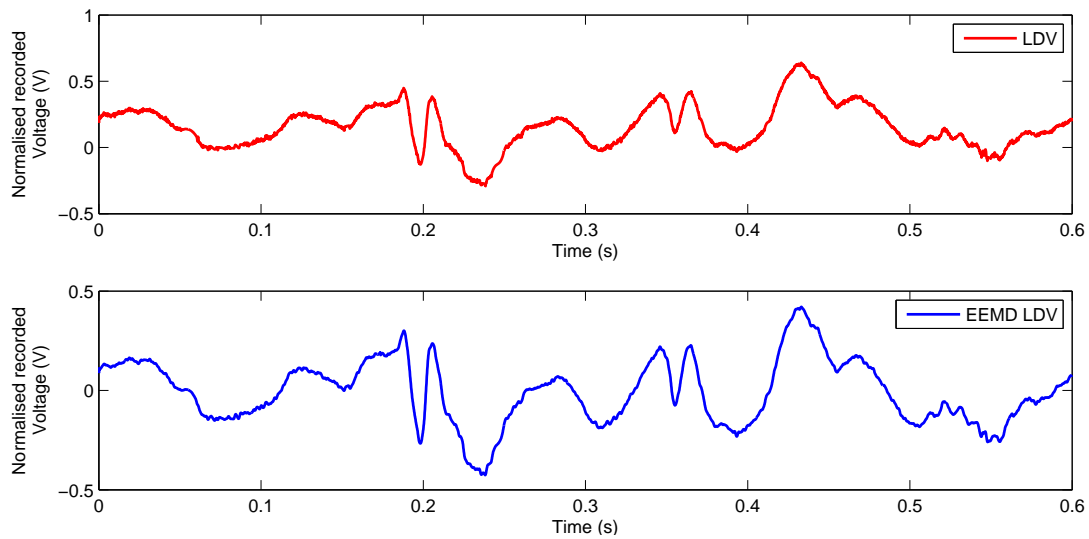
Figure 4.9: The laser Doppler vibrometer filtered by reconstruction of selected intrinsic mode functions. By selecting the less noisy IMFs for reconstruction, the signal is visibly reduced.

4.2.4   Overview of the denoising process

The denoising sequence creates two separate data streams. Stream 1 is the LDV, stethoscope and accelerometer data which has been filtered with a Butterworth band-pass filter, wavelet reconstruction and EEMD decomposition. Stream 2 is the LDV data which was filtered with a low-pass Butterworth filter and EEMD decomposition. The two streams are required by different methods of analysis: Stream 1 is used for feature extraction and classification and Stream 2 is used to characterize the LDV's velocity profile for various heart murmurs. The use of these streams is discussed further in Sections 5.2, 6.2, and 6.3.

4.3   Segmentation of the first and second heart sounds

Segmentation is the process whereby the recorded signal is divided into the systolic and diastolic components of each cycle so that time-specific features can be extracted for analysis and classification.

4.3.1   Complexity analysis

Segmentation is often accomplished using the ECG due to its simplicity and non-invasive nature (Burke and Nasor, 2002). The ECG used in this work, a model 1200-

HR from Norav medical, used the proprietary PC-ECG software which could only save up to 10 seconds of the recorded data at a time. The ZonicBook however could record far longer data series. A second segmentation method was implemented to segment the ZonicBook data where no corresponding ECG data was available. This method was based on using an eigenvalue spectrum (ES) technique as a method to gate a dynamic system, as outlined by Rezek and Roberts (1998). This method uses the complexity of a signal to create an envelope curve and was adopted by Nigam and Priemer (2005) for use with phonocardiogram data.

Visual inspection confirms that certain parts of a heart sound cycle appear much more structured than others. S1 and S2 are less complex than heart murmurs which are in turn less complex than the background noise between the murmurs and heart sounds and between the heart sounds. As a result the simplicity curve has a regular pattern. The intersection of the simplicity curve with a normalized threshold value can thus be used to identify the peaks which corresponded with the start of a new heart cycle. The simplicity curves for a normal and abnormal participant are shown in Figure 4.10.

Simplicity curves are calculated using an approach suggested by Nigam and Priemer (2005). Takens' theorem, known as the "method of delays", suggests that given a particular time series a (m,τ) data window should be visible for analyzing, where m elements are offset sequentially by τ. m is called the embedding dimension and τ is known as the embedding delay. The windowed data, transformed into an embedding matrix gives a good indication of the underlying dynamic system's complexity.

The signal, represented as $\mathbf{x} = \{x(k)\}, k = 1, \ldots, N$ is assumed to have a zero mean and be normalized so as to have unit variance. Set x_k to be a vector in space R^m, hereafter named the embedding space,

$$\mathbf{x_k} = [x(k), x(k+\tau), \ldots, x(k+\tau(m-1))]^T \tag{4.3}$$

With $\tau = T$, where T is a sample time increment, each $\mathbf{x_k}$ is created by moving the window one sample time increment on. Together, the $\mathbf{x_k}$ segments are used to construct a trajectory matrix where $P = N - (m-1)$

$$\mathbf{X} = \frac{1}{\sqrt{p}} \begin{bmatrix} \mathbf{x_1^T} \\ \mathbf{x_2^T} \\ \vdots \\ \mathbf{x_p^T} \end{bmatrix} \tag{4.4}$$

The embedding matrix is $\mathbf{X^T}$, the transpose of $\mathbf{X}$. According to Nigam and Priemer (2005), the eigenvalues, λ_k, of the correlation matrix $\mathbf{C} = \mathbf{XX^T}$ can be used to calculate H(i), a measure of entropy in the signal.

$$H(i) = -\sum_{k=1}^{m} \hat{\lambda}_k^i log\hat{\lambda}_k^i \text{ with } \hat{\lambda}_j^i = \frac{\lambda_j^i}{\sum_{k=1}^{m} \lambda_k^i}, j = 1, 2, \ldots, m \qquad (4.5)$$

The simplicity of the signal, S, is then given by

$$S = \frac{1}{\Omega^i}, \text{ where } \Omega^i = 2^{H(i)} \qquad (4.6)$$

Using Equations 4.3,4.4, 4.5 and 4.6 it is possible to calculate the simplicity curve with the following algorithm. Nigam and Priemer (2005) suggests m > 3 and fixes $\tau = 1$ and N = 50

1. Select suitable values for m and τ as well as an analyzing window of length N.

2. Align the window with the start of the signal

3. Iterate as follows: for $j = $ N:length(signal)

   a) Construct **X** over the windowed signal using Eq. 4.4

   b) Find the eigenvalues of $\mathbf{C} = \mathbf{XX^T}$

   c) Calculate $\mathbf{H_j}$ and $\mathbf{\Omega^i}$ using Eq. 4.5 and Eq. 4.6

   d) Calculate simplicity at time $j\tau$ by using Eq. 4.6

   e) Shift the analyzing window by one sample time increment and repeat steps a) to f)

An example of a calculated simplicity curve is shown for a normal and abnormal participant in Figures 4.10a and 4.10b respectively. Notice the peaks where the less complex S1 and S2 are prominent in the recorded data. The threshold value shown is discussed in Section 4.3.3.

4.3.2   ECG segmentation

Burke and Nasor (2002) published equations which were used to calculate the various segments on the ECG as illustrated in Figure 4.11.

$$T_{\text{P-wave}} = 0.57T_{\text{R-R}}^{1/2} - 0.33T_{\text{R-R}} - 0.14 \qquad (4.7)$$

$$T_{\text{P-Q segment}} = 0.56T_{\text{R-R}}^{1/2} - 0.33T_{\text{R-R}} - 0.17 \qquad (4.8)$$

$$T_{\text{P-Q interval}} = 1.12T_{\text{R-R}}^{1/2} - 0.65T_{\text{R-R}} - 0.31 \qquad (4.9)$$
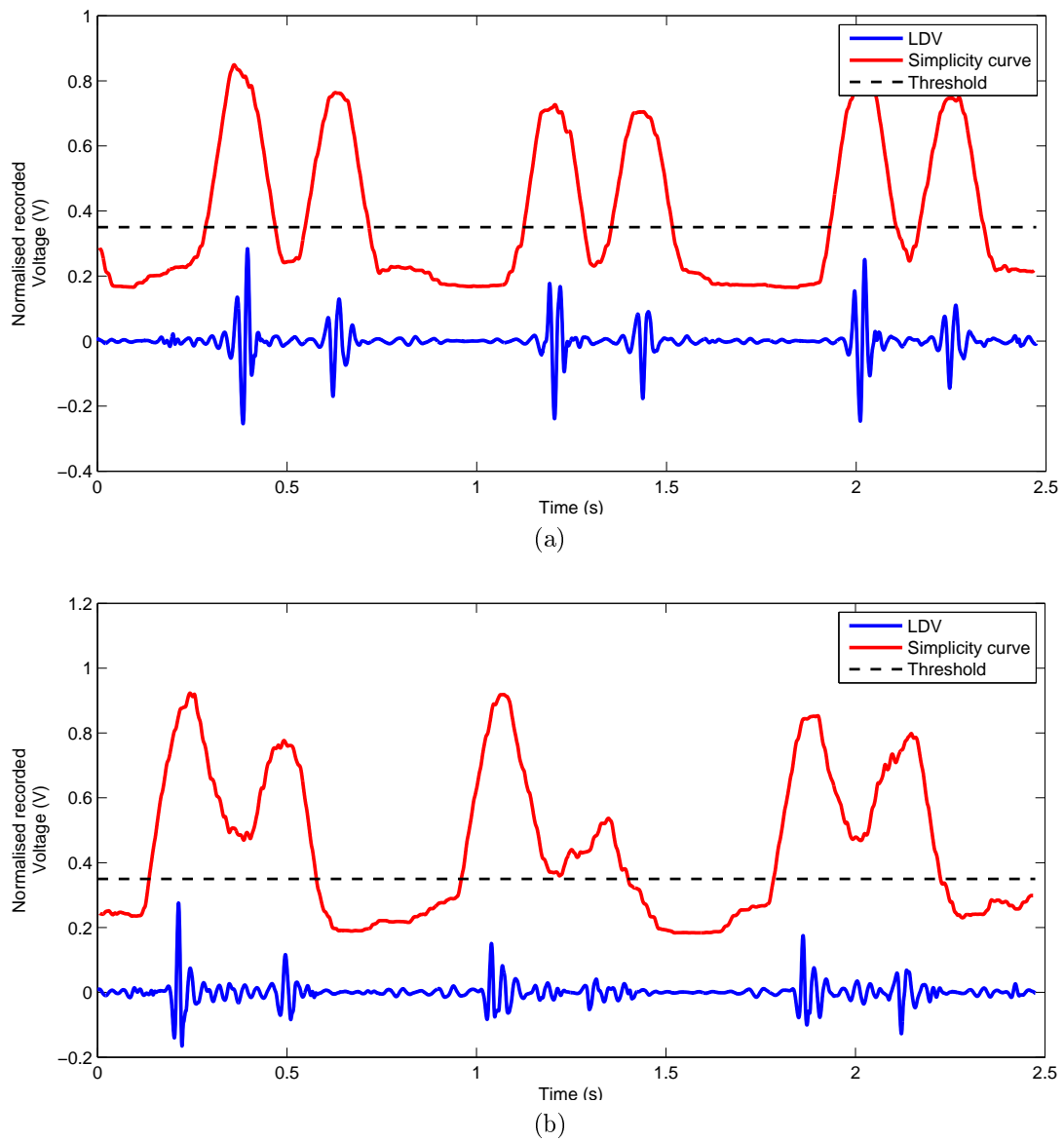
Figure 4.10: A simplicity curve calculated for the LDV signal from participants with (a) normal and (b) abnormal heart sounds. The normalized threshold value intersects with the simplicity curve at regular intervals. The intersection points were filtered and used to indicate the start of a first heart sound.
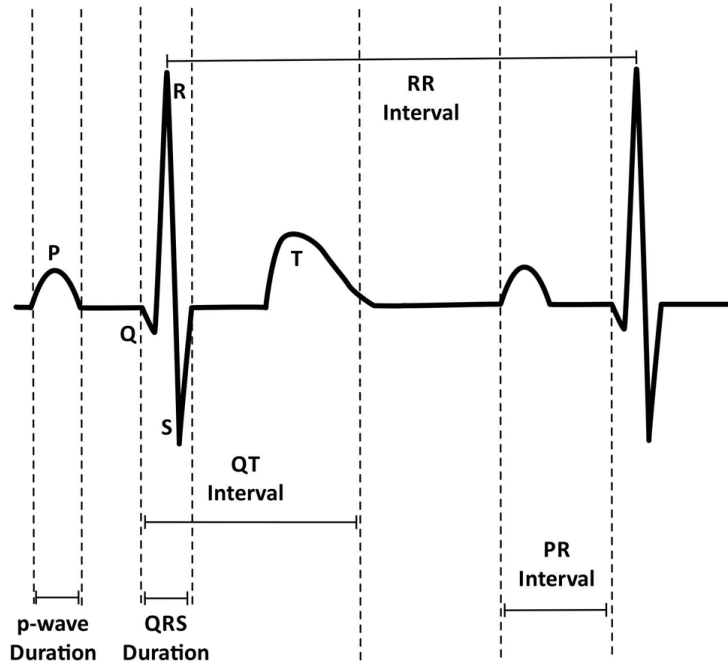
Figure 4.11: The electrical trace segments commonly seen on an ECG trace. The deflections indicate the strength of the electrical activity in the direction of the ECG lead.

$$T_{\text{QRS}} = -0.02T_{\text{R-R}}^{1/2} + 0.02T_{\text{R-R}} + 0.08 \tag{4.10}$$

$$T_{\text{Q-T interval}} = 1.65T_{\text{R-R}}^{1/2} - 0.84T_{\text{R-R}} - 0.46 \tag{4.11}$$

$$T_{\text{T-wave}} = 1.29T_{\text{R-R}}^{1/2} - 0.66T_{\text{R-R}} - 0.42 \tag{4.12}$$

$$T_{\text{S-T segment}} = 0.34T_{\text{R-R}}^{1/2} - 0.17T_{\text{R-R}} - 0.10 \tag{4.13}$$

Botha (2010) combined the above equations to calculate the start of diastole as

$$T_{\text{S-T segment}} = \frac{T_{\text{Q-T} - T_{\text{T-wave}}}}{2} \tag{4.14}$$

4.3.3 Combined ECG and complexity segmentation

The ECG data was used to determine the position of S1. The simplicity curve was normalized and different threshold values were used to calculate intersection points with the simplicity curve. The chosen normalized threshold value was that which produced simplicity curve intersection points that best corresponded with the segmentation calculated from the ECG data where it was available. The intersection points and the ECG segmentation points were iteratively compared for different normalized threshold values. The normalized threshold value which gave the best results over all the participant data was then calculated as 0.35. The intersection points that best corresponded with the start of the QRS-wave point, calculated from the ECG wave, were chosen as the start of systole. Figures 4.12a and 4.12b shows the segmented data from the simplicity curve for a normal and an abnormal participant respectively. The green dashed line is the segmentation which was calculated using the simplicity curve and the red dashed line indicates the ECG segmentation. Visual inspection of all participant data showed that the combined segmentation method outlined here has accuracy which is comparable to that of the trusted ECG segmentation methods.

4.3.4 The second heart sound

After the signal was segmented into full cycles (S1 to S1), the second heart sound (S2) could be extracted by considering each cycle individually. If no second peak was identified, or S2 was unusually late or early, Equation 4.14 was used to calculate the timing of S2. A reduced S2 could potentially be due to a pathology such as AS.

4.4 Chapter summary

The LDV data recorded during the clinical study showed signal dropouts, discussed in Section 4.2.1, which were removed to create an artifact-free recording. The dropout-free data was divided into two streams, Stream 1 and Stream 2. The recorded PA, stethoscope and Stream 1 LDV data were BP Butterworth filtered and further denoised using wavelet analysis as well as EEMD filtering. The denoised data were then segmented into the individual heart sound cycles using a combination of the available ECG data and a simplicity curve generated from the complexity analysis of the underlying signal, discussed in Section 4.3. These data are analyzed in Chapter 5 and used to train a classifier in Chapter 6. Stream 2 LDV data were passed through a LP Butterworth filter and are analyzed in Chapter 5.
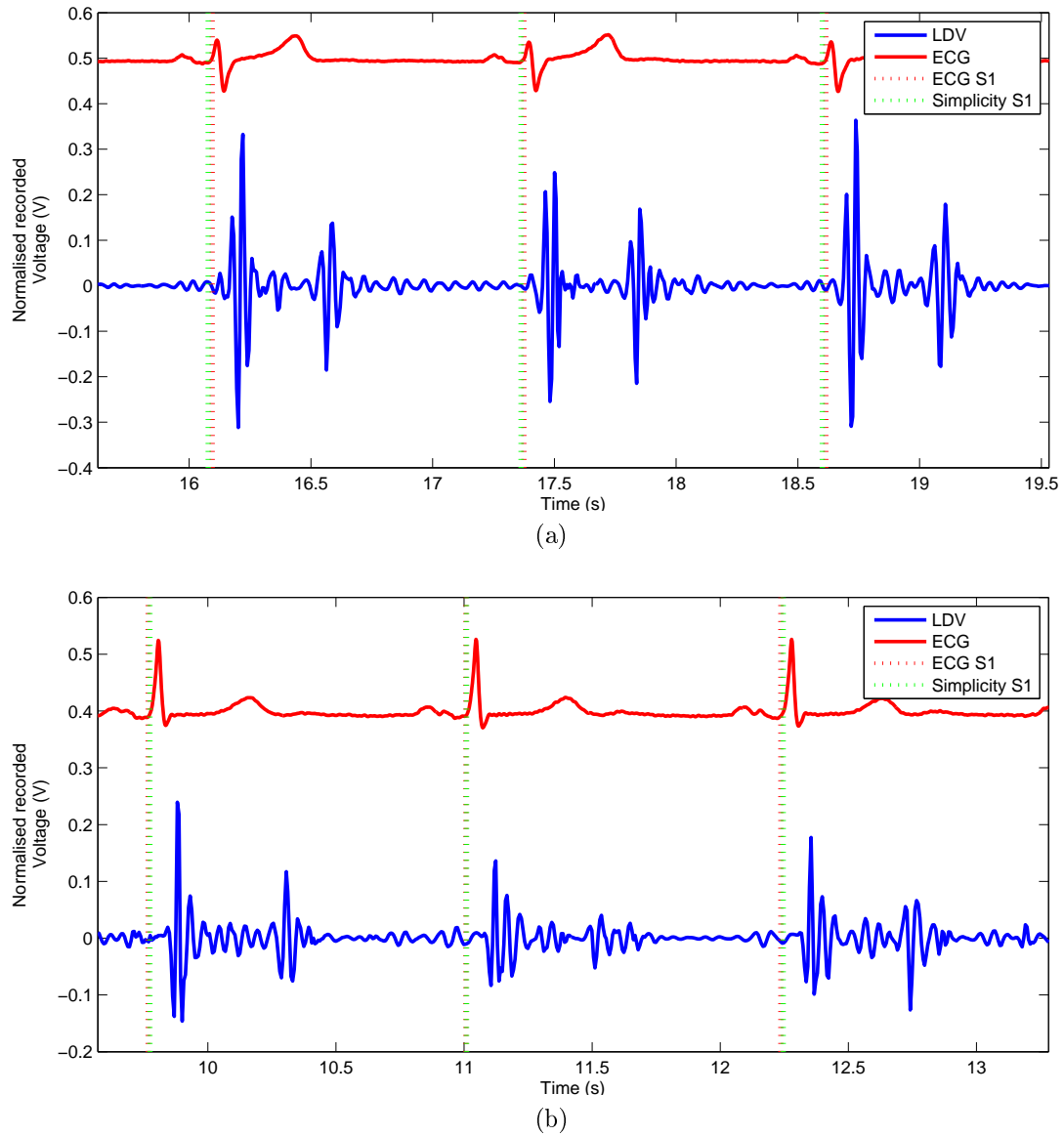
Figure 4.12: A comparison of segmentation results calculated from an ECG (red dotted line) and the simplicity curve (green dotted line) for a participant with (a) normal and (b) abnormal heart sounds. The ECG and simplicity curve methods give similar results. The simplicity curve is therefore a good alternative to the ECG for segmenting heart sound cycles when ECG data is not available.

Chapter 5

Comparing the LDV to existing instruments

5.1   Introduction

In the current work the LDV is explored as a non-contact tool for auscultation. In Section 5.2 the recorded LDV data from Stream 2 (as defined in Section 4.2) is analyzed for each pathology to understand how the underlying mechanics of the heart influences the LDV's velocity profile. In Section 5.3, in order to gauge the LDV's performance as a biomedical sensor, the LDV is compared to the PA for computing several medically significant qualities, such as heart rate, and investigating diagnostic indicators through the systolic/diastolic ratio. The PA is commonly used for basic biomedical uses such as calculating HR and is more widely researched than the LDV and thus forms a good benchmark for the LDV.

5.2   Pathological analysis

The Stream 2 LDV data shows a velocity profile which provides information regarding the underlying cardiac activity. The recorded participant data is analyzed in this section.

5.2.1   Background

Umberto *et al.* (2007) showed that the velocity profile of the LDV had features which could be related to certain events within the heart, in particular the closing of the four heart valves. These events as identified by Umberto *et al.* for a normal patient are shown in Figure 5.1. Figure 5.2 shows the data from a normal participant from the current study. The velocity profile recorded in this study shows a similar profile which can be related to the underlying cardiac events. The

phonocardiogram patterns associated with common heart murmurs are shown in Figure 2.3.
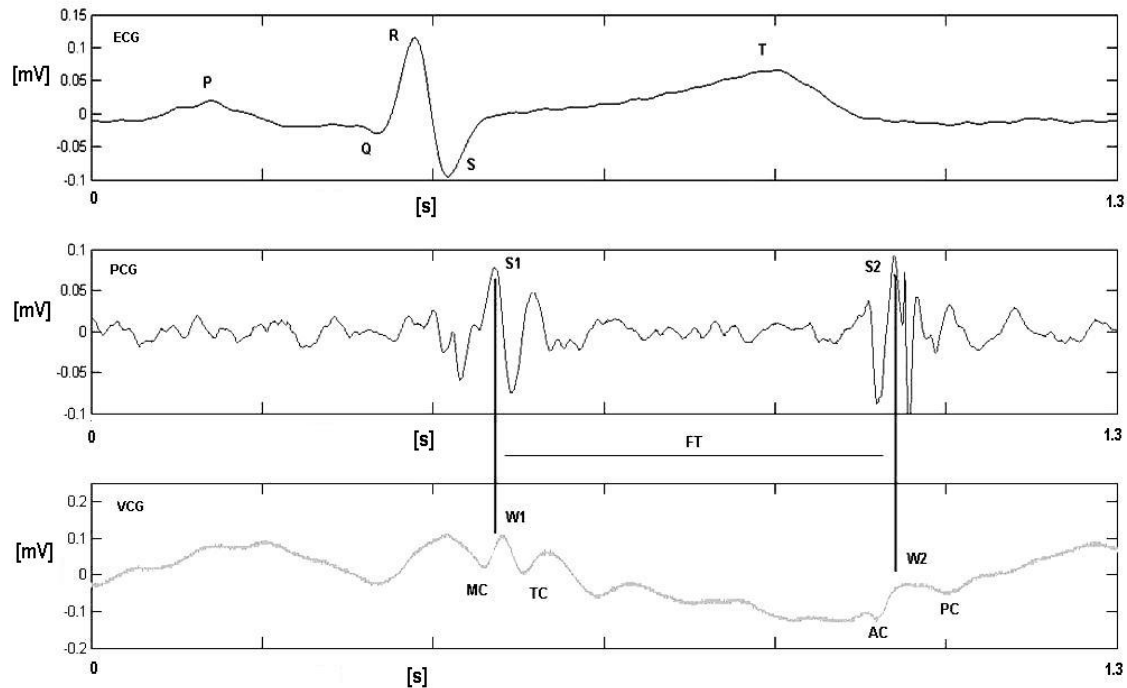
Figure 5.1: A synchronized recording of an ECG trace, phonocardiogram and LDV velocity profile. The markers indicate the timing where the heart valves close and show the peaks corresponding to the first and second heart sounds observed in the phonocardiogram (De Melis *et al.*, 2007).

As part of the same study, Umberto *et al.* (2007) used phonocardiogram data to characterize the heart murmurs experienced by their patients. Figure 5.2 shows that there is a close correlation between the BP butterworth filtered LDV data and phonocardiogram data, particularly in the location of the signal peaks. In this section, in contrast to Umberto *et al.* (2007), LDV data are used to characterize participant heart murmurs in order to demonstrate how recordings made by the LDV relate to the underlying heart mechanics.

5.2.2   Mitral regurgitation

Mitral regurgitation (MR) is a valvular condition where the mitral valve cannot close completely and as a result there is leakage from the ventricles back into the atrium as the heart pumps. MR is observed during auscultation as a pansystolic murmur, with a soft mitral component in the first heart sound. Mayo Clinic (2011)
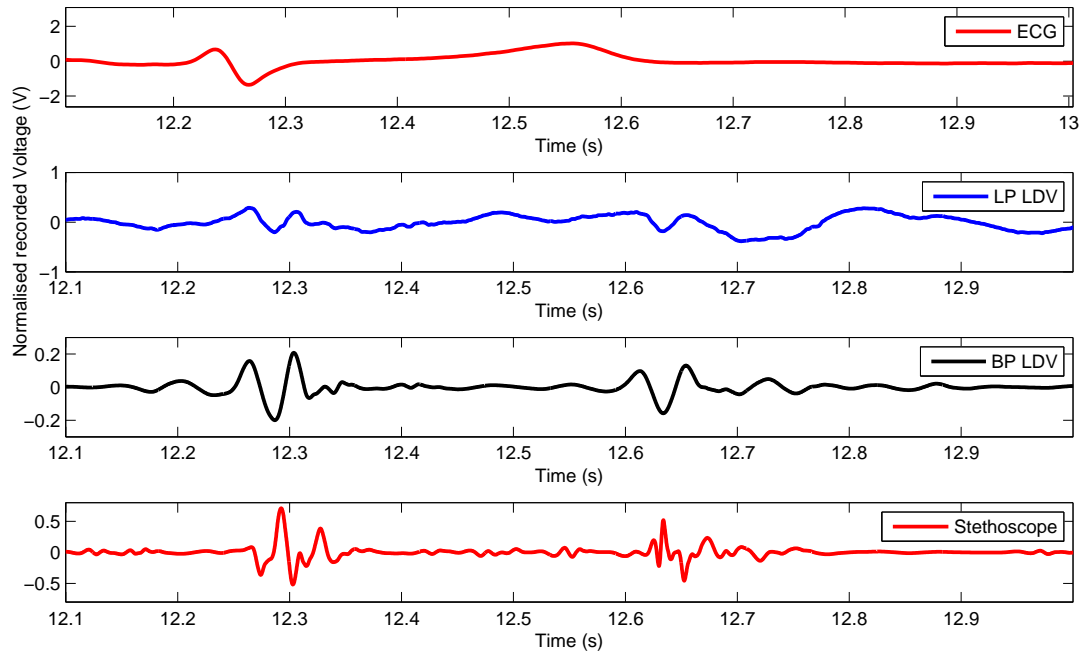
Figure 5.2: Velocity profile of the laser Doppler vibrometer with a synchronized ECG trace and stethoscope data for a participant with normal heart sounds.

lists common causes for MR as mitral valve prolapse, a previous heart attack and rheumatic fever.

Figure 5.3 shows the Stream 1 (LP filtered) and Stream 2 (BP filtered) LDV data for a single cycle of MR, as well as the corresponding ECG trace. Studying the data reveals that MR shows a rise and fall ("dip") during systole. As the blood is forced out of the ventricles during ventricular diastole, the velocity increases. The mitral valve, however, starts to allow some of the blood to return to the atrium which decreases the volume of blood which is pumped out of the heart. The redirection of the blood is likely the reason for the dip, as the blood is suddenly no longer being pumped out of the ventricles. This dip is found in the data from both MR patients as well as the patients who presented with the combination murmur of ASMR. This dip is also present, although less pronounced, in the participants with MSMR. This phenomenon was therefore attributed to the presence of the MR.

5.2.3   Mitral stenosis

Mitral stenosis (MS) is a valvular condition where the mitral valve does not open completely. MS is reported as occurring most often in adults who have suffered
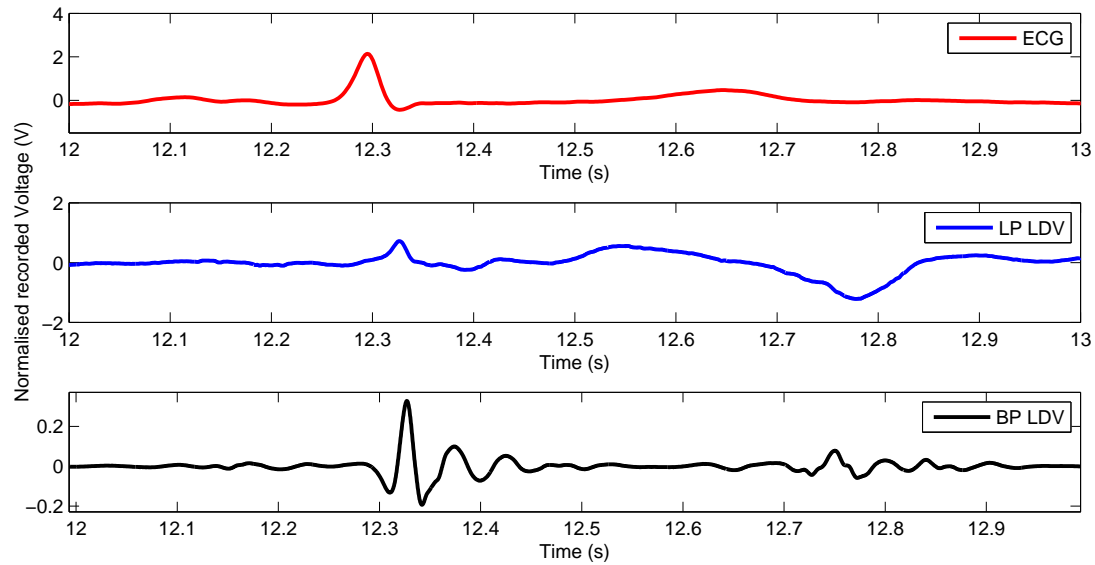
Figure 5.3: Synchronized ECG trace with the velocity profile of the laser Doppler vibrometer for a participant presenting with mitral regurgitation (MR). The velocity increases and decreases sharply in the area of the second heart sound as the blood is forced out of the ventricle and starts to push back into the atrium.

rheumatic fever. Less common causes are listed as calcium deposits which form around the mitral valve, radiation treatment to the chest and medications (Dima, 2012).

When ausculating a patient with a stethocope, MS is described as a rumbling sound which can be observed during diastole. As the mitral valve has decreased mobility, the atrial pressure is increased during the heart cycle. This increase in pressure forces the valve open and causes it to shut rapidly as the pressure gradient over it is elevated. MS patients often therefore have a loud S1 (Shub, 1999) as the valve is forced open, and an opening snap right after S2 as the valve closes. Figure 5.4 shows the Stream 1 (LP filtered) and Stream 2 (BP filtered) LDV data for two heart cycles as well as the corresponding ECG trace. A prominent S1 peak is visible which is consistent with the mitral valve closing forcefully. Another peak is visible at an average time of 0.1 s after S2 for this participant which is consistent with an opening snap in a patient with mild MS.

5.2.4   Aortic stenosis

Aortic stenosis (AS) is the valvular condition where the aortic valve is narrowed, thereby restricting the amount of blood which can flow from the heart to the body.
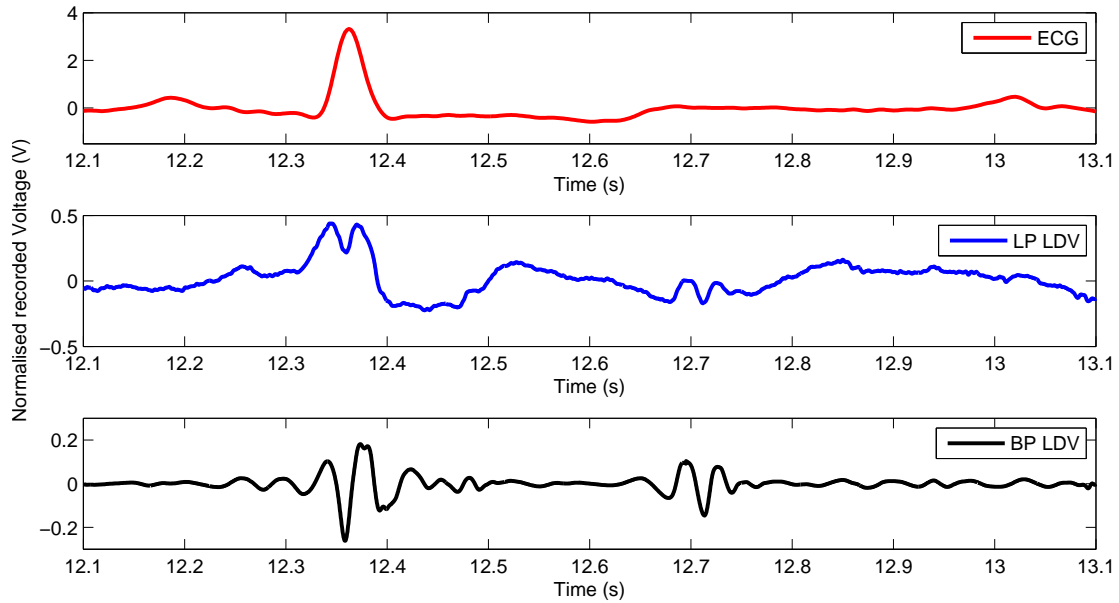
Figure 5.4: Synchronized ECG trace with the velocity profile of the laser Doppler vibrometer for a participant presenting with mitral stenosis (MS). MS traces consistently showed a sharp S1 peak and an opening snap just after S2.

The narrowed valve prohibits the free flow of blood from the ventricles to the rest of the body, slowing down the transfer of blood as the valve has to be forced open. AS is described during auscultation as a crescendo-decrescendo murmur heard during systole. During auscultation, severe AS patients do not have a strong S2. Figure 5.5 shows the Stream 1 (LP filtered) and Stream 2 (BP filtered) LDV data for two heart cycles as well as the corresponding ECG trace. A lack of S2 for a severe AS participant is also visible in the Stream 1 LDV data in Figure 5.5. The Stream 2 data in Figure 5.5 shows a strong dip in the velocity just after S1 as the valve creates resistance and the profile picks up again as the blood is increasingly forced through.

5.2.5   Combined murmurs

Patients sometimes present with more than one heart murmur. Figures 5.6 and 5.7 are examples of combinations of AS and MR as well as MS and MR respectively. These combination murmurs profiles resemble the profiles of their constituent features. The combination of AS and MR shows the strong dip in velocity just after S1 as well as the velocity increase and decrease at S2 which is common for MR recordings. The combination of MS and MR shows the sharp S1 peak found in MS
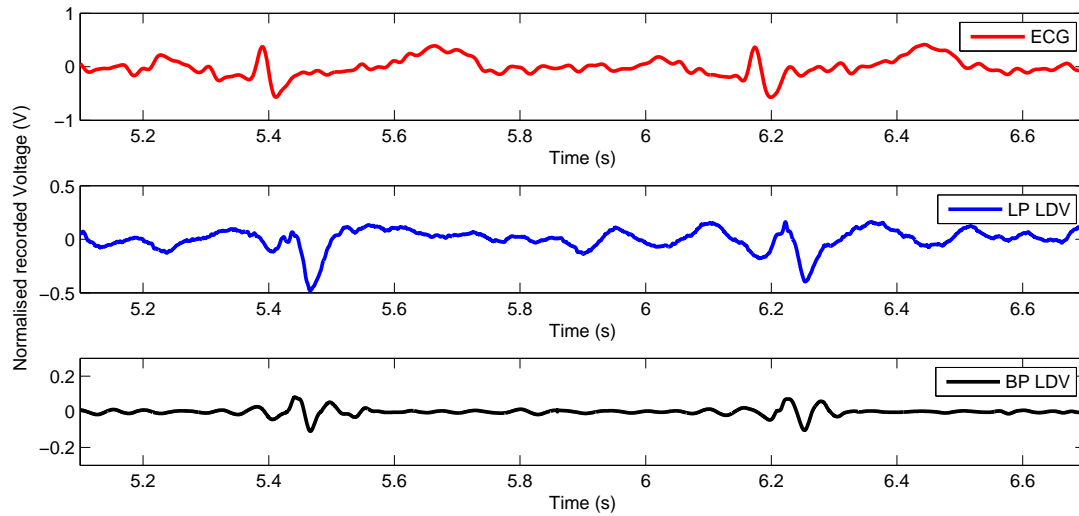
Figure 5.5: Synchronized ECG trace with the velocity profile of the laser Doppler vibrometer for a participant presenting with aortic stenosis (AS). There is a lack of a S2 peak, a common occurrence in severe AS patients.

recordings as well as the sharp "dip" at S2 which is common for MR recordings.

5.3 Comparing the piezoelectric accelerometer to the LDV

The fundamental purpose of this work is to gauge whether the LDV is suitable for automated diagnosis of heart sounds. In order to do this, it is helpful to contrast the LDV's performance to that of the PA, which has been widely used in the biomedical field. In this section, the PA is compared to the LDV for several common biomedical use cases.

5.3.1 Calculating heart rate

The ECG is considered to be the golden standard for heart rate (HR) monitoring. In the absence of an ECG, an accelerometer is preferred to a stethoscope for determining HR, as stethoscopes are prone to pick up motion artifacts, especially if the patient is performing an exercise stress test (Anh Dinh, 2011) or has difficulty in remaining stationary.

The HR of each participant was calculated using both the LDV and PA by using the normalized threshold and simplicity curve intersection points to find the start of S1 (see Section 4.3). Missing intersection points and false peaks were detected and
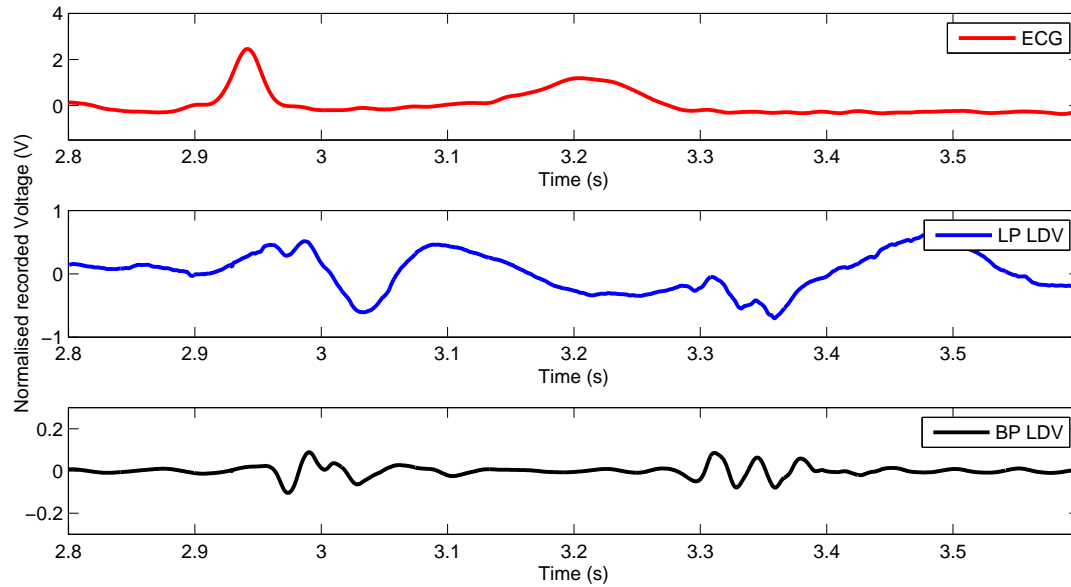
Figure 5.6: Synchronized ECG trace with the velocity profile of the laser Doppler vibrometer for a participant presenting with a combination of AS and MR. The velocity dips sharply just after S1 as with AS participants and an increase and decrease at S2 which is common for MR recordings.

the affected section then omitted from the data. The HR was then calculated by dividing the lengths of uninterrupted recordings by the number of S1 intersection points which were detected in that time. The overall participant HR was taken as the average over all the recordings for that participant.

The HR determined from LDV, PA and ECG data are shown in Table 5.1. The HR calculated from both the LDV and PA data corresponds closely to the HR calculated by the ECG. The patient with the highest deviation was Participant 13 (who was diagnosed with HOCM) which deviated 6.09% and 6.04% for LDV and PA respectively. The data shows that LDV and PA perform equally well in this task: the average difference over all the participants is 1.95% between the ECG and LDV and 1.65% between the ECG and PA. The results show that the LDV is a viable alternative to the ECG for calculating heart rates.

5.3.2 Using systolic/diastolic ratio as an diagnostic indicator

The ratio of systolic time/diastolic time was proposed by Gemignani *et al.* (2008) for use as an indicator of abnormal heart function. It was hypothesized that a

Table 5.1: Heart rate for ECG, LDV and PA shown in beats per minute (BPM) and percentage difference between the ECG and LDV, and ECG and PA calculated heart rates. The average difference indicates that the LDV is a viable alternative to the ECG and PA for determining a patient's HR.

	Heart rate in beats per minute (BPM)				
PAT	**ECG**	**LDV**		**PA**	
	BPM	**BPM**	**% Diff**	**BPM**	**% Diff**
1	59.58	59.30	0.47	59.75	0.29
2	60.59	58.83	2.90	60.38	0.35
3	57.93	58.36	0.74	58.44	0.88
4	57.56	57.64	0.14	56.87	1.20
5	93.72	95.73	2.14	95.97	2.40
6	73.85	69.81	5.47	71.63	3.01
7	76.91	74.60	3.00	75.99	1.20
8	62.4	62.87	0.75	62.50	0.16
9	68.95	71.35	3.48	69.91	1.39
10	49.31	48.65	1.34	48.37	1.91
11	58.2	57.61	1.01	58.08	0.21
12	70.86	71.15	0.41	72.90	2.88
13	51.92	53.40	2.85	54.48	4.93
14	74.99	75.41	0.56	74.97	0.03
15	76.84	75.37	1.91	76.32	0.68
16	76.38	77.75	1.79	76.52	0.18
17	49.72	50.58	1.73	50.30	1.17
18	71.97	67.58	6.10	67.62	6.04
19	64.64	64.15	0.76	66.08	2.23
20	62.87	61.92	1.51	61.85	1.62
Average			**1.95**		**1.64**
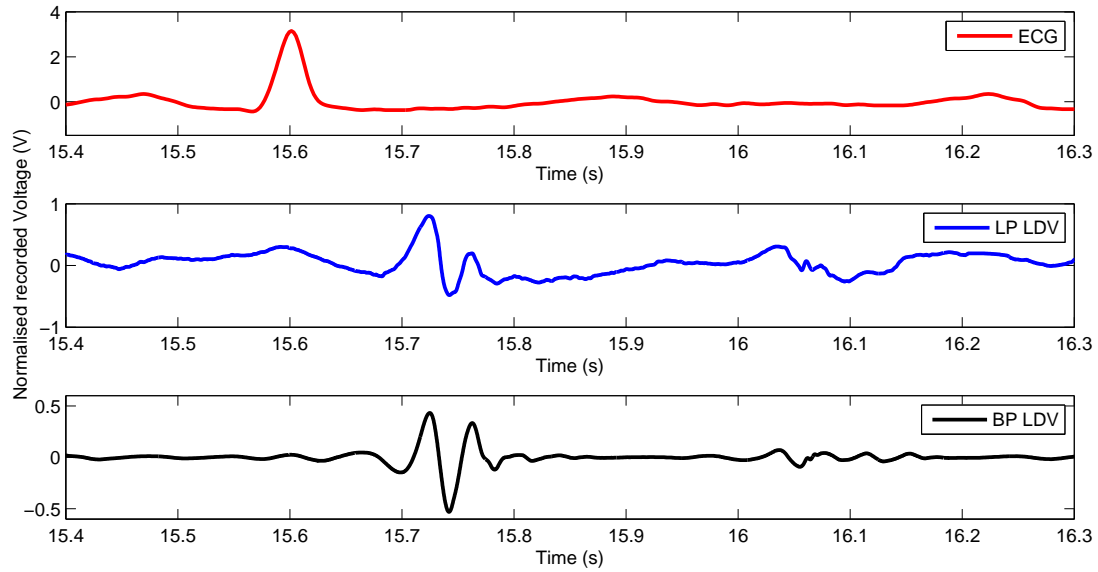
Figure 5.7: Synchronized ECG trace with the velocity profile of the laser Doppler vibrometer for a participant presenting with a combination of MS and MR. A sharp S1 peak is visible as found in MS recordings as well as the sharp "dip" at S2 which is common for MR recordings.

shortened diastolic time could indicate a problem with the patient's ventricular filling and perfusion.

The systolic/diastolic ratio was calculated for each participant group (e.g. AS, MS, etc). The ratios are graphically represented as histograms for inspection in Figures 5.8 and Figures 5.9. Figure 5.9 shows the difference in dispersion for Normal and Abnormal ratios as calculated from the PA data and Figure 5.8 shows the LDV equivalent. The majority of the ratios were lower for the normal participants than the abnormal participants for both the LDV and PA data, confirming the finding of Gemignani *et al.* (2008). The abnormal participant ratio data show a much flatter profile with a wider spread of values than the normal participant ratio data. This is due to the large number of different pathologies in the data. All of the individual abnormal pathologies ratio data were individually higher on average than the normal participant ratio data.

5.3.3   Determining chest wall velocity and position

Acceleration is the change of velocity over time and velocity is the change of position over time. The accelerometer data can therefore be compared with the velocity data of the LDV by means of numerical integration. The mathematical relationships
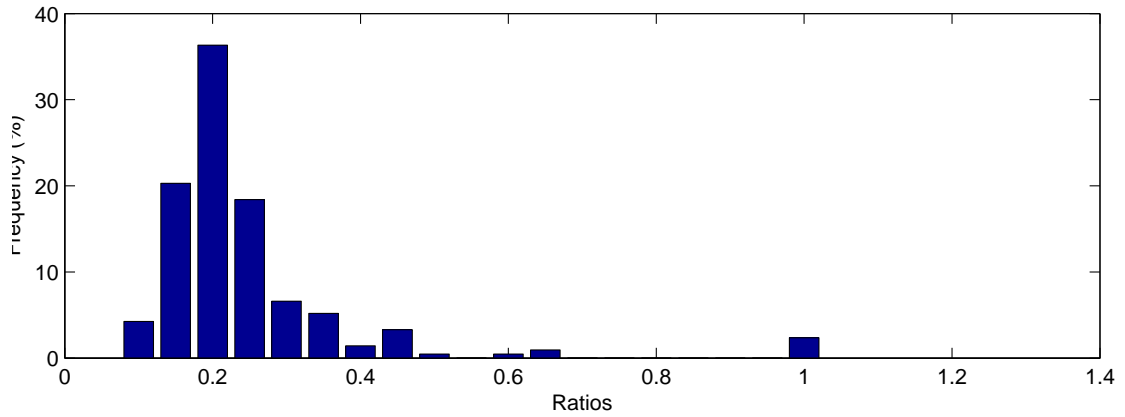
(a) All normal participants recorded with LDV
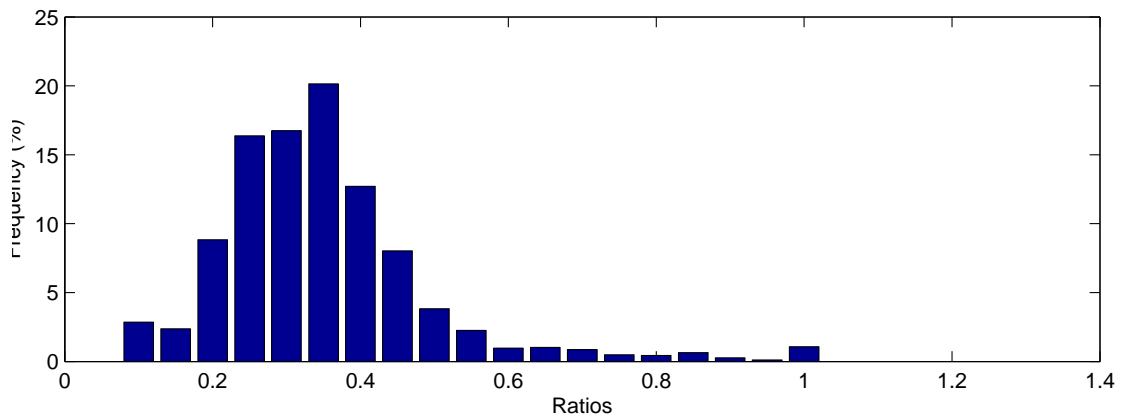
(a) All abnormal participants recorded with LDV

Figure 5.8: Histogram of systolic/diastolic ratio for LDV, shown as percentages. The systolic/diastolic ratios were on average lower for normal participants than abnormal participants. Notice the similarity between this Figure and Figure 5.9, which shows the same data for the PA.

between acceleration (a), velocity (v) and displacement (s) are given below with time t

$$a = \frac{\mathrm{d}v}{\mathrm{d}t} \text{ and } v = \frac{\mathrm{d}s}{\mathrm{d}t}, \text{ therefore } a = \frac{\mathrm{d}^2 s}{\mathrm{d}t^2} \tag{5.1}$$

In integral form, these can be written as:

$$v = v_0 + \int\limits_0^t a(t)dt \quad s = s_0 + \int\limits_0^t v(t)dt \tag{5.2}$$

The constants v_0 and s_0 are the initial conditions of the system. Unfortunately, these initial conditions are not available in most biomedical systems. Accelerometers also exhibit a phenomenon known as drift where a small DC offset is present
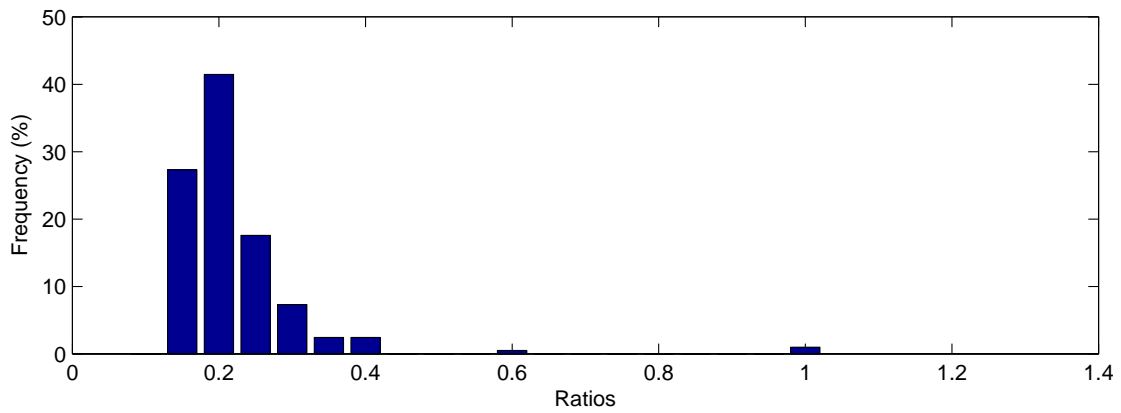
(a) All normal participants recorded with PA
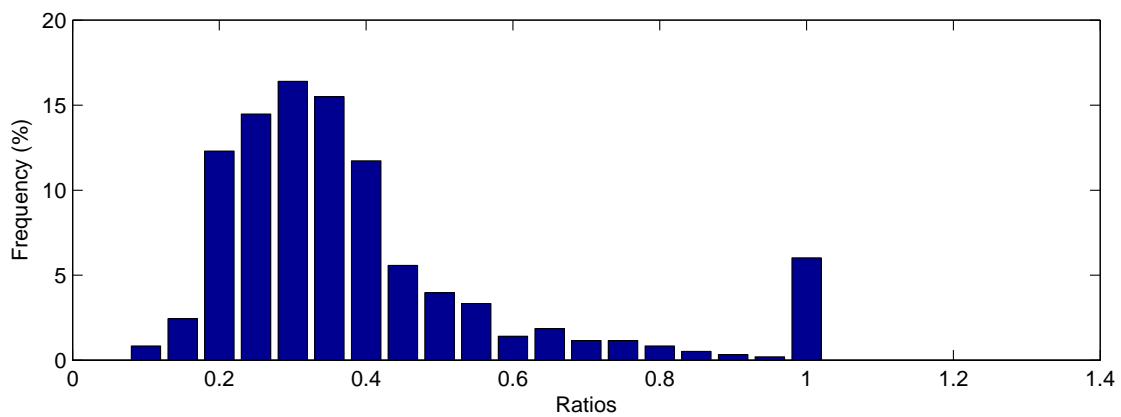
(a) All abnormal participants recorded with PA

Figure 5.9: Histogram of systolic/diastolic ratio for PA, shown as percentages. The systolic/diastolic ratios were on average lower for normal participants than abnormal participants. Notice the similarity between this Figure and Figure 5.8, which shows the same data for the LDV.

in the data. Drift is influenced by factors such as temperature and the sensor's grounding voltage in relation to the grounding voltage of the measuring equipment it is connected to. If not corrected for, drift can cause large numerical errors.

Slifka (2004) proposed the following procedure to determine velocity and displacement from accelerometer data without requiring initial conditions, while accounting for accelerometer drift:

1. Use a high pass filter to remove the accelerometer drift

2. Numerically integrate numerically to obtain velocity

3. Use a high pass filter to remove the DC component from the velocity data, eliminating the need for an initial velocity value.

4. Integrate the velocity to calculate position

5. Use a high pass filter to remove the low frequency content from the position signal, eliminating the need for an initial position measurement.

Slifka (2004) tested various filters for their suitability in the role of high pass filter in the proposed algorithm. The recommended scheme was based upon a modified FFT filtering technique whereby the coefficients of the lower frequency components of the FFT were modified before an inverse FFT was used to recreate the filtered signal.

Accelerometer data was gathered from the sternum (Xu *et al.*, 1996) as well as the apex of the heart (Phan *et al.*, 2008). These positions are marked in Figure 3.9. To compare the measurements from the LDV with that of the accelerometer, the acceleration data were transformed with the procedure described by Slifka (2004) as described in this Section. It was observed that the transformed data recorded on the sternum corresponded to the LDV data whereas the accelerometer data recorded from the apex area corresponded to the negative of the LDV data. The results of the double integration method are shown in Figures 5.10 and 5.11.

Figure 5.10 a) and Figure 5.11a) show accelerometer data recorded on the sternum of two participants. The accelerometer data which has been transformed to velocity data has the same sign as the LDV data. Figure 5.10 b) and Figure 5.11b) show the accelerometer data recorded on the apex of the heart. The transformed velocity data of the accelerometer has a reversed polarity to that of the LDV data. This behaviour was consistent for all participants. A potential physical explanation of this is as follows: the acceleration of the chest wall is an indirect measurement of the heart's motion. As the atria contract, the ventricles relax, and vice versa. It is expected that the contractions experienced by the atria or ventricles will be observed as an acceleration of the chest wall, whereas the relaxing atria or ventricles would show as deceleration. The difference in profile for accelerometer data recorded from the sternum and apex positions indicate that the accelerometer's position does affect the data recorded and could be explored in future work. The LDV could be considered as a replacement for the accelerometer if a system could ensure that the LDV recorded data from a single, consistent point on the participant's body.

The electric pulses of the ECG leads closest to the placements of the accelerometers (V1/V2 for the sternum and V3/V4 for the apex) were opposite in polarity, and in many cases were close to a mirror image of one another as well. The ECG is a measure of net electrical activity as seen by the various leads. Figure 5.12 shows the heart with the relative positions of leads V1 and V4–V6. In Figure 5.12 the depolarization vectors of the heart tissue which were drawn in show that the
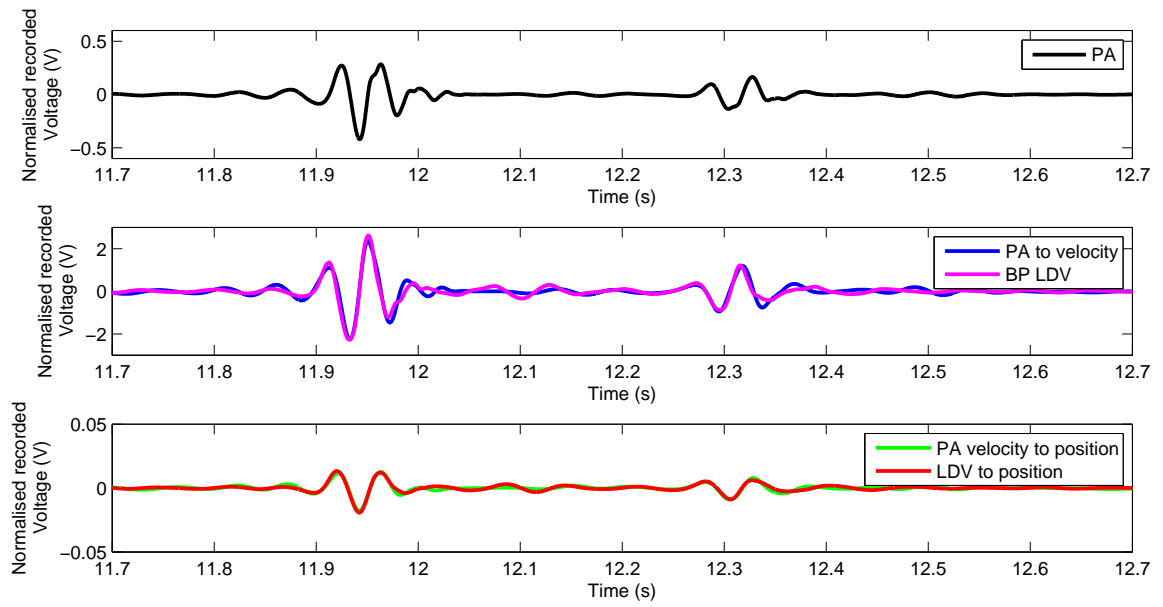
(a) Sternum
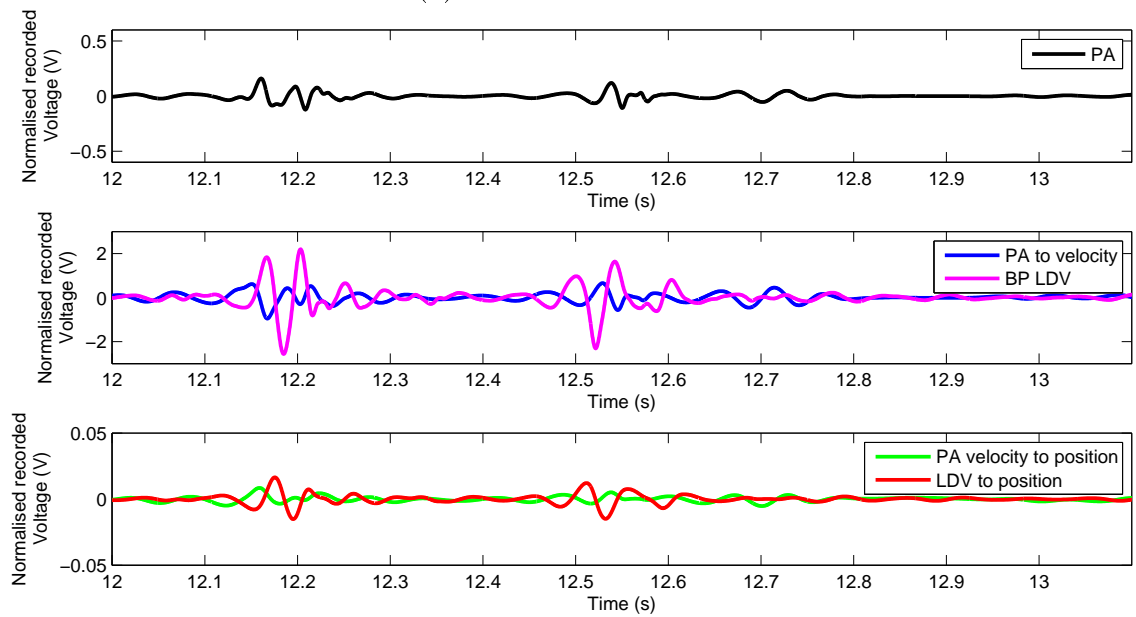
(b) Apex

Figure 5.10: Accelerometer data recorded on the sternum and apex of a normal partici-pant transformed to velocity and distance and compared to the LDV data. The PA data and LDV data have very similar profiles when the PA data is recorded on the sternum, but have opposite polarities when the PA data is recorded on the apex of the heart.
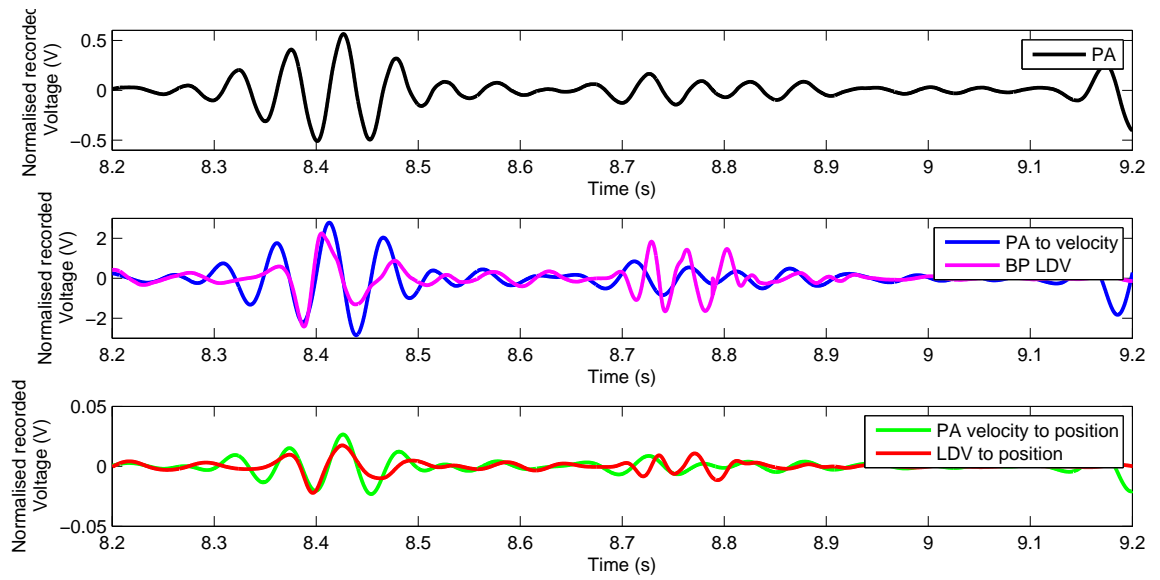
(a) Sternum
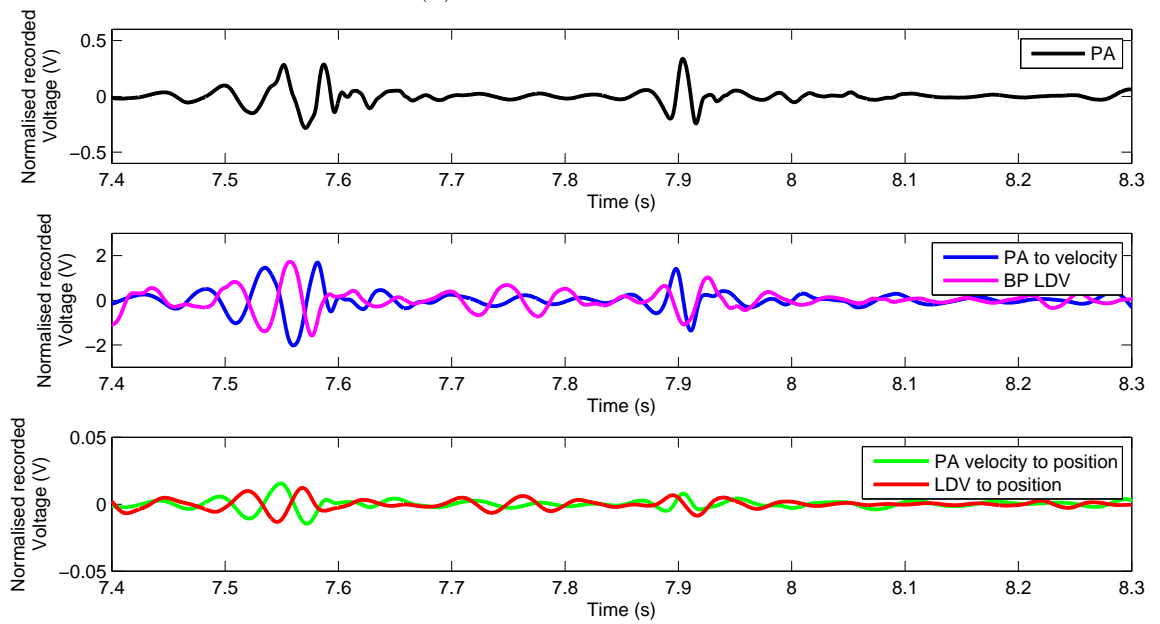
(b) Apex

Figure 5.11: Accelerometer data recorded on the sternum and apex of an abnormal participant transformed to velocity and distance and compared to the LDV data. The PA data and LDV data have very similar profiles when the PA data is recorded on the sternum, but have opposite polarities when the PA data is recorded on the apex of the heart.

depolarization wave of the inter ventricular septum is in the direction of lead V1 and the depolarization wave of the larger ventricular wall is in the direction of leads V4–V6. The lead therefore sees a net depolarization wave as moving "towards" or "away" from it. When a lead sees the wave as moving towards it, the deflection on the ECG curve is positive. A wave seen as moving away from the lead causes a a negative deflection.

The depolarization wave of the inter ventricular septum is much smaller than the ventricular wall due to the large difference in mass. The difference in magnitude of the two vectors is visible when studying the R-wave propagation in the leads (Ashley and Niebauer, 2004). Figure 5.13 shows the QRS complex of V1 and V6.

The different signs of the data recorded with the accelerometer at the apex and sternum are potentially due to the difference in cardiac activity seen at the same time at the atria and apex of the heart. In future work this could be explored with a second accelerometer.
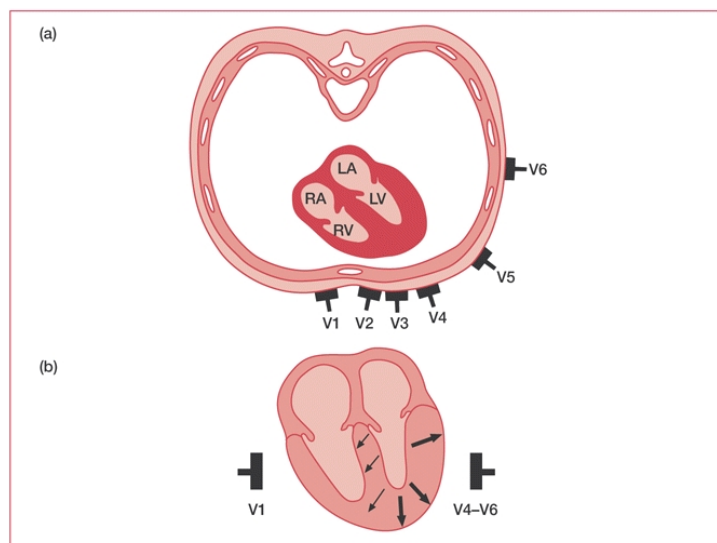
Figure 5.12: a) A cross section of the human chest and heart along with the relative positions of the chest leads of the ECG b) The depolarization vectors are shown with respect to the V1 and V6 ECG leads.

5.4   Chapter summary

The Stream 2 LDV data was analyzed for each of the recorded pathologies in order to investigate how the LDV's recordings relate to the underlying mechanics of the heart. The LDV was also compared to the PA in common biomedical applications. The LDV and PA were equally accurate in calculating HR when compared to the
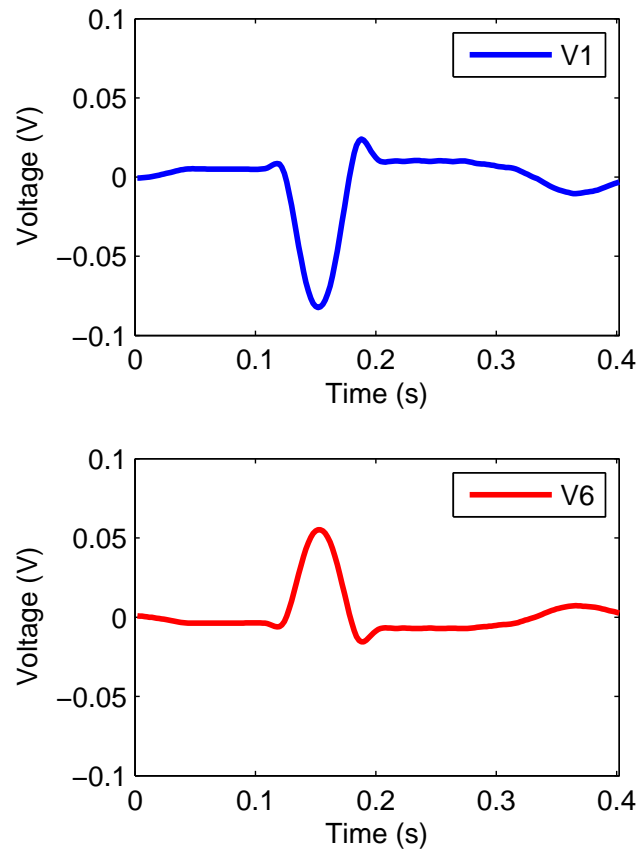
Figure 5.13: The QRS waveforms observed in the V1 and V6 leads recorded simultaneously. The recorded polarity is reversed for the leads.

HR calculated by the ECG. The LDV and PA both displayed the potential for use as a diagnostic tool when comparing the systolic/diastolic ratio of the recorded participants. The physical recorded waveform of the LDV and PA were also compared by using a double integration method to transform the PA data into velocity and distance quantities. The PA data which was transformed into velocity was compared to the LDV waveform. The LDV data were transformed into distance data and compared to the transformed PA distance data. The resultant curves showed that the directionality of the PA recorded signals were dependent on the position of the recorded PA data. The LDV could be a potential replacement for the accelerometer given further study into overcoming the limitations of a non-contact sensor recording a non-stationary point.

Chapter 6

Classification of heart sounds

6.1   Introduction

In order to explore the LDV's role as part of an autonomous auscultation system, the LDV data was used to train a proof of concept heart murmur classifier. During the data gathering phase data were collected from 17 unhealthy participants and 3 healthy participants. The ratio between healthy and unhealthy participants was based on the work of Jiang *et al.* (2007). It was, however, found during post processing of the data that there were too few healthy participants to train a classifier that could distinguish between normal and abnormal participants. This is likely due to the fewer number of participants in this work.

Due to the availability of a sufficient number of AS participants, it was possible to train a classifier which could successfully distinguish between participants presenting with AS and those who did not. In this chapter, the process of creating an automatic classifier to separate participants into those with and without AS, is discussed. In Section 6.2, the process of converting LDV recordings into classifier input is discussed. The classification technique is introduced in Section 6.3 and results are presented in Section 6.4.

6.2   Feature extraction

Jiang *et al.* (2007) created a support vector classifier (SVC) which could successfully diagnose various heart murmurs recorded by a stethoscope. They took 196 normal and 263 abnormal heart sound cycles from 6 healthy subjects and 30 unhealthy subjects. They reported a specificity of 99.9% and a sensitivity of 99.52% for classifying normal and abnormal sounds. They also reported discrimination rates of 86.88% for atrial fibrillation sounds, 89.98% for aortic valvular disorders and 90% for mitral valve disorders. Their classifier required only two features derived from the normalized power spectral density (PSD) of the signal: the bandwidth

60
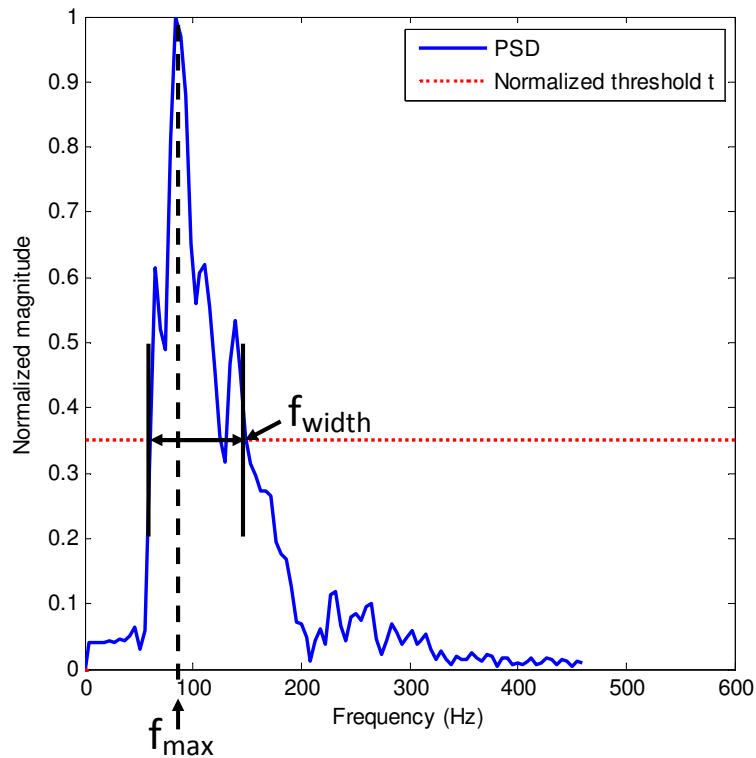
Figure 6.1: Extracted features f_{width} and f_{max} from a full heart sound cycle at normalized threshold value t.

(f_{width}) of the transformed signal at a specific normalized threshold value, t, and the frequency at which the maximum value of the curve occurred (f_{max}). The features f_{width} and f_{max} are shown in Figure 6.1. Jiang *et al.* (2007) tested threshold values of 0.1 to 0.5 with 0.1 increments and found that the accuracy of their classifier was not very sensitive to the threshold value.

In this work, the two feature scheme of Jiang *et al.* (2007) is used and expanded upon. A normalized threshold value of $t = 0.1$ to $t = 0.9$ in increments of 0.1 was used to create feature sets. These feature sets were then tested by feeding them into a KNN classifier. The threshold value from which the best classifier was trained was chosen as the threshold value for all subsequent classifiers. The effects of the feature sets and feature threshold choices are further discussed in Section 6.4, where it is shown that the normalized threshold value that leads to the most accurate predictions in this work is $t = 0.6$.

In the initial stages of this work, features were only extracted from the Stream 1 LDV data. In an attempt to increase the accuracy of the classification system, the same features were extracted from the PA data. A total of 12 features were therefore extracted for each heart sound cycle, 6 for the LDV data and 6 for the PA data.

Classifiers were trained for the LDV and PA feature data separately as well as the combination of PA and LDV data.

Various combinations of features were tested and it was found that the best results were obtained by using the f_{width} and f_{max} from the full cycle, as well as the diastolic and systolic segments of the cycle for the LDV data only. It was found that the PA data did not improve the results. This result seems to indicate that the PA data does not provide the classifier with any additional information that is not duplicated by the LDV. Table 6.1 shows the averaged feature values for each pathology.

Table 6.1: Averaged feature values per participant pathology

		Full		Diastole		Systole	
		f_{width}	f_{max}	f_{width}	f_{max}	f_{width}	f_{max}
LDV	**AS**	17.09	2.64	16.89	3.19	17.28	4.04
	ASMR	18.16	6.44	17.40	6.21	22.89	5.58
	MR	19.35	4.06	19.90	5.11	17.41	5.19
	MS	20.31	3.68	19.31	5.03	19.57	4.62
	Normal	19.01	3.80	18.95	4.70	20.15	5.45
	MSMR	20.50	5.46	21.15	7.94	19.73	5.66
PA	**AS**	26.9	6.28	27.12	9.12	26.58	5.93
	ASMR	25.40	8.40	23.88	8.68	25.31	5.55
	MR	18.33	5.63	18.04	6.16	20.21	5.74
	MS	23.42	8.71	23.03	7.75	24.97	11.39
	Normal	20.58	5.66	25.75	11.09	21.83	5.27
	MSMR	23.19	7.62	22.63	7.17	20.10	4.33

Figure 6.2 and Figure 6.3 shows the difference in feature values from LDV data, for the various recorded pathologies with feature thresholds of $t = 0.3$ and $t = 0.6$ for the LDV data respectively. Comparing Figure 6.2 and Figure 6.3 shows that a threshold value of $t = 0.6$ results in a more distinct distribution of feature values for each pathology. The visible separation of the features indicates that the parameterization is dividing the data into distinct clusters, which indicates an increased chance of correct classification. Section 6.4 discusses the best results achieved with the various feature sets presented in this section.

From Figure 6.3 it is possible to note that certain pathologies show definite patterns in their feature sets. The presence of AS, for example, shows features with much higher f_{width} and f_{max} values when compared to MS. The combination of AS and MR shows f_{width} and f_{max} values much closer to AS than MR, which means that for this dataset the presence of AS has a dominant effect on the feature values. Further, it can be noted that all the features shown are relevant to the pathologies.

No single feature or subset of features is sufficient to differentiate between the pathologies. The normal participants' features are not as tightly grouped as those of the abnormal pathologies. This indicates that there is substantial variability within the normal group itself and could indicate the need to add further features or modify the existing feature set.

6.3 Classification

Jiang *et al.* (2007) used a binary tree of SVM classifiers to systematically classify heart sounds and murmurs. A disadvantage of this approach is that it is sensitive to noisy data and does not provide a way to correct any incorrect classifications made at higher nodes of the tree, causing incorrect classifications to impact the accuracy of every node beneath them (Leha and Singh, 2011). In this work, k-nearest neighbors (KNN) was used to classify heart sounds.

6.3.1 K-Nearest neighbours classification

K-nearest neighbours (KNN) is extremely simple but robust classification algorithm, which operates on the principle that the sample data will most likely belong to the same class as its nearest neighbours. Figure 6.4 shows the basic principle of KNN classification (Bhatia, 2010).

KNN classifiers do not require training, are simple and easy to apply, are not strongly affected by noisy training data (for a suitably large K value) and perform well when a large set of training data is used. Unfortunately, their computational cost increases drastically with the dimensionality of the data, they use a large amount of memory and irrelevant attributes can negatively impact the classification results by distorting the distance metrics used to determine neighbours (Bhatia, 2010).

Various metrics can be used to measure the distance between two samples: Euclidean distance is commonly used, but more exotic measures such as Manhattan distance are useful in some cases. Additionally, a rule for deriving the label of a particular point, given the labels of the K neighbour points, is required. In this work a data point is assigned the label of the majority of its K-nearest neighbours. A tie-breaking rule is implemented if two or more labels have an equal number of neighbours. Other possible rules, such as distance weighted designs, are discussed in Dudani (1976).

6.3.2 Cross-validation

Cross validation (CV) is the process of iteratively dividing the data into separate test and training sets which can be used to access the accuracy of a classification
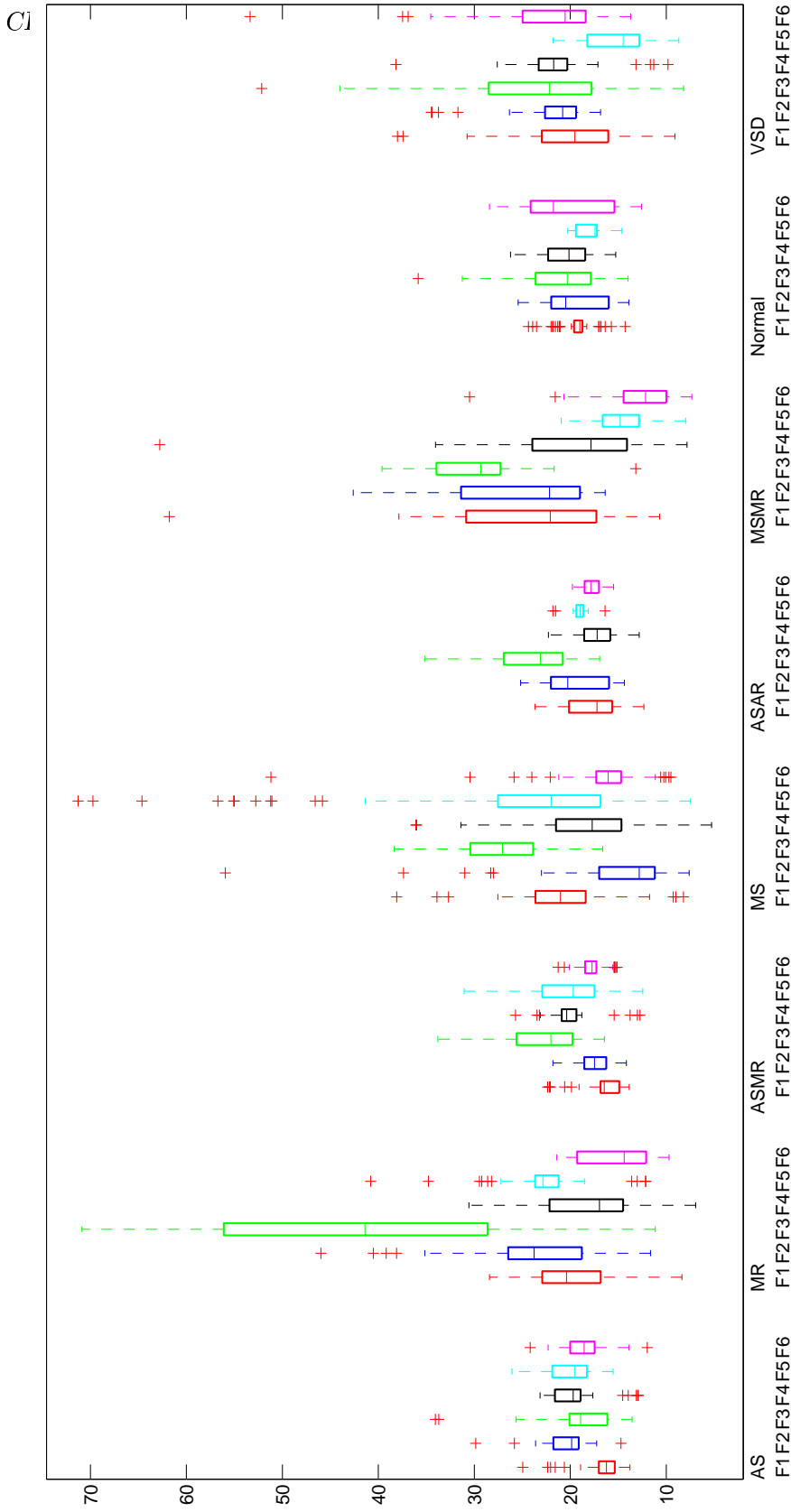
Figure 6.2: The range of feature values for the LDV data for each pathology at a normalized threshold value of $t = 0.3$. F1, F3 and F5 are f_{max} feature of the full, systolic and diastolic FFT curves respectively. F2, F4 and F6 are f_{width} feature of the full, systolic and diastolic FFT curves respectively. When compared to Figure 6.3, much less distinct feature groups can be observed.
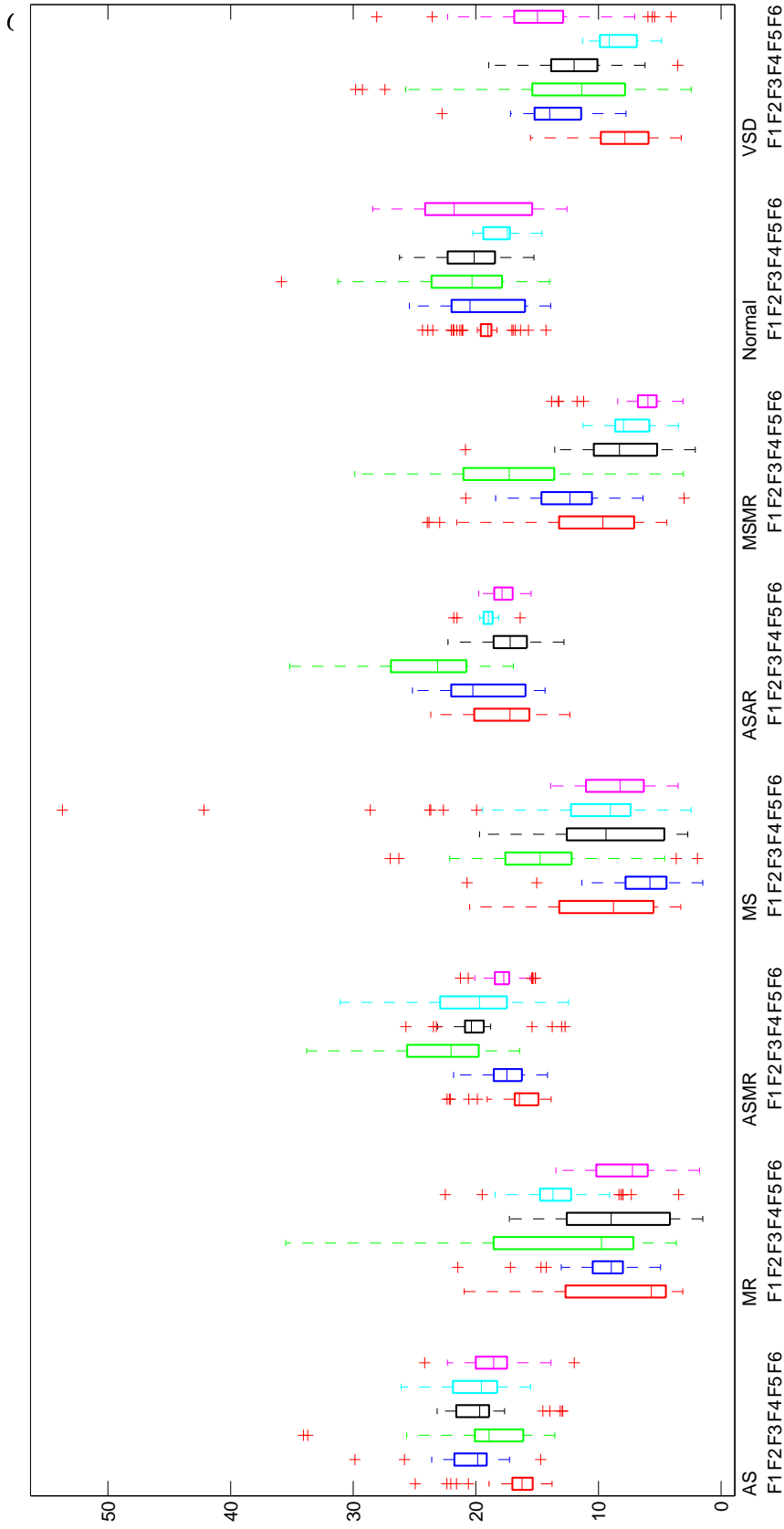
Figure 6.3: The range of feature values for the LDV data for each pathology at a normalized threshold value of $t = 0.6$. F1, F3 and F5 are f_{max} feature of the full, systolic and diastolic FFT curves respectively. F2, F4 and F6 are f_{width} feature of the full, systolic and diastolic FFT curves respectively. When compared to Figure 6.2, notice the more distinct groupings of features associated with each pathology.
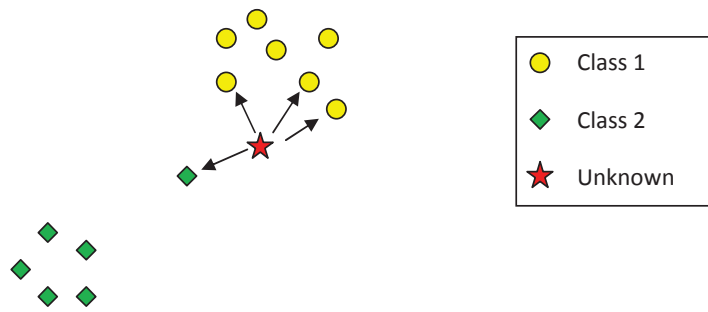
Figure 6.4: In KNN, a data point is assigned the label of the majority of its K-nearest neighbours. A tie-breaking rule is implemented if two or more labels have an equal number of neighbours.

technique. CV is an important step towards predicting the accuracy of a predictive model in the context of real-world application. When datasets are small, it becomes impractical to use a large part of the data set as test data only. Using cross-validation, a small number of data points can be removed at a time, leaving the majority of the points to build the prediction model (Simon *et al.*, 2003). Due to its efficient use of data, CV is ideally suited for the current work.

Cross-validation is often used to reduce the risk of overfitting, where the model is tuned to fit the set of data it trained with, at the expense of generalizability. Evaluating a model using cross-validation helps to avoid overfitting since the test data is by definition not a part of the training data set.

All of the LDV recordings made on all of the participants were segmented into heart sound cycles from which features could be extracted. Leave-one-out (LOO) cross validation was chosen to evaluate the classifier's performance. In order to minimize the bias within the classifier, the rest of the cycles of the participant currently being tested were removed from the training data. The participant was allocated the data label that occurred most frequently among their individually classified samples.

6.3.3   Model parameter choice

An advantage of KNN classifiers is that they do not require the choice of many model parameters and are not particularly sensitive to parameter choices. Applying Matlab's KNN classifier requires choosing three parameters: the number of nearest neighbours to consider, the distance metric and the classification rule. The choices for the rule and distance were the majority vote with a nearest tie-breaker and Euclidean distance. Both of these parameters are commonly used when applying KNN classification.

Table 6.2: Confusion matrix for the individually classified pathologies.

		Predicted								
		AS	**MR**	**ASMR**	**MS**	**ASAR**	**MSMR**	**N**	**VSD**	**HOCM**
	AS	35	12	12	6	4	5	10	10	6
	MR	24	5	8	9	6	15	19	11	3
	ASMR	41	14	5	6	4	4	11	6	8
Actual	**MS**	14	11	5	20	1	16	19	6	8
	ASAR	30	14	15	8	0	2	15	12	4
	MSMR	13	14	5	19	1	5	34	9	1
	N	19	11	8	14	5	22	8	8	4
	VSD	31	16	7	11	4	10	17	0	4
	HOCM	28	10	15	5	6	1	15	10	0

The results obtained from using different K values as well as different threshold values were compared. It was found that, when classifying AS or Not AS, K = 3 and a normalized threshold value of $t = 0.6$ classified the most patients correctly when using LOO CV.

6.4   Individual participant results

As mentioned in the introduction of this chapter, there was not enough unique data available to create a classifier which could differentiate between normal and abnormal participants or sensibly distinguish between the full set of pathologies. There were, however, a sufficient number of participants who presented with AS to create a classifier which could reliably distinguish between AS and those without AS, hereafter referred to as "not AS" participants. This seems to suggest that the chances of creating classifiers for other combinations of pathologies are good, given additional data. A confusion matrix is used to represent the performance of a classifier. A diagonal line of maximum values would indicate that the actual pathology of each participant was correctly predicted. The distribution of predicted pathologies, given as percentages for each actual pathology are shown in Table 6.2. The most frequent predictions are shown in green. From Table 6.2 it can be concluded that the classifier does not accurately predict individual pathologies, as is to be expected given the low number of participants exhibiting a given pathology.

There were enough AS participant recordings to allow an AS/not AS classifier to be trained. To illustrate the effect of the chosen feature set and threshold level, Table 6.3 compares the actual and predicted pathology for feature threshold levels of $t = 0.1, 0.3$ and 0.6. It is clearly visible that the threshold value as well as the chosen feature set does not drastically affect the accuracy of the classifier, which

Table 6.3: Comparison of KNN classification results for LDV data with K = 1 and $t = 0.1, 0.3$ and 0.6. Feature sets of f_{width} and f_{max} of the full cycle, systolic and diastolic components, and the combination of full cycle, systolic and diastolic components are given. AS is labeled with a numerical value of 2 and not AS is labeled with a numerical value of 1.

		Full cycle			**Systolic and diastolic**			**Full cycle, systolic and diastolic**		
		Normalized threshold value t								
PAT	**Actual**	**0.1**	**0.3**	**0.6**	**0.1**	**0.3**	**0.6**	**0.1**	**0.3**	**0.6**
1	1	1	1	1	1	1	1	1	1	1
2	1	1	1	1	1	1	1	1	1	1
3	2	1	2	1	1	2	1	1	2	2
4	2	2	1	1	2	1	1	2	2	1
5	1	1	1	1	1	1	1	1	1	1
6	1	1	1	1	1	1	1	1	1	1
7	2	2	2	2	2	2	2	2	2	2
8	1	1	1	1	1	1	1	1	1	1
9	1	1	1	1	1	1	1	1	1	1
10	1	1	1	1	1	1	1	1	1	1
11	1	1	1	1	1	1	1	1	1	1
12	2	1	1	1	1	1	1	1	1	1
13	1	1	1	1	1	1	1	1	1	1
14	1	1	1	1	1	1	1	1	1	1
15	1	1	1	1	1	1	1	1	1	1
16	1	1	1	1	1	1	1	1	1	1
17	1	1	1	1	1	1	1	1	1	1
18	2	1	2	2	1	2	2	2	1	2
19	1	1	1	1	1	1	1	1	1	1
20	1	1	1	1	1	1	1	1	1	1
Total correct		17	18	17	17	18	17	18	18	18
Total incorrect		3	2	3	3	2	3	2	2	2

is confirmed by the results obtained by Jiang *et al.* (2007) for their two-parameter classification scheme. The results obtained using the full cycle, systolic and diastolic components are more accurate than those of the full cycle or systolic and diastolic components individually. The correctly classified AS participants are highlighted in green and the incorrectly classified participants are highlighted in yellow for better visibility.

Table 6.4 shows the confusion matrix for the final AS/not AS classifier with K = 3, and a normalized feature threshold of $t = 0.6$. With the simplified classifi-

Table 6.4: Confusion matrix for the AS not AS classification.

		Predicted	
		AS	Not AS
Actual	AS	4	1
	Not AS	0	15

Table 6.5: Individual results for each pathology for AS or not AS classification as a percentage of the total number of cycles classified for K = 3 and a normalized threshold of $t = 0.6$.

Participant	1	2	3	4	5	6	7	8	9	10
Not AS	80	90	25	45	80	100	30	75	95	100
AS	20	10	75	55	20	0	70	25	5	0
Participant	**11**	**12**	**13**	**14**	**15**	**16**	**17**	**18**	**19**	**20**
Not AS	70	90	90	95	95	80	70	40	95	79
AS	30	10	10	5	5	20	30	60	5	21

cation scheme the classifier has much improved accuracy: 19 of the 20 participants were correctly identified as either AS or not AS. The results per participant for are shown in Table 6.5, and are listed as a percentage of the total number of cycles classified, with the higher percentage highlighted. Only Participant 12 was continuously misdiagnosed as not AS, regardless of the classifier used. Participant 12 was diagnosed by a cardiologist as having "mild AS", which may be affecting the classifier's ability to identify the participant as AS. From Table 6.5 it can be seen that for the majority of the correctly classified participants a high percentage of the samples are classified as one label. Only for Participant 4 and Participant 18 are there a near equal number of samples for each label. The tendency of samples to overwhelmingly be classified as one label or another indicates a high degree of similarity between the recordings of a single participant.

The fact that the data could be classified into participants who presented with AS and those who did not demonstrates the theoretical soundness of the classification scheme. It is likely that, given more data, it would be possible to train classifiers able to distinguish between other pathologies.

6.5   Sensitivity and specificity

Sensitivity and specificity are the common measure of the performance of a classifier. They are used as statistical measures for determining how accurately a classifier predicts data. Sensitivity and specificity are defined as follows

$$\text{Sensitivity } = \frac{TP}{TP + FN} \text{ and Specificity } = \frac{TN}{TN + FP} \tag{6.1}$$

where TP, FN, TN and FP are defined as

TP - true positives (participants who were correctly classified as AS)

FN - false negatives (participants who were incorrectly classified as Not AS)

TN - true negatives (participants who were correctly classified as Not AS)

FP - false positives (participants who were incorrectly classified as AS)

In classifying AS participants, the current classifier has an 80% sensitivity and 100% specificity in classifying AS and Not AS participants, although the value of these results is questionable due to the low sample size.

6.6   A comparison to the diagnosis of cardiologists using auscultation

The cardiologists were asked to perform manual auscultation with their stethoscopes without knowing what the echocardiogram revealed as the true diagnosis. The cardiologists all correctly identified the patients as either normal or abnormal. One patient was incorrectly identified as having PS, but the echocardiogram revealed that the diagnosis was actually VSD.

The comparison between the cardiologists and the classifier is superficial at this point. The number of participants recorded in the study is not sufficient to accurately compare the performance of a cardiologist to the classification achieved in the current study. As the data currently stands, the cardiologists have a sensitivity of 100% for classifying AS and Not AS participants, which is more accurate than the classifier. This is unsurprising since the cardiologists have been trained on a large data set for many years. They are thus the benchmark for any proposed classification system.

6.7   Chapter summary

Frequency domain features were extracted from the LDV data and used to train a KNN classifier which could distinguish between participants who presented with AS and those who did not. The KNN classifier's results were presented and analyzed

and found to have a sensitivity of 100% and specificity of 80%. The classification results were compared to the diagnosis results of cardiologists and indicate that classification using the LDV is indeed possible.

Chapter 7

Conclusions and recommendations

7.1 Introduction

The LDV has been compared to a phonocardiogram (De Melis *et al.*, 2007) and PA and been used to identify events such as the opening and closing of the heart valves (Umberto *et al.*, 2007). This project explored the LDV's abilities as an autonomous auscultation device. In the following sections the various conclusions are drawn and where applicable recommendations are made for future work.

7.2 The laser Doppler vibrometer as an auscultation device

The LDV has been compared to other auscultation devices, such as the stethoscope. Work done by researchers from the University of Marche showed that data generated by the LDV could be post-processed to yield a chest wall velocity profile or an output similar to that of the phonocardiogram. This finding was confirmed in the current work. That the LDV can produce an output similar to the phonocardiogram is of particular significance since the phonocardiogram is familiar to cardiologists. This bodes well for the use of the LDV in a clinical setting. Since the Stream 1 LDV data has a wave shape similar to the phonocardiogram, future work could include the LDV data as an audible aid to cardiologists.

7.3 Denoising

The Stream 1 LDV signal as well as the accelerometer and stethoscope signals were denoised with a band-pass Butterworth filter, wavelets and EEMD. The Stream 2 LDV data was denoised using a low-pass Butterworth filter and EEMD. The denoising process was effective at removing signal dropouts as well as noise for both

72

streams of data. The post-processing was not done in real time as there was no need for a instantaneous display of any results. The current implementation of EEMD would be prohibitively expensive were real time classification required.

The LDV is inherently prone to the occurrence of signal dropouts, discussed in Section 4.2.1. Dropouts cannot be avoided while measuring, but they can be reduced (Gatzwiller *et al.*, 2002). Proper perpendicular alignment of the measurement beam with the measurement surface, adequate focus of the laser beam, an optimal measurement distance and good surface reflectivity are listed as factors which would reduce the number of dropouts experienced.

7.4 Data acquisition and hardware

7.4.1 The LDV and external noise

The LDV was found to be extremely sensitive to vibrations of the frame upon which it was mounted. Contact with the frame during recording had to be minimized as any external vibrations prevented the recording of usable data. The developed segmentation method in Section 4.3 proved to be mostly immune to these variations as any disturbance drastically changed the complexity of the processed signal. The segmentation algorithm therefore excluded these cycles from the usable dataset. While this process ensured that the externally introduced artifacts did not distort the classification data, it did reduce the number of cycles available for classification.

For future work it is recommended that the LDV is mounted on a structure which has no contact with the individual conducting the study or the participant whose data is being recorded. The LDV's sensitivity to vibrations necessitates that it be securely mounted during use and will make the development of a hand-held LDV auscultation device challenging.

7.4.2 The vibration surface

Umberto *et al.* (2007) used retro-reflective tape to enhance the signal of the LDV used in their study. They reported that the application of retro-reflective tape to the participant significantly reduced the occurrence of signal dropouts. Initially, identical retro-reflective tape was used in the current study, but was removed after it was found that it degraded the LDV signal. A likely cause of this discrepancy is the much larger distance between the participant and the LDV unit in the work of Umberto *et al.* (2007) than in the current work.

Despite the poor results from the retro-reflective tape, it was found that small paper sticker greatly improved the signal quality of the LDV. The sticker gave the LDV a measurement surface which was uniform in both texture and colour. Stickers of various colours were tested and it was found that a white sticker resulted in the

best signal quality. Because of the variation of signal quality with the sticker colour, it is likely that the skin tone of the participants as well as the variation of skin tone of a single patient would likely influence signal quality. The presence of chest hair was found to cause erratic behaviour in the recordings as the individual hairs would move in and out of the laser's beam as the patient breathed, causing signal spikes at unpredictable intervals.

7.5   The piezoelectric accelerometer

The study found that the accelerometer recordings on the sternum and apex of the heart were similar but had opposing polarities. The integration of the accelerometer data to velocity was shown to be effective as it compared well with the signal obtained from the LDV data, as shown in Figures 5.10 and 5.11. The accelerometer placed at the sternum had the same sign as that of the LDV data, and the same sign was observed in both the data which had been integrated to calculate the velocity and position data. The accelerometer data from the apex, however, had an opposite sign to that of the LDV data. The LDV was also tested against the PA, as the PA is more commonly used in the biomedical field. The LDV and PA produced very similar results when used to calculate HR and analyze systolic versus diastolic signal ratios, indicating that the LDV is a viable instrument in those common use cases.

7.6   The stethoscope

The stethoscope used in this study did not perform to the satisfaction of the author. The original stethoscope meant for use in the study was destroyed by a fellow student shortly before clinical trials began, leaving inadequate time for a new stethoscope to be tested in a clinical setting. The choice was made to make the new stethoscope battery-powered, but unfortunately the batteries depleted more rapidly than was anticipated. Some participants therefore do not have usable stethoscope data. It is therefore recommended that a new electronic stethoscope be developed or bought for use in any future studies.

7.7   Segmentation

The ECG system could only record 10 seconds of data at a time. A segmentation algorithm was developed which combined the standard of segmentation by the ECG with a simplicity curve approach, first described by Nigam and Priemer (2005). The segmentation performed using the simplicity curve compared well to that of the ECG. The ECG data was recorded on a different laptop to the LDV, accelerometer

and stethoscope and as such the two data streams had to be synchronized. A sinusoidal signal was introduced as an artifact into both of the streams which could then be synchronized automatically during post processing. Despite the effectiveness of segmentation using simplicity curves, future work should consider using an ECG able to record more data as segmentation using the ECG remains the gold standard for segmentation in biomedical research.

The combined segmentation approach of using the simplicity curve and ECG data meant that most of the usable cycles were correctly extracted from the recorded data. The method proved to be immune to noisy data as the simplicity curve would reflect the presence of noise rather than the more simple heart sounds. The effect of the number of extracted heart sound cycles was not investigated in the current work. It would be sensible to assume that a larger number of cycles would ensure more confidence in the output of the classifier. The topic could be included in future work as a point of interest.

7.8 Feature extraction

Six LDV features were extracted for each heart sound cycle. FFTs were calculated separately for the full cycle as well as for the systole and diastole of the cycle. From each FFT curve the signal bandwidth was calculated at a threshold value and the position of the maximum frequency was extracted. Various combinations of features were tested and it was found that all six LDV features gave the best classification results (see Table 6.5). The PA data was tested alone as well as in combination with the LDV data, but did not significantly improve the classification.

The feature set used in this work is far smaller than the features used by Botha (2010) and Visagie (2007), which means the classifier is computationally cheaper than the preceding projects. Botha (2010) and Visagie (2007) had a far larger data set, which means the robustness of their systems have been tested to a greater extent than the classifier in the current work. KNN classifiers are not complicated systems, and therefore the choice and testing of features for its input is a straightforward process. The features extracted from the FFT data proved to be adequate for the KNN classifier.

No morphological data from the velocity profiles was used to extract any features. Future research could include such features in order to further improve classifier performance.

7.9 Classification

KNN classification uses the nearest data points to the unclassified data point to decide what that point should be classified as. KNN classifiers are simple and

robust, making them well suited for dealing with potentially noisy data.

When the two feature classification system was tested, the classifier could not differentiate between normal and abnormal participants, even though the normal to abnormal participant ratio was similar to the work of Jiang *et al.* (2007) from whom the two-feature classification system was adapted. Further investigation yielded that a reason for this could be that there were too few normal participants recorded. The classifier was therefore trained to differentiate between AS and Not AS participants, as a larger number of AS participants had been recorded. This improved the classification results marginally. By adding the systolic and diastolic features, totalling 6 features, acceptable accuracy was obtained. The normal/abnormal classification however, still suffered from poor performance even with the new feature set. The conclusion was drawn that more normal participants were required, which was an oversight in the planning for the clinical trial. The original time line for the work also did not allow more participants to be recorded by the time the lack of data became apparent. The classification between participants with AS and those without resulted in a classifier with a specificity of 100% and a sensitivity of 80%.

The data recorded for the current work did not include innocent heart murmurs, which are an important subsection of detectable heart murmurs. Future work should therefore include innocent heart murmurs which could either be grouped as "normal" or as a completely separate pathology depending on the classification results obtainable. With a larger data group attention could also be given to the severity of the various heart murmurs, which could not be done in the current work.

Leave-one-out cross-validation was applied at the participant level. For each participant, a set of features from each heart cycle was classified using the training data from all other participants. The label most frequently allocated to the individual heart cycles of a participant was the overall label allocated to that participant.

Future work could explore different classification schemes. There are many variations of KNN classifiers which could be tested or an entirely different classifier could be evaluated. Possible classification schemes to investigate include neural networks, support vector classifiers or random forest classifiers.

7.10 Physical and other limitations of the LDV against mechanical auscultation

The LDV as a biomedical sensor has only recently become an active research topic (De Melis *et al.*, 2007; Umberto *et al.*, 2007). As such, there are still a variety of limitations to be overcome and open problems to be solved before the LDV can enter mainstream use. In this section, some of these will be discussed.

The LDV is prone to signal dropouts, as discussed in Section 4.2.1. These

dropouts could affect the Stream 1 waveform shape, potentially making it unrecognizable to cardiologists used to interpreting phonocardiograms. Real-time filtering techniques could be investigated to remove signal dropouts, in order to overcome this limitation.

The current LDV is large and not suitable for hand-held use. In Section 5.3.3 it was discussed that the measurement position could affect the recorded data. Since it is not attached to the participant, any relative motion between the LDV and the participant could distort the recorded measurements. Relative motion can be introduced by the participant moving or the LDV's position being unstable, such as would be the case with a hand-held device. The LDV is not attached to the point of measurement in any physical way. As a result, non-stationary participants cannot be recorded with the LDV alone, as the LDV does not track the measurement point in the same way a contact sensor would. A tracking system could be implemented to automatically hold the point of measurement of the LDV constant, irrespective of movement of the participant, however it may prove challenging to ensure that critical diagnostic information is not lost in this compensation process. As both a stethoscope and a PA are attached to the participant being recorded, they are not subject to either of these problems.

The LDV must be mounted securely at a constant distance from the subject to record reliable data. In contrast, the stethoscope and PA are small and light, making them easy to maneuver and attach to surfaces. The LDV would need to become more compact to be suitable for comparable biomedical purposes.

Finally, the LDV requires surface preparation to ensure a consistent recording. Factors such as the presence of chest hair influence the accuracy of the LDV recordings. A smooth, consistent surface on the participant greatly improved recordings. The stethoscope and PA do not have this restriction.

7.11 Project objectives

7.11.1 Record simultaneous data from the LDV, accelerometer and stethoscope and synchronize it with ECG data

Data was successfully recorded with the LDV, accelerometer and stethoscope and ECG. The data was synchronized using a "coil box" discussed in Section 3.2.5 which introduced an artifact sinusoidal signal to both the DAQ and ECG. The artifact signal could then be aligned during post-processing.

7.11.2 Find features which can be used to classify various heart murmurs

Six frequency domain features were identified for both the LDV and PA data which could be used to adequately classify the recorded data. The chosen features were the bandwidth of the FFT at a specific threshold value as well as the frequency at which the maximum of the FFT occurred. These two features were extracted for each full heart sound cycle as well as the systolic and diastolic components of the signal.

7.11.3 Implement a proof of concept classifier for automated diagnosis of heart murmurs using the LDV data

A KNN classifier was chosen as a proof-of-concept classifier for the current work. KNN classifiers have been proven to be resistant to noisy data and are computationally inexpensive in the context of the current work. The classifier proved that an automated classification system based on LDV data could be developed. The classifier could accurately distinguish between participants that presented with AS and those who did not. Lack of data means that no absolute conclusions can be made for the classification of the LDV data, but it is clear that its recordings have diagnostic value. Future work should include a larger number of healthy participants in particular.

7.11.4 Characterize the LDV output for various heart murmurs and compare its output to the well-known phonocardiogram and PA recordings

A comparison of the velocity profiles which were recorded for each participant indicated that certain morphological features could be identified as unique to specific heart murmurs. These features were briefly highlighted and discussed in Section 5.2. A BP filtered LDV signal also shows the characteristic morphological shapes commonly seen in phonocardiogram recordings which directly relate to the vibrations of the chest as they are translated to sound. The positions used to record the LDV data was taken from the work done by (De Melis *et al.*, 2007; Umberto *et al.*, 2007) however the results of this study shows that other positions may yield other diagnostically relevant results. This could be pursued in future work.

Appendices

Appendix A

Specification sheets

ICP® ACCELEROMETER

Model Number		Revision: C
352A24		ECN #: 27171

Performance	ENGLISH	SI	
Sensitivity(± 10 %)	100 mV/g	10.2 mV/(m/s²)	
Measurement Range	± 50 g pk	± 490 m/s² pk	
Frequency Range(± 5 %)	1.0 to 8000 Hz	1.0 to 8000 Hz	
Frequency Range(± 10 %)	0.8 to 10,000 Hz	0.8 to 10,000 Hz	
Frequency Range(± 3 dB)	0.4 to 12,000 Hz	0.4 to 12,000 Hz	
Resonant Frequency	≥ 30 kHz	≥ 30 kHz	
Broadband Resolution(1 to 10,000 Hz)	0.0002 g rms	0.002 m/s² rms	[1]
Non-Linearity	≤ 1 %	≤ 1 %	[2]
Transverse Sensitivity	≤ 5 %	≤ 5 %	
Environmental			
Overload Limit(Shock)	± 5000 g pk	± 49,050 m/s² pk	
Temperature Range(Operating)	-65 to +250 °F	-54 to +121 °C	
Temperature Response	See Graph	See Graph	
Electrical			
Excitation Voltage	18 to 30 VDC	18 to 30 VDC	
Constant Current Excitation	2 to 20 mA	2 to 20 mA	
Output Impedance	≤ 300 ohm	≤ 300 ohm	
Output Bias Voltage	8 to 12 VDC	8 to 12 VDC	
Discharge Time Constant	0.4 to 1.5 sec	0.4 to 1.5 sec	
Settling Time(within 10% of bias)	<8 sec	<8 sec	
Spectral Noise(1 Hz)	80 µg/√Hz	785 (µm/s²)/√Hz	[1]
Spectral Noise(10 Hz)	15 µg/√Hz	147 (µm/s²)/√Hz	[1]
Spectral Noise(100 Hz)	4 µg/√Hz	39 (µm/s²)/√Hz	[1]
Spectral Noise(1 kHz)	1 µg/√Hz	9.8 (µm/s²)/√Hz	[1]
Electrical Isolation(Base)	≥ 10⁸ ohm	≥ 10⁸ ohm	
Physical			
Sensing Element	Ceramic	Ceramic	
Sensing Geometry	Shear	Shear	
Housing Material	Anodized Aluminum	Anodized Aluminum	
Sealing	Epoxy	Epoxy	
Size (Height x Length x Width)	0.19 in x 0.48 in x 0.28 in	4.8 mm x 12.2 mm x 7.1 mm	
Weight	0.03 oz	0.8 gm	[1]
Electrical Connector	3-56 Coaxial Jack	3-56 Coaxial Jack	
Electrical Connection Position	Side	Side	
Mounting	Adhesive	Adhesive	

CE [3]

OPTIONAL VERSIONS

Optional versions have identical specifications and accessories as listed for the standard model except where noted below. More than one option may be used.

RH - RoHS Compliant
Supplied Accessory : Model RH030A10 Coax Cable, 10 ft (3 m), 3-56 plug to 10-32 plug, RoHS compliant. replaces Model 030A10

NOTES:
[1] Typical.
[2] Zero-based, least-squares, straight line method.
[3] See PCB Declaration of Conformance PS023 for details.

Typical Sensitivity Deviation vs Temperature

SUPPLIED ACCESSORIES:
Model 030A10 Coax Cable, 10 ft (3 m), 3-56 plug to 10-32 plug. (1)
Model 039A28 Removal Tool (1)
Model 080A109 Petro Wax (1)
Model ACS-1 NIST traceable frequency response (10 Hz to upper 5% point). (1)

Entered:		Engineer: SS	Sales: KH	Approved: RM	Spec Number:		
Date: 8-23-07		Date: 8-23-07	Date: 8-23-07	Date: 8-23-07	12320		

PCB PIEZOTRONICS™
VIBRATION DIVISION
3425 Walden Avenue, Depew, NY 14043

Phone: 716-684-0001
Fax: 716-685-3886
E-Mail: vibration@pcb.com

All specifications are at room temperature unless otherwise specified.
In the interest of constant product improvement, we reserve the right to change specifications without notice.
ICP® is a registered trademark of PCB Group, Inc.

NORAV
medical

1200HR High Resolution ECG

Technical Specifications

Lead	Standard 12 leads
Defibrillation protection	Protected against 360 J discharge
Lead OFF detection	Detached Lead or Offset >0.5 V
Pacemaker Pulse detection	From 0.1 to 2ms at 2 to 700mv
Sensitivity	5, 10, 20, 40 mm/mV
Horizontal scale	12.5, 25, 50, 100 mm/sec
Signal dynamic range	20mV
DC max. input	± 330mV
Resolution	**16 bits** (0.3 μV/LSB)
ECG maximum sampling rate	16,000 samples per second
Input impedance	> 100Mohm
CMMR	> 100 dB
Frequency range (-3db)	0.05 – 300 Hz
Low pass filter	20, 35, 40 Hz
Base line filter	Yes
Line noise filter	50/60Hz
Communication interface	USB
Power supply	5V$^{\pm 5\%}$
Current consumption	<200mA$^{\pm 10\%}$
Size	17 x 9 x 3 cm
Weight	300 gram
Safety standard	IEC 60601-1, EN 60601-1-2 IEC 60601-2-25, IEC 60601-2-27, EC11
Operating temperature	0^{0}C to +50^{0}C
Storing temperature	-40^{0}C to +70^{0}C
Humidity	0–85%
Certification	CE, FDA approved

- Ideal for Heart Rate Variability, Signal Averaged ECG and Exercise applications
- Very High resolution ECG processing
- Easy interface to EMR (Electronic Medical Records) and HIS (Hospital Information Systems)
- Right side and Posterior chest leads
- On-line filtering and automatic Base line correction.
- Free Software updates for the life of system.
- Export test results into formats: JPEG, XML, Plain text, GDT, native RAW data.
- Network Storage enabled.
- A4 format plain paper printing during the test (thermal printer is optional)
- "Scroll Back" during stress test to see episodes that might have been overseen. (S2)
- Controls many models of treadmills and ergometers (including GE, Schiller, Quinton)
- Full disclosure of entire stress study.(S1,S2)
- Remote View via Network (S2)
- Enables post processing of saved data (S2)
- ST measurements
- Arrhythmia detection, print and capture VPB and SVPB (S2)
- Blood pressure equipment interface
- Standard as well as unlimited user programmed Stress test protocols(S1,S2)

Distributed By:

Optional Software: Stress**,** Heart Rate Variability, QT Variability, Late Potentials, ECG Measurement, Interpretation, NEMS(Norav ECG Management System)

*Specifications are subject to changes without notice.

1200HR(1)280807

www.norav.com

Appendix B

Specialist report card and consent form

PROJECT - Application of laser Doppler vibrocardiography for human heart auscultation

Investigator – Suretha Koegelenberg (082 969 0388)

Patient ID	DATE	SPECIALIST/CLINICIAN

Normal   /   Abnormal

S1   S2

Diagnosis/Comments:

PARTICIPANT INFORMATION LEAFLET AND CONSENT FORM

TITLE OF THE RESEARCH PROJECT:

Application of laser Doppler vibrocardiography for human heart auscultation

REFERENCE NUMBER:

PRINCIPAL INVESTIGATOR: Suretha Koegelenberg

ADDRESS:
Room M517, Fifth Floor, Mechanical and Industrial Engineering Building
Corner of Banghoek and Joubert Street
Stellenbosch

CONTACT NUMBER: +27 (0) 21 808 4376

You are being invited to take part in a research project. Please take some time to read the information presented here, which will explain the details of this project. Please ask the study staff or doctor any questions about any part of this project that you do not fully understand. It is very important that you are fully satisfied that you clearly understand what this research entails and how you could be involved. Also, your participation is **entirely voluntary** and you are free to decline to participate. If you say no, this will not affect you negatively in any way whatsoever. You are also free to withdraw from the study at any point, even if you do agree to take part.

This study has been approved by the **Health Research Ethics Committee (HREC) at Stellenbosch University** and will be conducted according to the ethical guidelines and principles of the international Declaration of Helsinki, South African Guidelines for Good Clinical Practice and the Medical Research Council (MRC) Ethical Guidelines for Research.

What is this research study all about?

The study wich you have been invited to participate in will be conducted in Tygerberg Hospital, Cape Town. A maximum of 100 individuals will participate in this study, all of whom are from Tygerberg Hospital.

The project goal is to test and compare different types of sensors in their ability to record heart sounds. One sensor in particular, the laser Doppler vibrometer, is of particular interest to this project.

A laser Doppler vibrometer uses a laser beam to read the velocity of the object it is pointed at using physics phenomenon known as the Doppler Effect. This system will be used to pick up the movement of your chest.

The other sensors are basic mechanical or electrical sensors which need physical contact to pick up your heart's vibrations. These sensors are a type of accelerometer

(piezoelectric), a stethoscope with a built in microphone, and an electrocardiograph (ECG).

If you agree to participate in this study, the following procedure will be followed:
1. You will be required to sign this consent form
2. When prompted, please proceed to the recording area
3. Once inside the recording area, you will be examined by a doctor from the cardiology clinic.
4. The investigator will then place the electrode stickers for the ECG system on you and perform a quick calibration test
5. The recording process will then be started. The sensors will be used simultaneously to acquire the necessary data.
6. When the investigator prompts you to do so, put on the necessary safety glasses.
7. When satisfactory recordings have been made, all the sensors and stickers will be removed and you will be free to leave the recording area

Your involvement in this study is a single recording session, after which no further involvement will be required.

Why have you been invited to participate?

You have been classified as either having normal or abnormal heart sounds, and are capable of making an informed choice to willingly participate.

What will your responsibilities be?

You as a participant will be required to follow the investigator's prompts in order to ensure that good quality recordings can be made.

Will you benefit from taking part in this research?

There will be no direct benefit for you as a participant.

Are there in risks involved in your taking part in this research?

The laser Doppler vibrometer is a Class 3B laser system, which can cause eye damage if your eyes are exposed to the beam.

You, as a participant will be equipped with protective eye glasses and will be shielded from the beam during the recording process. There is therefore no risk to you.

Who will have access to your medical records?

The medical professional will indicate whether you are classified as having normal or abnormal heart sounds. This will be recorded along with the data acquired from the sensors. The data will be stored anonymously, which means that no personal data can be linked to you, the participant.

It is a possibility that the research records must be reviewed by the ethics council, study monitors or study sponsors. The records will be stored as strictly anonymous, and so no personal information will be available to any person involved in this study.

Will you be paid to take part in this study and are there any costs involved?

No you will not be paid to take part in the study. There will be no costs involved for you, if you do take part.

Is there anything else that you should know or do?

➢ You can contact Dr ……………….………..…….. at tel ……………..………… if you have any further queries or encounter any problems.

➢ You can contact the **Health Research Ethics Committee** at 021-938 9207 if you have any concerns or complaints that have not been adequately addressed by your study doctor.

➢ You will receive a copy of this information and consent form for your own records.

Declaration by participant

By signing below, I ……………………………….…………. agree to take part in a research study entitled *(insert title of study)*.

I declare that:

- I have read or had read to me this information and consent form and it is written in a language with which I am fluent and comfortable.

- I have had a chance to ask questions and all my questions have been adequately answered.

- I understand that taking part in this study is **voluntary** and I have not been pressurised to take part.

- I may choose to leave the study at any time and will not be penalised or prejudiced in any way.

- I may be asked to leave the study before it has finished, if the study doctor or researcher feels it is in my best interests, or if I do not follow the study plan, as agreed to.

Signed at *(place)* ....…….......………….. on *(date)* …………..………….. 2005.

....
Signature of participant   **Signature of witness**

Declaration by investigator

I *(name)* ……………………………………….……… declare that:

- I explained the information in this document to ………………………………..

- I encouraged him/her to ask questions and took adequate time to answer them.
- I am satisfied that he/she adequately understands all aspects of the research, as discussed above
- I did/did not use a interpreter. (*If an interpreter is used then the interpreter must sign the declaration below.*

Signed at (*place*) ....……......…………….. on (*date*) …………...……….. 2005.

....
Signature of investigator   ....
Signature of witness

Declaration by interpreter

I (*name*) …………………………………………..……… declare that:

- I assisted the investigator (*name*) …………………………………………. to

   explain the information in this document to (*name of participant*)

   …………...…………………………….. using the language medium of

   Afrikaans/Xhosa.

- We encouraged him/her to ask questions and took adequate time to answer them.
- I conveyed a factually correct version of what was related to me.
- I am satisfied that the participant fully understands the content of this informed consent document and has had all his/her question satisfactorily answered.

Signed at (*place*) ....……......…………….. on (*date*) …………...………………..

....
Signature of interpreter   ....
Signature of witness

List of References

3M (2012). Stethoscope anatomy.
  Available at: `http://solutions.3mae.ae/wps/portal/3M/en_AE/Littmann/stethoscope/education/stethoscope-anatomy/`

Agarwal, V. and Tsoukalas, L. (2007). Denoising electrical signal via empirical mode decomposition. In: *Bulk Power System Dynamics and Control - VII. Revitalizing Operational Reliability, 2007 iREP Symposium*, pp. 1 –6.

Amit, G. (2009). *Automatic analysis of vibro-acoustic heart signals: combining signal processing and computationa learning techniques for non-invasive evaluation and monitoring of cardiac function.* PhD, Tel Aviv University.

Anh Dinh, Younhee Choi, S.-B.K. (2011). A heart rate sensor based on seismocardiography for vital sign monitoring systems. *IElectrical and Computer Engineering (CCECE), 2011 24th Canadian Conference on. IEEE*.

Antoniak, C. (2011). Extended x-ray absorption fine structure of bimetallic nanoparticles. *Beilstein journal of nanotechnology*, vol. 2, no. 1, pp. 237–251.

Ashley, E. and Niebauer, J. (2004). *From Cardiology Explained.* London Remedica. ISBN 1901346226.

Avargel, Y. and Cohen, I. (2011). Speech measurements using a laser doppler vibrometer sensor: Application to speech enhancement. In: *Hands-free Speech Communication and Microphone Arrays (HSCMA), 2011 Joint Workshop, IEEE*, pp. 109 –114.

Bedford, E. (1972). Cardiology in the days of laennec. the story of auscultation of the heart. *British heart journal*, vol. 34, no. 12, pp. 1193–8.

Bentley, P., Grant, P. and McDonnell, J. (1998). Time-frequency and time-scale techniques for the classification of native and bioprosthetic heart valve sounds. *Biomedical Engineering, IEEE Transactions on*, vol. 45, no. 1, pp. 125 –128. ISSN 0018-9294.

Beyar, R., Levkovitz, S., Braun, S. and Palti, Y. (1984). Heart-sound processing by average and variance calculation - physiologic basic and clinical implications. *Biomedical Engineering, IEEE Transactions on*, vol. BME-31, no. 9, pp. 591 –596. ISSN 0018-9294.

Bhatia, N. (2010). Survey of nearest neighbor techniques. *International Journal of Computer Science and Information Security*, vol. 8, no. 2, pp. 302–305.

Botha, J. (2010). *Autonomous auscultation of the human heart.* Master's thesis, University of Stellenbosch.

Burke, M. and Nasor, M. (2002). The time relationships of the constituent components of the human electrocardiogram. *Journal of Medical Engineering & Technology*, vol. 26, no. 1, pp. 1–6.

Chen, W., Wang, S., Chuai, X. and Zhang, Z. (2012). Random noise reduction based on ensemble empirical mode decomposition and wavelet threshold filtering. *Advanced Materials Research*, vol. 518–523, pp. 3887–3890.

Cho, S. and Yejin, S. (2013). Extraction of significant features using empirical mode decomposition and its application. vol. 1.

Cummings, B. (2004). Pearson education inc.

Cunningham, P. and Delany, S. (2007). k-nearest neighbour classifiers.

Daliman, S. and Sha'ameri, A. (2003). Time-frequency analysis of heart sounds and murmurs. In: *Information, Communications and Signal Processing, 2003 and Fourth Pacific Rim Conference on Multimedia. Proceedings of the 2003 Joint Conference of the Fourth International Conference on, IEEE*, vol. 2, pp. 840 – 843.

Dalmay, F., Antonini, M., Marquet, P. and Menier, R. (1995). Acoustic properties of the normal chest. *European Respiratory Journal*, vol. 8, no. 10, pp. 1761–1769.

De Melis, M., Morbiducci, U. and Scalise, L. (2007). Identification of cardiac events by optical vibrocardiograpy: comparison with phonocardiography. In: *Engineering in Medicine and Biology Society, 2007. EMBS 2007. 29th Annual International Conference of the IEEE, IEEE*, pp. 2956 –2959. ISSN 1557-170X.

Dima, C. (2012). Mitral stenosis.
Available at: http://emedicine.medscape.com/article/155724-overview

Dudani, S. (1976). The distance-weighted k-nearest-neighbor rule. *Systems, Man and Cybernetics, IEEE Transactions on*, vol. SMC-6, no. 4, pp. 325 –327. ISSN 0018-9472.

Gatzwiller, K., Ginn, K., Betts, A. and Morel, S. (2002). Practical aspects of successful laser doppler vibrometry based measurements. *Proceedings of 21 st International Modal Analysis Conference (IMAC-XXI), Kissimmee, Florida.*

Gautschi, G. (2002). *Piezoelectric sensorics: force, strain, pressure, acceleration and acoustic emission sensors, materials and amplifiers.* Springer, Verlag Berlin Heidelberg.

Gemignani, V., E., B., Faita, F., Giannoni, M., Pasanisi, E., Picano, E. and Bombardini, T. (2008). Assessment of cardiologic systole and diastole duration in exercise stress tests with a transcutaneous accelerometer sensor, ieee. *Computers in Cardiology*, vol. 35, pp. 153–156.

Grillo, D., Pasquino, N., Angrisani, L. and Lo Moriello, R. (2012). An efficient extension of the zero-crossing technique to measure frequency of noisy signals. In: *Instrumentation and Measurement Technology Conference (I2MTC), 2012 IEEE International, IEEE*, pp. 2706 –2709. ISSN 1091-5281.

Hök, B., Bythell, V. and Bengtsson, M. (1988). Development of a wireless stethoscope for auscultatory monitoring during anesthesia. *Medical & Biological Engineering & Computing*, vol. 26, no. 3, pp. 317–320.

IOtech (2001). Zonicbook-medallion systems guide.
Available at: `ftp://ftp.measurementcomputing.com/Manuals/ZonicBook%20Systems%20Manual.pdf`

Jiang, Z., Choi, S. and Wang, H. (2007). A new approach on heart murmurs classification with svm technique. In: *In Proceedings of the 2007 International Symposium on Information Technology Convergence, IEEE Computer Society*, pp. 240–244.

Johnson, L. (2003). *Essential Medical Physiology.* Elsevier Science. ISBN 9780080472706.
Available at: `Online via Elsevie`

Karpman, L., Cage, J., Hill, C., Karpman, V. and Cohn, K. (1975). Sound envelope averaging and the differential diagnosis of systolic murmurs. *American Heart Journal*, vol. 90, no. 5, pp. 600–606.

Katzir, S. (2003). The discovery of the piezoelectric effect. *Archive for History of Exact Sciences*, vol. 57, pp. 61–91. ISSN 0003-9519.
Available at: `http://dx.doi.org/10.1007/s00407-002-0059-5`

Kofman, S., Bickel, A., Eitan, A., Weiss, A., Gavriely, N. and Intrator, N. (2012). Discovery of multiple level heart-sound morphological variability resulting from

changes in physiological states. *Biomedical Signal Processing and Control*, vol. 7, no. 4, pp. 315 – 324. ISSN 1746-8094.
Available at: `http://www.sciencedirect.com/science/article/pii/S1746 80941100084X`

Kumar, D., Carvalho, P., Antunes, M., Paiva, R. and Henriques, J. (2010). Heart murmur classification with feature selection. In: *Engineering in Medicine and Biology Society (EMBC), 2010 Annual International Conference of the IEEE, IEEE*, pp. 4566 –4569. ISSN 1557-170X.

Lammers, W. (2013). Murmurs.
Available at: `http://www.fmhs.uaeu.ac.ae/wlammersteach/D.CVS/D.3. %20The%20contracting%20heart/D304CardiacMurmursFiles/murmurs.jpg`

Lee, D. and Yamamoto, A. (1994). Wavelet analysis: Theory and applications. *HP Journal Online*, vol. 45, p. 44.

Leha, G. and Singh, C. (2011). Feature extraction and classification for ocr of gurmukhi script. *International Journal of Engineering Research and Applications (IJERA)*, vol. 1, no. 4, pp. 1736–1739.

Liang, H., Lukkarinen, S. and Hartimo, I. (1997). Heart sound segmentation algorithm based on heart sound envelogram, ieee. In: *Computers in Cardiology 1997*, pp. 105 –108. ISSN 0276-6547.

Livanos, G., Ranganathan, N. and Jiang, J. (2000). Heart sound analysis using the s transform. In: *Computers in Cardiology 2000, IEEE*, pp. 587 –590. ISSN 0276-6547.

Maredza, M., Hofman, K.J. and Tollman, S.M. (2011). A hidden menace: Cardiovascular disease in south africa and the costs of an inadequate policy response. *SA Heart Journal*, vol. 8, no. 1, pp. 48–57.

Mayo Clinic (2011). Mitral valve regurgitation-causes.
Available at: `http://www.mayoclinic.com/health/mitral-valve-regurg itation/DS00421/DSECTION=causes`

Messer, S., Agzarian, J. and Abbott, D. (2001). Optimal wavelet denoising for phonocardiograms. *Microelectronics Journal*, vol. 32, no. 12, pp. 931 – 941. ISSN 0026-2692.
Available at: `http://www.sciencedirect.com/science/article/pii/S0026 269201000957`

MetroLaser Inc. (2010). Vibromet 500v laser doppler vibrometer introductory paper.
Available at: `http://www.metrolaserinc.com/Vibromet500.htm`

Mokhlessi, O., Rad, H., Mehrshad, N. and Mokhlessi, A. (2011). Application of neural networks in diagnosis of valve physiological heart disease from heart sounds. *American Journal of Biomedical Engineeringl*, vol. 1, no. 1, pp. 26–34.

Nigam, V. and Priemer, R. (2005). Simplicity based gating of heart sounds. pp. 1298–1301.

Noble, W. (2006). What is a support vector machine? *Nature Publishing Group*, vol. 24, pp. 1565–1567.

Noimanee, S., Tunkasiri, T., Siriwitayakorn, K. and J., T. (2007). Design considerations for aural vital signs using pzt piezoelectric ceramics sensor based on the computerization method. *Sensors*, vol. 7, no. 12, pp. 3192–3208.

Norav Medical Inc. (2011). Pc-based ecg.
Available at: `http://www.norav.com/en/Rest-1200.html`

NursingMedic (2010). Anatomy of the heart.
Available at: `http://nursingmedic.blogspot.com/2010/11/anatomy-of-heart.html`

PCB Piezotronics (2012). Introduction to piezoelectric accelerometers.
Available at: `http://www.pcb.com/techsupport/tech_ accel.php`

Phan, D.H., Bonnet, S., Guillemaud, R., Castelli, E. and Pham Thi, N.Y. (2008). Estimation of respiratory waveform and heart rate using an accelerometer. In: *Engineering in Medicine and Biology Society, 2008. EMBS 2008. 30th Annual International Conference of the IEEE, IEEE*, pp. 4916 –4919. ISSN 1557-170X.

Rangayyan, R. (2001). *Introduction to Biomedical Signals, in Biomedical Signal Analysis: A Case-Study Approach*, pp. 1–59. John Wiley & Sons, Inc. ISBN 9780470544204.
Available at: `http://dx.doi.org/10.1002/9780470544204.ch1`

Reiser, S.J. (1979). The medical influence of the stethoscope. *Scientific American*, vol. 240, pp. 148–156.

Revision World (2012). Human circulatory system.

Rezek, I. and Roberts, S. (1998). Stochastic complexity measures for physiological signal analysis. *Biomedical Engineering, IEEE Transactions on*, vol. 45, no. 9, pp. 1186 –1191. ISSN 0018-9294.

Ricke, A., Povinelli, R. and Johnson, M. (2005). Automatic segmentation of heart sound signals using hidden markov models. In: *Computers in Cardiology, 2005, IEEE*, pp. 953 –956.

Rosowski, J., Nakajima, H. and Merchant, S. (2008). Clinical utility of laser-doppler vibrometer measurements in live normal and pathologic human ears. *Ear and hearing*, vol. 29, no. 1.

Safara, F., Doraisamy, S., Azman, A., Jantan, A. and Ranga, A. (2012). Wavelet packet entropy for heart murmurs classification. vol. 2012.

Salerno, D.M., Zanetti, J.M., Green, L.A., Mooney, M.R., Madison, J.D. and Tassel, R.A.V. (1991). Seismocardiographic changes associated with obstruction of coronary blood flow during balloon angioplasty. *The American Journal of Cardiology*, vol. 68, no. 2, pp. 201 – 207. ISSN 0002-9149.
Available at: `http://www.sciencedirect.com/science/article/pii/00029 14991907446`

Scalise, L. (2012). Non contact heart monitoring. *Advances in Electrocardiograms - Methods and Analysis, PhD, InTech.*
Available at: `http://www.intechopen.com/books/advances-in-electrocardiograms-methods`

Scalise, L., Castellini, P., Morbiducci, U., Del Gaudio, C., D'Avenio, G., Grigioni, M. and Tomasini, E. (2004). In: *Laser vibrometry for the study of prosthetic mechanical heart valves.*

Scalise, L., De Melis, M., Morbiducci, U., Segers, P. and Tomasini, E. (2008). From cardiac to respiratory rate, from cardiac sounds to pulse velocity a non contact, unified approach for the monitoring of vital signs by means of optical vibrocardiography. In: *Eighth International Conference on Vibration Measurements by Laser Techniques: Advances and Applications*, pp. 70980S–70980S. International Society for Optics and Photonics.

Scire, J. (2010). Laser stethoscope for use in noisy spacecraft environments.
Available at: `http://sbir.gsfc.nasa.gov/SBIR/abstracts/10/sbir/phase1/SBIR-10-1-X12.01-8856.html`

Shah, S., Marcus, G., Gerber, I., McKeown, B., Vessey, J., Jordan, M., Huddleston, M., Foster, E., Chatterjee, K. and Michaels, A. (2008). Physiology of the third heart sound: Novel insights from tissue doppler imaging. *Journal of the American Society of Echocardiography l*, vol. 21, no. 4, pp. 394–400.

Shub, C. (1999). Cardiac physical examination: clinical "pearls" and application. vol. 8, no. 5, pp. 9–13.

Simon, R., Radmacher, M.D., Dobbin, K. and Mcshane, L.M. (2003). Pitfalls in the use of DNA microarray data for diagnostic and prognostic classification. *Journal of the National Cancer Institute*, vol. 95, no. 1, pp. 14–18.

Singh, D., Febbo, P., Ross, K., Jackson, D., Manola, J., Ladd, C., Tamayo, P., Renshaw, A., D'Amico, A.V., Richie, J., Lander, E., Loda, M., Kantoff, P., Golub, T. and Sellers, W. (2002). Gene expression correlates of clinical prostate cancer behavior. *Cancer cell*, vol. 1, no. 2, pp. 203–209.
Available at: `http://linkinghub.elsevier.com/retrieve/pii/S153561080` `2000302`

Slifka, L. (2004). *An accelerometer based approach to measuring displacement of a vehicle body.* Master's thesis, Master of Science in Engineering, Department of Electrical and Computer Engineering, University of Michigan–Dearbornn.

Smith, D., Ozawa, Y. and Craige, E. (1983). Chest wall velocity and the second heart sound. an improved sensor of s2 splitting. *Circulation*, vol. 67, no. 6, pp. 1304–11. `http://circ.ahajournals.org/content/67/6/1304.full.pdf+html`.
Available at: `http://circ.ahajournals.org/content/67/6/1304.abstract`

Stethographics (2012). Auscultory sites.
Available at: `http://www.stethographics.com/heart/main/sites.html`

Steyn, K. (2007). Heart disease in south africa.
Available at: `http://www.mrc.ac.za/chronic/heartandstroke.pdf`

Sweeney, K., McLoone, S. and Ward, T. (2012). The use of ensemble empirical mode decomposition with canonical correlation analysis as a novel artifact removal technique. *IEEE transactions on bio-medical engineering*, vol. 60, no. 1, pp. 97–105.

Telleen, S. (2013). Derived copy of cardiac muscle and electrical activity.
Available at: `http://cnx.org/content/m47785/1.1/`

ThinkLabs (1995). Thinklab product guide.
Available at: `http://www.stethoscope.com/`

Umberto, M., Scalise, L., de Melis, M. and Grigioni, M. (2007). Optical vibrocardiography: a novel tool for the optical monitoring of cardiac activity. *Annals of Biomedical Engineering*, vol. 35, pp. 45–58.

Unser, M. and Aldroubi, A. (1996). A review of wavelets in biomedical applications. *Proceedings of the IEEE*, vol. 84, no. 4, pp. 626 –638. ISSN 0018-9219.

Vanlanduit, S., Guillaume, P. and Schoukens, J. (2002). On-line robust processing techniques for elimination of measurement drop-out. *Measurement Science and Technology*, vol. 13, no. 8, p. 1183.

Visagie, C. (2007). *Screening for abnormal heart sounds and murmurs by implementing neural networks.* Master's thesis, University of Stellenbosch.

Wang, C., Trivedi, S., Jin, F., Stepanov, S., Chen, Z., Khurgin, J., Rodriguez, P. and Prasad, N. (2007). Human life signs detection using high-sensitivity pulsed laser vibrometer. *Sensors Journal, IEEE*, vol. 7, no. 9, pp. 1370 –1376. ISSN 1530-437X.

WHO (2010). World health organization report on noncommunicable diseases in south africa.
Available at: http://www.who.int/nmh/countries/zaf-en.pdf

Wilson, R.A., Bamrah, V.S., Lindsay, J.J., Schwaiger, M. and Morganroth, J. (1993). Diagnostic accuracy of seismocardiography compared with electrocardiography for the anatomic and physiologic diagnosis of coronary artery disease during exercise testing. *American journal of Cardiology*, vol. 71, no. 7, pp. 539–545.

Wisconsin-Madison (2007). A basic introduction to neural networks.
Available at: http://pages.cs.wisc.edu/ bolo/shipyard/neural/local.html

Wu, Z. and Huang, N. (2009). Ensemble empiracle mode decomposition: a noise-assisted data analysis method. *Advances in Adaptive Data Analysis*, vol. 1, no. 1, pp. 1–41.

Xu, L., Wang, Y., Yao, Y., Feng, C., Zhao, Y. and Meng, M.-H. (2010). Comparison of six envelope extraction methods based on abnormal heart sounds. In: *Biomedical Engineering and Informatics (BMEI), 2010 3rd International Conference on, IEEE*, vol. 2, pp. 813–817.

Xu, W., Sandham, W., Fisher, A. and Conway, M. (1996). Wavelet transform analysis of the seismocardiogram. In: *Time-Frequency and Time-Scale Analysis, 1996., Proceedings of the IEEE-SP International Symposium on, IEEE*, pp. 481–484.

Yoganathan, A., Gupta, R., Corcoran, W., Udwadia, F., Sarma, R. and Bing, R. (1976*a*). Use of the fast fourier transform in the frequency analysis of the second heart sound in normal man. *Medical and biological engineering*, vol. 14, no. 1, pp. 455–460. ISSN 0025-696X.
Available at: http://dx.doi.org/10.1007/BF02476124

Yoganathan, A., Gupta, R., Udwadia, F., Wayen Miller, J., Corcoran, W., Sarma, R., Johnson, J. and Bing, R. (1976*b*). Use of the fast fourier transform for frequency analysis of the first heart sound in normal man. *Medical and biological engineering*, vol. 14, pp. 69–73. ISSN 0025-696X.
Available at: http://dx.doi.org/10.1007/BF02477093

Zhang, X., Kinnick, R., Pittelkow, M. and Greenleaf, J. (2008). Skin viscoelasticity with surface wave method. In: *Ultrasonics Symposium, 2008. IUS 2008. IEEE*, pp. 651 –653.